Modelling of a Floating Piston Expander employed in a 10 K Cryocooler

by

Gunaranjan Chaudhry

B.Tech., Mechanical Engineering
Indian Institute of Technology, Delhi, 2003

Submitted to the Department of Mechanical Engineering in Partial Fulfilment of the Requirements for the Degree of Master of Science in Mechanical Engineering

at the

Massachusetts Institute of Technology

September 2005

Signature of Author.....

Gunaranjan Chaudhry
Department of Mechanical Engineering
August 19, 2005

Certified by.....

...ngineering
... Supervisor

Accepted by.....

.....
...allit Anand
Chairman, Department Committee on Graduate Students

Modelling of a Floating Piston Expander employed in a 10 K Cryocooler

by

Gunaranjan Chaudhry

Submitted to the Department of Mechanical Engineering on August 19, 2005 in Partial Fulfilment of the Requirements for the Degree of Master of Science in Mechanical Engineering

ABSTRACT

A single stage of a 3-stage Collins-type cryocooler designed to provide 1 W of cooling at 10 K was constructed and tested. A single stage of the cryocooler consists of a compressor, a counter-flow heat exchanger, and an expander to expand the working fluid. The work of the expanding cold gas is transmitted up a floating piston and is dissipated by gas flows in and out of a warm volume. Flow through the cold volume is controlled by smart electromagnetic valves.

Models were developed to describe the thermodynamic processes that make up the expander cycle. In the first iteration, models were developed to determine the equilibrium states at various points in the cycle by assuming the thermodynamic processes that made up the expander cycle to be quasi-static. These models were used to determine appropriate values of parameters such as the cut-off volume, the recompression volume, and warm end reservoir pressures for expander operation.

Experiments were done to determine the efficiency of the floating-piston expander. Tests were also done to determine the characteristics of the heat exchanger and compare them with the design characteristics. Finally, the stage was run as a refrigerator with zero heat-load.

It was observed that the quasi-static models did not adequately describe the performance of the expander as most of the processes did not go to equilibrium. Therefore, these models were improved by incorporating the dynamics of the piston motion, the fluid flow through the warm and cold volumes, and the fluid flow through the high-pressure passages of the heat exchanger.

Thesis Supervisor: Joseph L. Smith, Jr.
Title: Professor of Mechanical Engineering

ACKNOWLEDGEMENTS

I would like to thank Prof. Smith and Prof. John Brisson for their guidance throughout the project. They were always willing to lend me a helping hand in the lab and in the shop, and made this project an incredible learning experience. I would also like to thank Mike Demaree for his assistance.

This project would not have been possible without the technical support of AMTI. Most of the equipment was manufactured by AMTI. Chuck Hannon was responsible for the design of most of the components of the machine. Brady Krass set up the electronics and developed the Labview Virtual Instruments used to control the expander.

I would also like to thank my fellow Cryogenic- and Fuel Cell-Lab mates for the entertaining, occasionally enlightening, discussions in the office, and for their help and support.

Finally, I should probably thank my sister Suparna, who claims to have encouraged me in times of emotional lows, to have reminded me that I could do it, and to have told me to get back to work when I was just sitting around, surfing the web!

CONTENTS

LIST OF FIGURES

CHAPTER 1 – INTRODUCTION

1.1 Background

Large-scale cryogenic refrigerators are able to achieve high thermodynamic efficiencies. However, most small-scale cryocoolers are not able to achieve high efficiencies, because the mechanically complex configurations that are used in a large-scale system are not feasible at a small scale. Compactness is typically achieved by using mechanically simple designs. The work covered by this thesis concentrates on the development of a cryocooler that achieves both efficiency and compactness by substituting the mechanical complexity of the cold end of the cryocooler with electronic complexity, which is much easier to manage.

Cryogenic refrigerators typically consist of a system of pre-coolers and expanders to cool the working fluid to a low temperature. In the proposed cryocooler, the expander employs a floating piston to extract work from the working fluid. The floating piston eliminates the need for mechanical linkages. The piston motion is actuated by smart electromagnetic valves which require no mechanical linkages or mechanical valve timing mechanisms at the cold end. Expander work is dissipated at the warm end of the cryocooler.

1.2 The Collins Cycle and the Modified Collins Cycle

The cycle employed in the proposed cryocooler is based upon the Collins cycle (Fig. 1.1), which is used to liquefy helium on a commercial scale. The cycle employs a stack of heat exchangers in which compressed helium is cooled. A portion of the gas is cooled by expansion. The cool expanded gas joins the low-pressure gas from the next heat exchanger stage in the low-pressure side of the heat exchanger stack. The effect of this is to cool the remaining high-pressure gas to near the exhaust temperature of the expander. In this way, high-pressure helium is cooled down in three expansion stages. The liquefaction takes place through a Joule-Thomson valve.

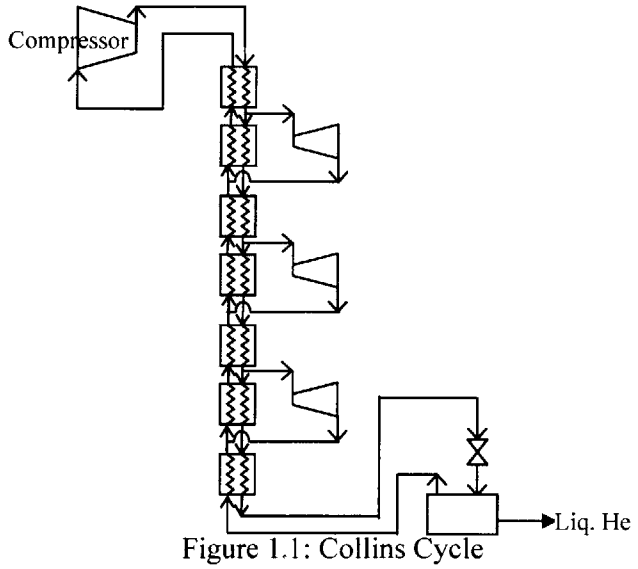

Figure 1.1: Collins Cycle

The proposed cryocooler has a slightly different configuration (Fig. 1.2). A separate heat exchanger is associated with each expansion stage. High-pressure helium from the compressor is split up into three different streams. A heat exchanger for each stage pre-cools the high-pressure stream entering the stage. The pre-cooled stream is cooled further by expansion. Except in the 3rd stage, the exhaust from the expander is split up into two streams. The larger stream returns to the compressor through the low-pressure side of the heat exchanger. The smaller stream goes to the low-pressure side of the heat exchanger in the next stage. This helps increase the pre-cool associated with the next stage. With this configuration, the 3rd stage is pre-cooled to a very large extent and is able to cool the load at 10 K.

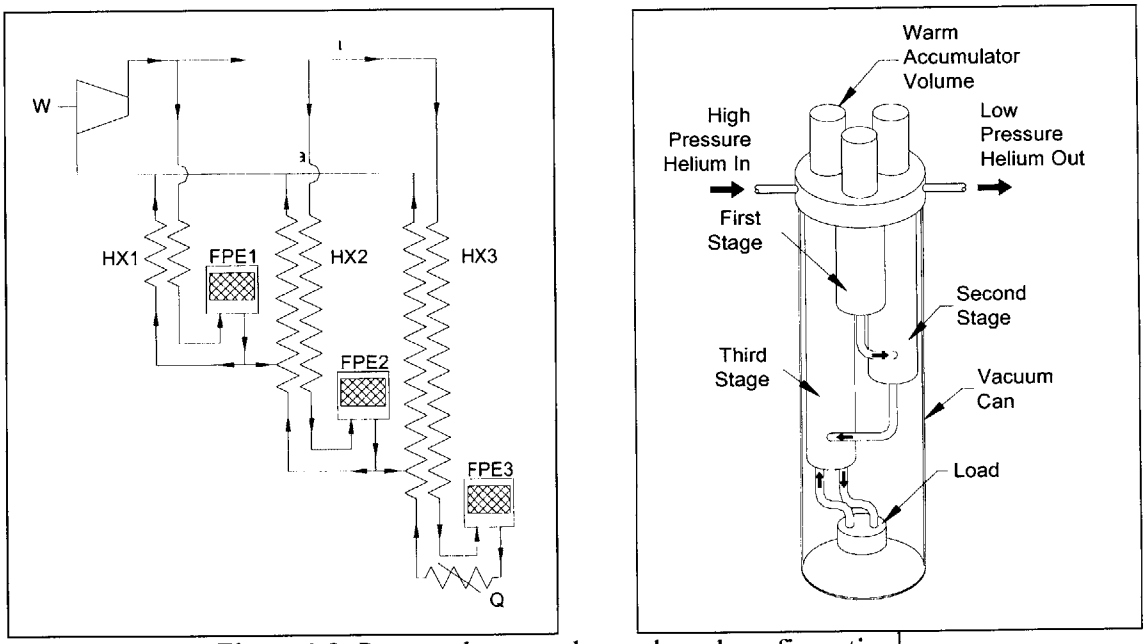

Figure 1.2: Proposed cryocooler cycle and configuration[1]

1.3 Previous Work

Cold electromagnetic valves to control flows in cryogenic applications were first developed by J.A.Crunkleton[2]. Crunkleton, who was interested in reducing the size and mechanical complexity of the valves at the cold end of a cryocooler, developed a low-loss solenoid valve for a new cryocooler developed by Boreas.

In 2001, K.M.Ceridon[3] developed methods for the design and manufacture of electromagnetic valves. The focus of her work was on the design and testing of low-loss valves used to transport helium between cold volumes. A Gifford-McMahon cryocooler was retrofitted with an external flow loop and the cold electromagnetic valves were placed inline of this loop. This allowed the valves to be tested in conjunction with a cycle of known performance.

Around the same time, R.E.Jones[4] was developing a prototype of a floating piston expander to be used in an expansion engine. He constructed a proof-of-principle expander and demonstrated that

a piston without any physical connections, driven solely by a pressure differential, could be used to extract work from the working fluid. He also developed a control routine to run the expander cycle.

In 2003, M.J.Traum[5] developed procedures for the design and manufacture of electromagnetic valves for use in a cryocooler running the modified Collins cycle to provide 1 W of cooling at 10 K. These "smart" valves were integrated into the cold end of a single stage of the cryocooler employing a floating piston expander.

The work covered by this thesis focuses on the integration of the cold end design developed by Traum and the floating piston expander developed by Jones into a single stage of a cryocooler capable of providing efficient cooling at 10 K.

1.4 About this thesis

A single stage prototype to simulate the 3rd stage of the cryocooler assembly was developed in collaboration with AMTI. The reason for the development of the 3rd stage was to demonstrate the ability of the cycle to provide cooling at 10 K. The stage consisted of a floating piston expander, a heat exchanger and a helium compressor.

Quasi-static models developed in MS Excel to describe the thermodynamic processes making up the expander cycle are discussed in Chapter 2. These models were used to determine appropriate values of parameters such as the cut-off volume, the recompression volume, and warm end reservoir pressures for expander operation.

The cold end design, slightly modified from the one developed by Traum, is described in Chapter 3. Also described is the rig developed to test the expander-heat exchanger stage and the Labview routine used to control the expander.

Chapter 4 details the tests done to determine the characteristics of the heat exchanger – specifically, the NTU and the pressure drop – and compare them with the design characteristics. The pressure drop tests were particularly significant since the impedance of the heat exchanger was suspected of limiting the performance of the expander.

Chapter 5 contains details of experiments done on the stage. The first series of tests were done to determine the efficiency of the floating-piston expander. Due to limitations of the flow-meter, the results were not deemed to be accurate. The stage was then run as a refrigerator with zero heat-load. Along the way, certain design problems were identified and rectified.

It was observed that the quasi-static models did not adequately describe the performance of the expander as most of the processes did not go to equilibrium. Therefore, these models were improved by incorporating the dynamics of the piston motion, the fluid flow through the warm and cold volumes, and the fluid flow through the high-pressure passages of the heat exchanger. These models, explained in Chapter 6, gave some insights into the operation of the expander and were used to suggest design modifications to the stage to ensure better performance.

CHAPTER 2 – STATIC MODELLING OF THE FLOATING PISTON EXPANDER

A schematic of the expander system is shown in Figure 2.1. A piston without any linkages "floats" between the cold and warm volumes in the cylinder. The cold end valves control the flow of high-pressure gas into and low-pressure gas out of the cold volume. The warm volume is connected to four intermediate pressure reservoirs A, B, C and D ($P_A > P_B > P_C > P_D$) through the warm end valves V_1, V_2, V_3 and V_4 respectively. The throttling of gas into and out of the warm volume controls the motion of the piston.

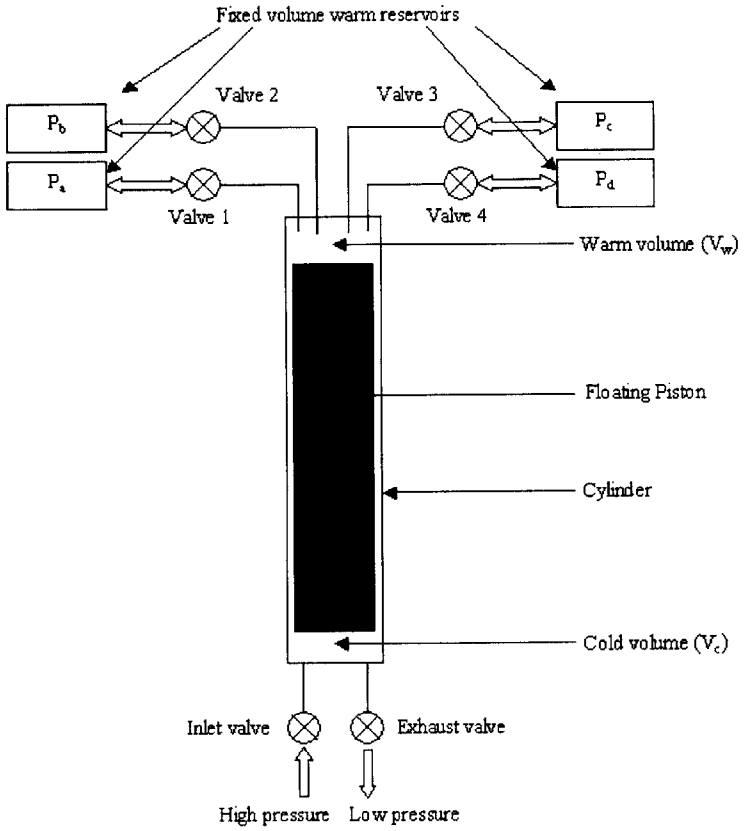

Figure 2.1: Schematic of Floating-Piston Expander

In order to determine appropriate operational parameters for control of the floating piston expander, models were developed for all the processes that made up one expander cycle. The models assumed the working fluid to be an ideal gas. It was assumed that all the processes went to equilibrium. Since the piston freely floats between the warm and cold volumes, it was also assumed that the pressure in both volumes was equal except when the piston was flush against the top or the bottom of the cylinder.

2.1 Expander Cycle

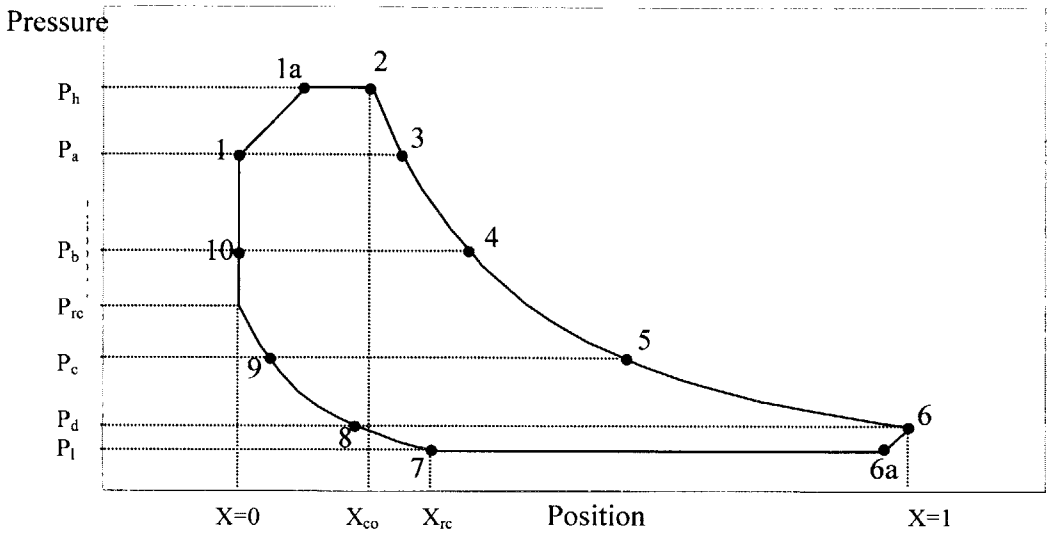

Figure 2.2: Pressure-Position diagram for the expander cycle

The warm-end-pressure – piston-position diagram for the gas is shown in Figure 2.2. The cycle starts at State 1, with the piston in its bottommost position (X = 0). In an ideal cylinder, this would correspond to zero volume in the cold end. However, there is always a dead volume associated with a piston-cylinder arrangement. At State 1, the pressure in the warm volume is equal to the pressure in reservoir A. At this point, all valves are closed. The expander goes through the following processes:

Process 1-1a (Blow-in): The inlet valve is opened. Helium at the cycle high pressure (P_h) enters the cold volume. The piston moves up, compressing the gas in the warm volume. The process stops when the pressure in the cylinder reaches P_h.

Process 1a-2 (Intake): The inlet valve is kept open and the warm end valve V_1 (leading to reservoir A) is opened. Helium flows from the warm volume into reservoir A. High pressure helium continues to flow into the cold volume, maintaining the pressure inside the cylinder at P_h. When the piston has reached a cut-off position X_{co}, the inlet valve is closed.

Process 2-3 (First expansion): The warm valve V_1 is kept open. Helium from the warm volume flows into reservoir A. The pressure in the cylinder decreases. The helium in the cold volume expands so that the pressure in the cold end matches the pressure in the warm end. When the pressure in the cylinder falls to P_a, valve V_1 is closed.

Process 3-4 (Second expansion): The warm valve V_2 is opened. Helium now flows from the warm volume into reservoir B. The helium in the cold volume expands further. This process continues until the pressure in the cylinder reaches P_b, at which point valve V_2 is closed.

Process 4-5 (Third expansion): Warm valve V_3 is opened. Helium flows from the warm volume into reservoir C, while the helium in the cold volume expands. V_3 is closed when the pressure in the cylinder equals P_c.

Pressure 5-6 (Fourth expansion): Warm valve V_4 is opened. Helium flows from the warm volume into reservoir D. The helium in the cold volume continues to expand. V_4 is closed when the cylinder pressure equals P_d. In an ideal expander cycle, the pressure in reservoir D is maintained at a level which ensures that the piston reaches the topmost position (X = 1) just as the pressure reaches P_d.

Process 6-6a (Blow-out): The exhaust valve is opened. Because the pressure in the cylinder (P_d) is greater than the outlet pressure (P_l), helium from the cold volume flows through the exhaust valve. The pressure in the cylinder falls, and the helium in the warm volume begins to expand. This process continues until the pressure in the cylinder equals P_l.

Process 6a-7 (Exhaust): The exhaust valve is kept open, and the warm valve V_4 is opened. Helium from reservoir D (at a pressure P_d) flows into the warm volume. The piston moves downwards, forcing the helium in the cold volume out through the exhaust valve. Throughout this process, the pressure in the cylinder stays at P_l. This process continues till the piston has reached the recompression position X_{rc}, at which point the exhaust valve is closed.

Process 7-8 (First recompression): Valve V_4 is kept open. Helium from reservoir D continues to flow inside the warm volume. The piston moves down, compressing the helium in the cold volume. The process continues until the pressure in the cylinder equals P_d. At this point, V_4 is closed.

Process 8-9 (Second recompression): Warm valve V_3 is opened and helium from reservoir C enters the warm volume. The piston moves down and the pressure in the cylinder rises to P_c, at which point V_3 is closed.

Process 9-10 (Third recompression): Warm valve V_2 is opened and helium from reservoir B enters the warm volume until the cylinder pressure reaches P_b. V_2 is closed at the end of the process.

Process 10-1 (Fourth recompression): Valve V_1 is opened and helium from reservoir A enters the warm volume. The pressure inside the cylinder rises to P_a, at which point the valve is closed and the cycle is repeated.

It is possible that the piston will reach the bottom dead centre at some point during one of the four recompression processes. If this happens, the pressure in the cold volume will not change until Process 1-1a begins. The pressure in the warm volume will continue to increase as described above. Thus there will be a pressure differential across the piston until the cycle reaches state 1.

2.2 Modelling of Processes

In order to evaluate the temperature, pressure, volume and mass in the warm and cold volumes at every state, thermodynamic models of each process were developed. The properties of each state were determined in terms of the properties of the preceding state.

Process 1-1a: The pressure in both the warm and cold regions at State 1a is P_h. The remaining properties of the gas in the warm region at State 1a were determined by modelling the warm region as a fixed mass going through an isentropic compression. The cold displacement volume was modelled as an open system with perfect mixing, ensuring a uniform temperature. The gas entering the cold volume was assumed to be at a constant intake temperature (T_{in}). The work done by the cold volume was assumed to be equal to the work done on the warm volume. As the sum of the warm and cold volumes in the cylinder is a constant, the cold volume was calculated by subtracting the warm volume from the total volume, which was the sum of the swept volume, the cold end clearance volume and the warm end clearance volume. The temperature and mass were determined from the First Law for the open system.

First Law for an open system (neglecting changes in K.E. and P.E.):

$$\frac{dE}{dt} = \dot{Q} - \dot{W} + \dot{m}(h_{in} - h_{out}) \qquad \ldots(2.1)$$

Integrating this equation for the cold volume over the process 1-1a,

$$(m_{1a}T_{1a} - m_1T_1)_{cold}C_v = -W_{cold} + (m_{1a} - m_1)_{cold}C_pT_{in} \qquad \ldots(2.2)$$

The expression for the work is given by $W_{cold} = -W_{warm} = \dfrac{(P_1V_1 - P_{1a}V_{1a})_{warm}}{\gamma - 1}$ $\ldots(2.3)$

Substituting the work into Eq. 2.2,

$$m_{1a,cold} = \left(\frac{(P_{1a}V_{1a} - P_1V_1)_{cold}C_v}{R} + \frac{(P_{1a}V_{1a} - P_1V_1)_{warm}}{\gamma - 1}\right)\frac{1}{C_pT_{in}} + m_{1,cold} \qquad \ldots(2.4)$$

$$m_{1a,cold} = \left(\frac{(P_{1a}V_{1a} - P_1V_1)_{cold} + (P_{1a}V_{1a} - P_1V_1)_{warm}}{\gamma R}\right)\frac{1}{T_{in}} + m_{1,cold} \qquad \ldots(2.5)$$

Process 1a-2: The pressure in both the warm and cold regions at State 2 is P_h. The cold volume at state 2 is V_{co} (the cut-off position times the piston area) + $V_{c,cl}$ (cold end clearance volume). The warm volume was obtained by subtracting this from the total volume. The temperature and mass of the cold region were determined by modelling the cold region as an open system, as in Process 1-1a, but with the additional condition of it being at constant pressure. The warm displacement volume was modelled as an open system at a constant pressure and no entropy generation. A second law analysis of the mass left in the warm region at State 2 showed that the temperature also stayed the same. Hence the mass ratio from State 1a to 2 equalled the volume ratio.

Integrating the First Law equation for the cold volume over the process 1a-2,

$$(m_2T_2 - m_{1a}T_{1a})_{cold}C_v = -W_{cold} + (m_2 - m_{1a})_{cold}C_pT_{in} \qquad \ldots(2.6)$$

$$(m_2T_2 - m_{1a}T_{1a})_{cold}C_v = -P_h(V_2 - V_{1a})_{cold} + (m_2 - m_{1a})_{cold}C_pT_{in} \quad \ldots(2.7)$$

$$(P_2V_2 - P_{1a}V_{1a})_{cold}\frac{C_v}{R} + P_h(V_2 - V_{1a})_{cold} = (m_2 - m_{1a})_{cold}C_pT_{in} \quad \ldots(2.8)$$

$$m_{2,cold} = \frac{(P_2V_2 - P_{1a}V_{1a})_{cold}}{RT_{in}} - m_{1a,cold} \quad \ldots(2.9)$$

The Second Law equation for the mass staying in the warm volume over the process 1a-2:

$$dS = C_p \ln\frac{T_2}{T_{1a}} - R\ln\frac{P_2}{P_{1a}} = 0 \quad \ldots(2.10)$$

Since $P_{2,warm} = P_{1a,warm}$, $T_{2,warm} = T_{1a,warm}$

Process 2-3: The pressure in both the warm and cold regions at State 3 is P_a. The remaining properties of the cold region were determined by modelling the cold region as a fixed mass undergoing an isentropic expansion. The warm volume was calculated by subtracting the cold volume from the total volume. The temperature and mass of the warm region at State 3 were calculated by modelling the mass of gas left in the warm region at State 3 as having undergone an isentropic expansion, since it is assumed that the process occurs quickly enough that there is no heat transfer between the gas and the walls.

For the warm volume, $P_2V_2 = m_2RT_2$ and $P_3V_3 = m_3RT_3$

From the Second Law, $P_2^{1-\gamma}T_2^{\gamma} = P_3^{1-\gamma}T_3^{\gamma}$

$$m_{3,warm} = \left(\frac{P_3V_3}{RT_3}\right)_{warm} = \left(\frac{P_3V_3}{RT_2}\left(\frac{P_3}{P_2}\right)^{\frac{1-\gamma}{\gamma}}\right)_{warm} = \left(\frac{P_2V_3}{RT_2}\left(\frac{P_3}{P_2}\right)^{\frac{1}{\gamma}}\right)_{warm} \quad \ldots(2.11)$$

Equations for Processes 3-4, 4-5 and 5-6 were determined in the same way as for Process 2-3. The pressures at States 4, 5 and 6 are P_b, P_c and P_d respectively.

Process 6-6a: The pressure at State 6a is equal to P_l. The warm region was modelled as a fixed mass going through an isentropic expansion. The cold volume was calculated from the known warm volume. The mass of gas left in the cold region at State 6a was modelled as having undergone an isentropic expansion (the same model as that used for the gas left in the warm volume during the expansion processes). The temperature and mass of the gas leaving the cold region were obtained from the open system First Law equation for the cold volume.

Process 6a-7: The pressure at State 7 is equal to P_l. The cold volume at State 7 is equal to V_{rc} (the recompression position times the piston area) + $V_{c,cl}$. The analysis for the Process 6a-7 required to get the temperatures and masses in the warm and cold regions was very similar to that for the Process 1a-2, the only difference being that the cold region model for Process 1a-2 was equivalent to the warm region model for Process 6a-7 and vice versa.

In order to determine the remaining states, a recompression pressure P_{rc} was calculated. This pressure was equal to the pressure of the cold region if it was allowed to expand isentropically from the volume at state 7 to the minimum volume $V_{c,cl}$.

The analysis for the remaining processes required to get the temperatures and masses in the warm and cold volumes was very similar to that for the Process 1-1a. The cold region model for Process 1-1a was equivalent to the warm region models for these processes.

Process 7-8: The warm volume pressure at State 8 is P_d. The cold volume pressure at this state is equal to the minimum of P_d and P_{rc}. If P_{rc} is less than P_d, it indicates that the piston is at the lowest possible position and the gas in the cold volume cannot be compressed further. The cold volume properties were determined by modelling it as a fixed mass undergoing an isentropic compression from P_7 to P_8. The warm volume was modelled as an open system with perfect mixing, ensuring a uniform temperature. The warm volume work was calculated from the cold volume work, which was equal and opposite.

Process 8-9: The warm volume pressure at State 9 is P_c. If the piston is already at the lowest position, the cold end properties do not change; if not, the cold volume pressure is equal to the minimum of P_c and P_{rc}, and the rest of the analysis is identical to that for the previous process. The warm volume equations are similar to those for determining State 8.

Equations for Processes 9-10 and 10-1 were determined in the same way as for Process 8-9. The warm end pressures at States 10 and 1 are P_b and P_a respectively.

The equations described above are listed in Appendix A. These equations are based on a non-dimensional form of the ideal gas law $PV=mRT$. The ideal gas equation is written in the form $P^*X^*=m^*T^*$, where P^* is a non-dimensional temperature, X^* is the non-dimensional position variable which can be used in place of the volume as the cross-sectional area of the piston is uniform ($X^* = 0$ corresponds to the lowest piston position and $X^* = 1$ corresponds to the highest piston position), m^* is a non-dimensional mass and T^* is a non-dimensional temperature. For each stage, three equations are specified; the fourth unknown can be determined from $P^*X^*=m^*T^*$.

2.3 Steady State Operation of the Expander

For steady state operation of the expander, there must not be any net flow of mass into or out of any of the four reservoirs. This is needed to ensure that each of the reservoirs stay at the same pressure throughout the operation. The cycle high and low pressures as well as the cold end and warm end clearance volumes do not change. If the cut-off and recompression volumes are kept at a constant level, the cycle will consistently repeat itself.

The solution of the equations described in the previous section depends on the values of six controllable parameters - the pressures in each of the reservoirs, the cut-off volume and the recompression volume.

Since the total mass of the gas in the four reservoirs and the warm volume is fixed, setting the net mass flow equal to zero for any three of the reservoirs will ensure that the net mass flow is equal to zero for the fourth reservoir, since the warm volume returns to the same initial state after every cycle. Thus, three constraints are required to ensure steady state operation

2.3.1 Ideal cycles

In the ideal expander cycle, the piston reaches the topmost position at the same time that the pressure in the cylinder equals the pressure in reservoir D. This leads to an additional constraint.

While there were six parameters, there were only four constraints for an ideal expander cycle in steady state. Therefore, the values of the cut-off and recompression volumes were fixed and the equations were solved to get values of the four reservoir pressures. This was done for different values of pressure of the inlet stream.

The system of equations was solved by entering the equations into an MS Excel worksheet and using the Excel solver. Fig. 2.3 shows a screenshot of the Excel worksheet. The solver solves for the following:

- the warm volume properties at each of the states 1 through 10
- the cold volume properties at each of the states 1 through 7, as well as the pressure, temperature and mass of gas in the cold volume when the piston reaches the bottom dead centre
- the pressures in each of the four reservoirs

The solver required an initial guess to get started. In order to get a solution that made physical sense, the initial values had to be reasonably close to the final result. It took a few iterations to come up with the solution the first time the solver was used. Once the first feasible solution was obtained, it was used as the initial guess for all the solver runs that followed. Surprisingly, Excel did a pretty good (read quick) job of coming up with the solution.

A solution does not exist for all values of cut-off and recompression volumes. It was observed that while solutions could be found for a large range of recompression volumes, the corresponding range for cut-off volumes was a lot smaller.

The lower and upper limits on the cut-off volume were obtained by solving the set of equations as an optimisation problem. The lower limit was obtained by defining the objective function of the optimisation problem as the minimum of the cut-off volume subject to all the equations and constraints defined above. The upper limit was obtained by defining the objective function of the problem as the maximum of the cut-off volume subject to all the equations and constraints defined above. The range of feasible cut-off volumes for an expander operating at a specified pressure ratio are given in Table 2.1. All volumes in the table are expressed as a fraction of the swept volume. It was ensured the recompression volume had a value of at least 0.1 in all cases.

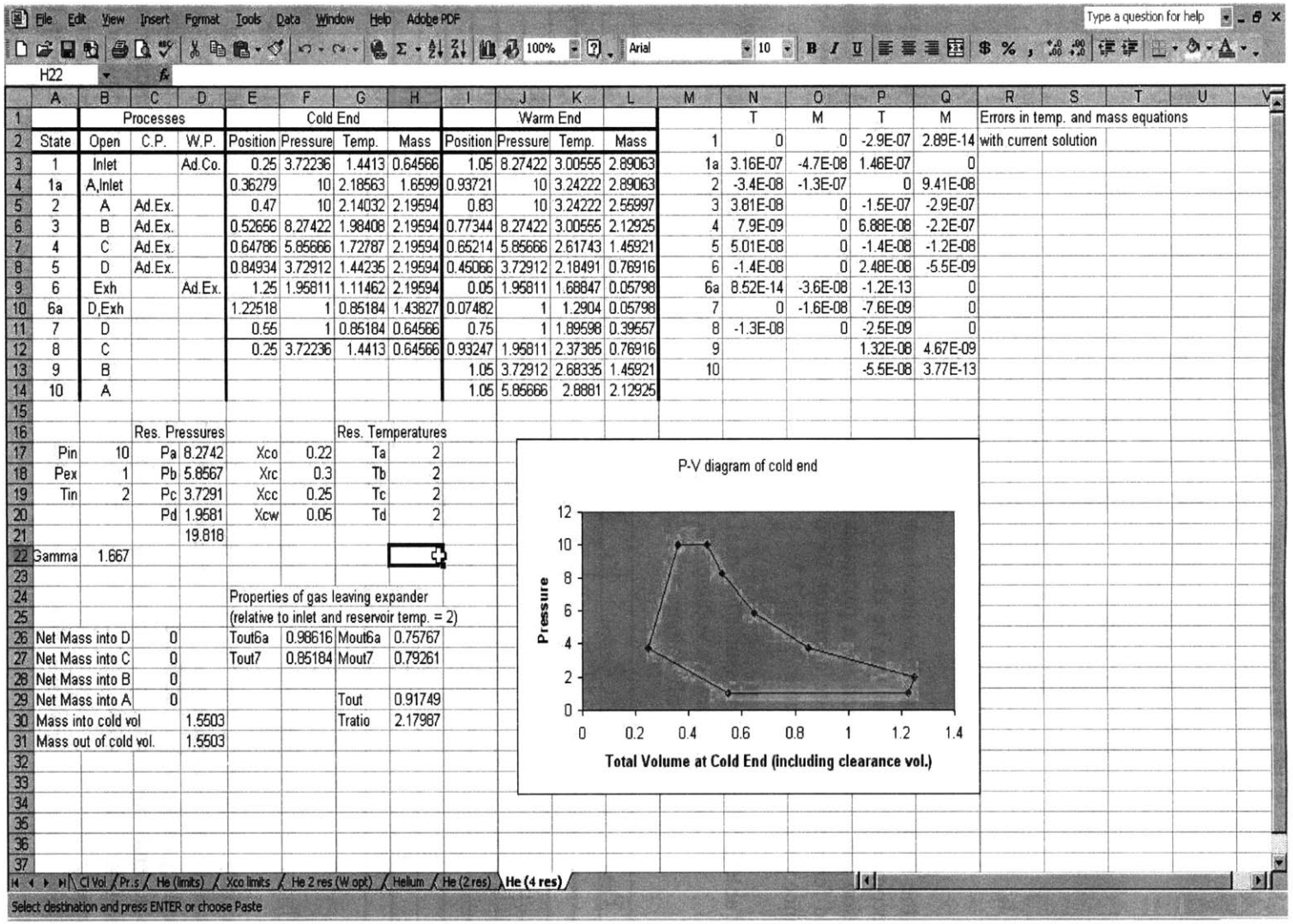

	A	B	C	D	E	F	G	H	I	J	K	L	M	N	O	P	Q	R	S	T	U
1		Processes				Cold End				Warm End				T	M	T	M	Errors in temp. and mass equations			
2	State	Open	C.P.	W.P.	Position	Pressure	Temp.	Mass	Position	Pressure	Temp.	Mass	1	0	0	-2.9E-07	2.89E-14	with current solution			
3	1	Inlet		Ad.Co.	0.25	3.72236	1.4413	0.64566	1.05	8.27422	3.00555	2.89063	1a	3.16E-07	-4.7E-08	1.46E-07	0				
4	1a	A,Inlet			0.36279	10	2.18563	1.6599	0.93721	10	3.24222	2.89063	2	-3.4E-08	-1.3E-07	0	9.41E-08				
5	2	A	Ad.Ex.		0.47	10	2.14032	2.19594	0.83	10	3.24222	2.55997	3	3.81E-08	0	-1.5E-07	-2.9E-07				
6	3	B	Ad.Ex.		0.52656	8.27422	1.98408	2.19594	0.77344	8.27422	3.00555	2.12925	4	7.9E-09	0	6.88E-08	-2.2E-07				
7	4	C	Ad.Ex.		0.64786	5.85666	1.72787	2.19594	0.65214	5.85666	2.61743	1.45921	5	5.01E-08	0	-1.4E-08	-1.2E-08				
8	5	D	Ad.Ex.		0.84934	3.72912	1.44235	2.19594	0.45066	3.72912	2.18491	0.76916	6	-1.4E-08	0	2.48E-08	-5.5E-09				
9	6	Exh		Ad.Ex.	1.25	1.95811	1.11462	2.19594	0.05	1.95811	1.68847	0.05798	6a	8.52E-14	-3.6E-08	-1.2E-13	0				
10	6a	D,Exh			1.22518	1	0.85184	1.43827	0.07482	1	1.2904	0.05798	7	0	-1.6E-08	-7.6E-09	0				
11	7	D			0.55	1	0.85184	0.64566	0.75	1	1.89598	0.39557	8	-1.3E-08	0	-2.5E-09	0				
12	8	C			0.25	3.72236	1.4413	0.64566	0.93247	1.95811	2.37385	0.76916	9			1.32E-08	4.67E-09				
13	9	B							1.05	3.72912	2.68335	1.45921	10			-5.5E-08	3.77E-13				
14	10	A							1.05	5.85666	2.8881	2.12925									
15																					
16			Res. Pressures				Res. Temperatures														
17	Pin	10	Pa	8.2742	Xco	0.22	Ta	2													
18	Pex	1	Pb	5.8567	Xrc	0.3	Tb	2													
19	Tin	2	Pc	3.7291	Xcc	0.25	Tc	2													
20			Pd	1.9581	Xcw	0.05	Td	2													
21				19.818																	
22	Gamma	1.667																			
23																					
24					Properties of gas leaving expander																
25					(relative to inlet and reservoir temp. = 2)																
26	Net Mass into D	0			Tout6a	0.98616	Mout6a	0.75767													
27	Net Mass into C	0			Tout7	0.85184	Mout7	0.79261													
28	Net Mass into B	0																			
29	Net Mass into A	0					Tout	0.91749													
30	Mass into cold vol			1.5503			Tratio	2.17987													
31	Mass out of cold vol.			1.5503																	

Figure 2.3: Excel Worksheet

Table 2.1: Limits for cut-off volumes (Working fluid: Helium)
(Cold end clearance volume = 0.25, Warm end clearance volume = 0.05)

P_{inlet}/P_{outlet}	Minimum Cut-Off Volume X_{co}	Maximum Cut-Off Volume X_{co}
15	0.194	0.321
14	0.183	0.328
13	0.182	0.332
12	0.182	0.332
11	0.181	0.331
10	0.179	0.331
9	0.178	0.33

Once the limits for the cut-off volume have been determined, appropriate values of the cut-off and recompression volumes can be chosen and the reservoir pressures required for steady state operation can be determined for a particular value of the inlet pressure. The reservoir pressures needed for ideal steady-state operation for a particular set of values of cold-end and warm-end clearance volumes are given in Table 2.2.

Table 2.2: Reservoir pressures for ideal steady-state operation (Working fluid: Helium)
(Cold end clearance volume = 0.25, Warm end clearance volume = 0.05)
(Cut-off volume = 0.22, Recompression volume = 0.3)

P_{inlet}/P_{outlet}	P_A/P_{outlet}	P_B/P_{outlet}	P_C/P_{outlet}	P_D/P_{outlet}
15	12.28	8.75	5.74	2.94
14	11.48	8.17	5.34	2.74
13	10.68	7.59	4.93	2.55
12	9.88	7.01	4.53	2.35
11	9.07	6.43	4.13	2.15
10	8.27	5.86	3.73	1.96
9	7.40	5.20	3.33	1.76
8	6.53	4.55	2.94	1.57
7	5.66	3.89	2.55	1.37

2.3.2 Incorporation of non-ideal behaviour into the model

In the ideal expander cycle, the piston reaches the topmost position at the same time that the pressure in the cylinder equals the pressure in reservoir D. This may not always be the case. Depending on the values of the cut-off volume and the pressure in reservoir D, the pressure in the cold end may equal the pressure in reservoir D at a position below the topmost piston position. It is also possible that the pressure in the cold end may not have dropped down to the pressure in reservoir D even though the piston has reached the topmost position. The equations described above will hold true for the first case, but a slight modification has to be made in the equations used to calculate states 3 through 6 in order to incorporate the second case.

The position of the piston at states 3 through 6 was previously calculated by modelling the gas in the cold region as undergoing an adiabatic expansion. In this modified model, the position of the

piston is the minimum of the value calculated from the adiabatic expansion model and the topmost position possible. The pressure in the cold end is then calculated from the pressure-volume relation for an adiabatic process. The equations used to calculate the properties of the warm end stay the same. The modified equations for the cold end are listed in Appendix A3.

The solution technique for a non-ideal cycle is quite similar to that for an ideal cycle. The only difference is that since the piston does not reach the topmost position at the same time that the pressure in the cylinder equals the pressure in reservoir D, there is one less constraint than in the ideal case. This allows one of the four reservoir pressures to be arbitrarily fixed. However, solutions do not exist for all values of reservoir pressures. Therefore, additional inequality constraints need to be added to ensure that physically impossible solutions are not obtained.

2.4 Cycle Stability

It would have proven difficult to ensure that the pressures in the reservoirs at the warm end were identical to the theoretical values required for steady state. It was, therefore, important to study the behaviour of the expander and to ensure that it did not become unstable when these pressures were not exact.

The Excel worksheet developed to analyse the stability of the cycle differed from the previous one in one major way. While the steady-state worksheet solved a set of non-linear equations simultaneously to determine the solution, the cycle-stability worksheet converged to a solution by iterating over a number of expander cycles. A set of initial conditions in the expander – state 1 of the steady-state solution of the expander cycle for the same cut-off and recompression volumes – was entered. The initial reservoir pressures were given values that were slightly different from the values required for steady-state operation. Each expander state was calculated from the previous state using the equations developed earlier. After an entire expander cycle was completed, the reservoir pressures were updated. The first state of the next cycle was calculated from the last state of the previous cycle. The process continued until the changes in pressure of each reservoir over an expander cycle became negligibly small.

In order to do this transient analysis, the pressure in each reservoir was calculated at the end of every expander cycle. This was done by calculating the change in the mass of each reservoir over an expander cycle. The change of mass calculation over one process during which a particular reservoir is open is described in Appendix B. In every expander cycle, reservoirs A and D are open through three processes (1a-2, 2-3 and 10-1 for A; 5-6, 6a-7 and 7-8 for D), while reservoirs B and C are open through two processes (3-4 and 9-10 for B; 4-5 and 8-9 for C). The overall change in mass of gas in a particular reservoir is equal to the sum of changes over all the processes during which that particular reservoir is open.

It was observed that if the reservoir pressures were not identical to their theoretical values for an ideal cycle, the system adjusted the warm end pressures so that a steady state was ultimately obtained. It was also observed that no matter what the individual reservoir pressures were, the system came to the same steady state if the sum of the pressures in the four reservoirs was the same. An example is shown in Appendix C.

This result led to an important conclusion. All the four reservoirs have the same volume and are at the same temperature. Hence, the constant of proportionality relating the pressure to the mass is the same for all the reservoirs.

$P_a=Km_a$ $P_b=Km_b$ $P_c=Km_c$ $P_d=Km_d$

Hence the total mass in the warm end (assuming negligible mass in the warm end of the expander, which has a much smaller volume than the reservoirs) is directly proportional to the sum of the pressures in the four reservoirs.

$$m_{total,warm} \propto P_a + P_b + P_c + P_d$$

Thus it can be concluded that the only independent variables which affect the steady state operating conditions are the cut-off volume, the recompression volume and the mass in the warm end. If the difference between the actual and theoretical warm end masses is not much, the cycle operates at conditions very close to the ideal operating conditions, i.e., either the piston is nearly at its topmost position at state 6 (if the actual mass is a little lower than the theoretical mass), or the pressure in the cold end has nearly dropped down to the pressure in D when the piston reaches the topmost position (if the actual mass is a little higher than the theoretical mass). If there is a significant difference between the actual and theoretical values, a steady state will still be obtained, but the cycle will operate at conditions that are quite different from the ideal operating conditions.

The program developed to study cycle stability converges to the non-ideal steady-state solution (described in the previous section) after a large number of iterations if all operating parameters are kept the same. This is expected as these are different approaches to the same problem. In the non-ideal steady-state case, a solution is obtained by solving simultaneous non-linear equations and by specifying one particular reservoir pressure, while the cycle-stability program converges towards the solution by specifying the sum total of the reservoir pressures. In essence, the iteration is done automatically by Excel in the steady-state worksheet, and manually by the user in the cycle-stability worksheet.

2.5 Transient Operation

If there is a change in the inlet high pressure, the pressures in the four reservoirs at the warm end must be adjusted. From the solution of the ideal cycle at various values of the inlet pressure, it was seen that the mass required in the warm end for ideal steady-state operation increases linearly with the inlet pressure over the range of operation of the cryocooler.

From the stability analysis, it was seen that the steady state operating conditions were a function only of the total mass in the warm end and not of the individual reservoir pressures. Therefore, the pressures in the four reservoirs can be adjusted just by increasing or decreasing the mass in one of the reservoirs. This makes it very convenient to tune the cycle while it is running. Over a number of expander cycles, this mass will redistribute itself over all the four reservoirs. It is important, however, to ensure that during the process of redistribution, the expander does not go

through a state which causes it to stop. Thus, the effect of changing the mass in a particular reservoir on the expander performance was studied for all the four reservoirs at the warm end.

The program used to study transient analysis was the same as that used for analysis of cycle stability, except for one modification. Depending on an expected value of rate of cycle-high-pressure increase, the required rate of change in warm-reservoir-mass was calculated. After every five cycles, the inlet pressure was updated and the mass of reservoir A was increased by the amount calculated above. There was one constraint – since the extra mass would come from the compressor, the pressure in A could not exceed the cycle high pressure. The program was kept running until the cycle constraints were violated or the cycle had achieved a new equilibrium (this was an indication that the expander would not stop).

This experiment was repeated for reservoirs B, C and D. After this transient analysis for an increasing inlet pressure was complete, the experiment was repeated for reservoirs A, B, C and D while the inlet pressure decreased.

It was found that neither taking mass out of reservoir A when the inlet pressure was decreasing nor putting mass into A when the inlet pressure was increasing caused any problems. However, putting mass into A drove its pressure very close to the cycle high pressure. In a real machine, the low pressure differential would slow the intake stroke down considerably.

In the case of reservoir B, neither taking mass out when the inlet pressure was decreasing nor putting mass in when the inlet pressure was increasing created any significant problems. When the inlet pressure was falling sharply, taking mass out of reservoir A was a better option than taking mass out of B, as in the latter case, the decrease in mass in A took some time and caused the inlet pressure to fall below the pressure in reservoir A.

Taking mass out of C when the inlet pressure was decreasing caused the cycle to stop, because the decrease in mass in reservoir A took a long time, which led to inlet pressure falling below the pressure in reservoir A. However, putting mass into reservoir C when the inlet pressure was increasing did not present any problems.

An analysis of reservoir D showed that the cycle encountered problems in both cases – decreasing inlet pressure and increasing inlet pressure. When mass was taken out of D, the decrease in mass of reservoir A was not fast enough to keep the pressure in reservoir A below the falling inlet pressure. When mass was put into D, the increase in the pressure of reservoir D caused too much blow-out.

Therefore, it was concluded that in the case of decreasing inlet pressures, mass should be taken out of reservoir A, while in the case of increasing inlet pressures, the extra mass could be put into either reservoir B or reservoir C. If the extra mass was put into reservoir B, the pressure of reservoir D during the transient region was less than the ideal value. Consequently, even though the piston would make a full stroke, the low pressure differential between reservoir D and the outlet pressure would be quite low and hence blow-out would take longer. On the other hand, if the extra mass was put into reservoir C, the pressure of reservoir D during the transient region

was more than the ideal value. Therefore, the piston would not make a full stroke during this time.

2.6 Warm-End Bleed

In order to reduce the extent of the blow-in and blow-out processes, both of which are highly irreversible, it is important that the pressure in reservoir A be reasonably close to the high-pressure and the pressure in reservoir D be close to the low-pressure. During early experiments, it was found that the warm end settled down to an equilibrium where this was not the case. This happened even though the expander model indicated that it was possible to run cycles with a relatively high pressure in A and low pressure in D.

It was decided to bleed high-pressure gas into reservoir A and bleed gas from reservoir D to the low-pressure side to remedy the problem. This configuration represents a hybrid of the "closed" warm-end configuration modelled so far and a previously suggested open configuration, in which the high-pressure and low-pressure lines connect directly to the warm volume (Figure 2.4)

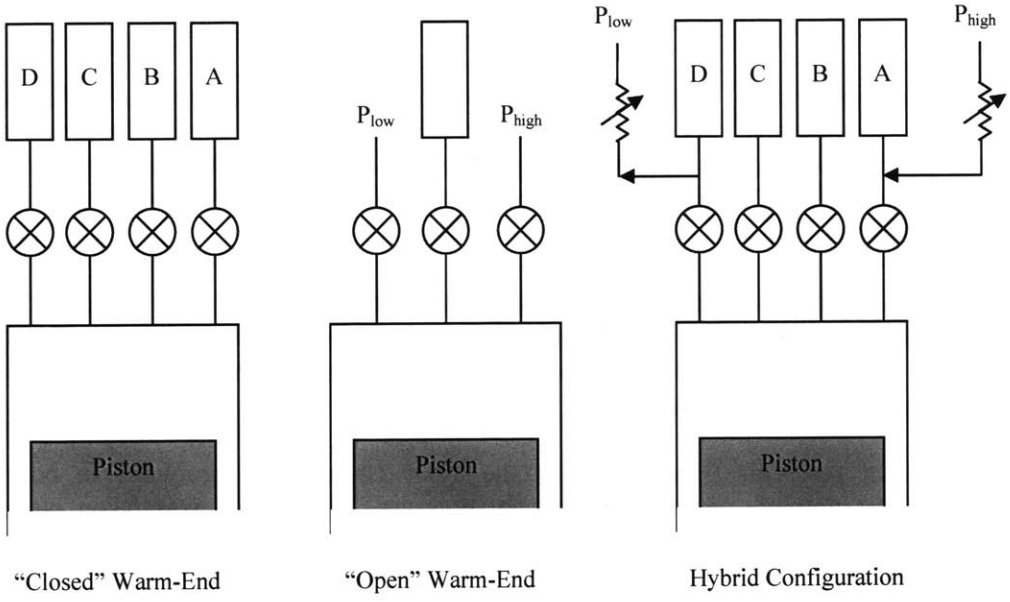

Figure 2.4: Warm End Configurations

The models developed were modified to determine whether this configuration was stable. The pressures in A and D were no longer determined by the system of equations, but were pre-specified. The constraints of there being no net flow out of reservoirs A and D were removed. It was found that the system of equations did have a solution in which the bleed flow into A equalled the bleed flow out of D. The net mass flow out of A during a single cycle was balanced by the bleed flow into A; therefore, at steady state, the pressure in A was the same at the beginning of every cycle. Similarly, the pressure in D was the same at the beginning of every

cycle. The steady state solution indicated that the hybrid configuration would work. When implemented, it was found that the hybrid configuration did work and allowed much better control of the pressures in reservoirs A and D.

The throttle valves perform another useful function – they automatically adjust the mass of gas in the warm end if the compressor pressure changes. If there is an increase in the high-pressure, the flow into A increases. As the bleed flow out of D stays the same initially, there is a net increase in mass in the warm end. This continues until the redistribution of mass in the warm end balances the two bleed flows. Similarly, a drop in the high-pressure leads to a drop in mass in the warm end.

Even though experiments showed that the static models did not accurately describe the performance of the expander, the models served several significant purposes. They helped in an understanding of the operation of the expander. The parameter values that were determined were reasonably accurate and proved to be helpful in tuning the expander, both during setup and operation. In addition, the equations developed for use in the static model were used in a later expander model which included the dynamics of the fluid flow and the motion of the piston.

CHAPTER 3 – EXPERIMENTAL APPARATUS

3.1 A Description of the Cold End of the Expander

The cold end of the prototype expander used in this test rig is based on the design developed by Traum[5] in 2003. The detailed mechanical design was done by C.L.Hannon and the fabrication done at AMTI. A few modifications were made to the design, all of which were done to improve sealing. A schematic of the cold end is shown in Figure 3.1.

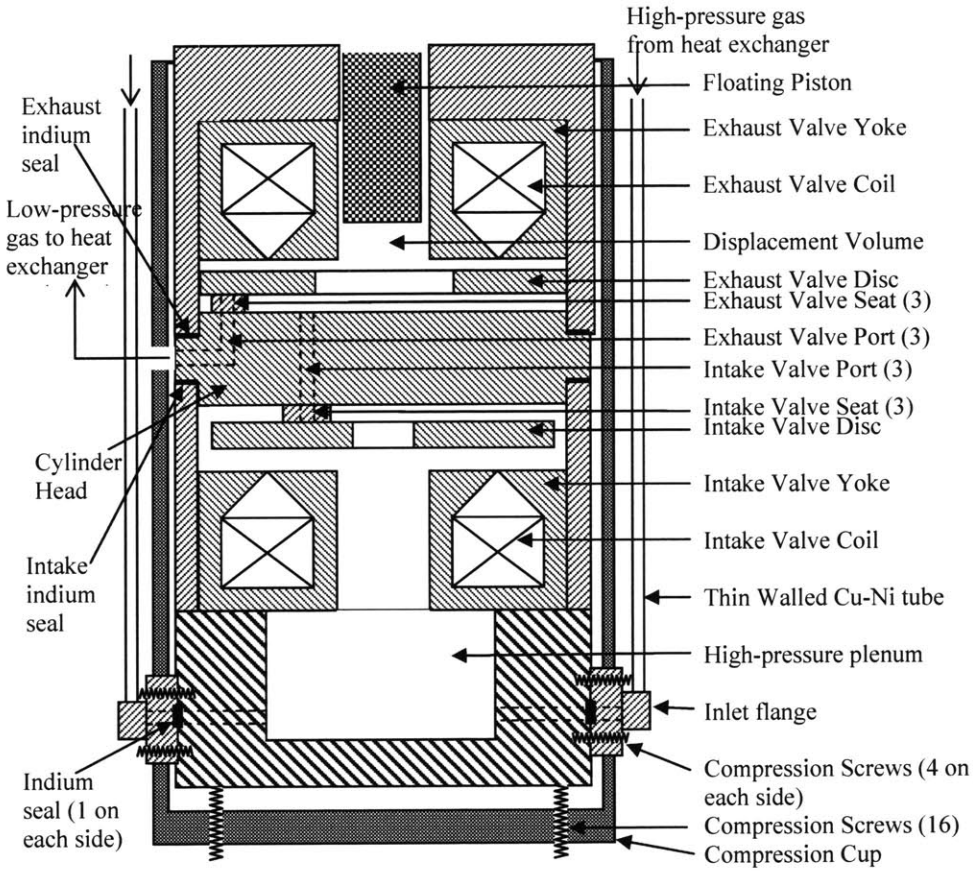

Figure 3.1: Expander Cold End

3.1.1 Electromagnetic Valves

At the heart of the cryocooler design lie the smart electromagnetic valves which control the flow into and out of the cold volume. Electromagnetic valves score over mechanically actuated valves in two important ways. They eliminate the need for mechanical linkages, and hence have lower dissipation rates. Secondly, the valve timing can be modified according to operational requirements. Therefore, the cycle can be run optimally at conditions other than the design operating condition. These valves basically replace mechanical complexity with electrical complexity, which is a lot easier to handle.

The valve actuating mechanism consists of an electromagnetic valve, a valve disc and a set of permanent magnets embedded in the cylinder head. The valve disc is held down against three valve seats on the cylinder head by the magnetic field of the permanent magnets. When the valve is to be opened, a current is passed through the electromagnetic valve coil. The magnetic field generated pulls the valve disc off the valve seats, and gas is free to flow through the valve ports. When the valve is to be closed, the current is turned off and the disc springs back onto the valve seats due to the attractive force of the permanent magnets.

The electromagnetic valves were designed by Traum[5] using the QuickField finite element package. As there were a number of geometric parameters which dictated the performance of the valve, an evolutionary design procedure was employed, wherein the parameters were modified in the order of their perceived importance to valve performance. The valves were then tested to verify that they would generate the required amount of force for opening.

The valves were manufactured from ferromagnetic 430 stainless steel. They consist of a mandrel, around which copper wire is coiled, and a cover, which fits over the mandrel-coil assembly. The entire assembly was potted with Stycast 2850 epoxy to fill up the void spaces. The valve discs were also made of 430 stainless steel. They were lapped to an optical flat surface with 1 micron alumina grit and polished to a mirror finish.

The valve discs seal against Kel-F seats epoxied to the cylinder head. The intake ports consist of three through-holes in the cylinder head. The exhaust ports are L-shaped and go from the exhaust face of the cylinder head to the periphery. Eighteen permanent magnets are epoxied into recesses in both faces of the cylinder head. As the intake Kel-F seats are located near the centre of the disc, three additional Kel-F bumpers are epoxied on the intake face near the periphery to prevent the intake disc from cocking. The bumpers are lapped to a height about 0.001 inches lower than the valve seats. The valve seats are themselves lapped with 1 micron alumina grit. The reason for choosing three valve ports was that if there were more than three ports, it would be difficult to ensure that all the seats lay in a single plane, which would lead to sealing problems.

In order to minimise the Joule heating in the valve coils, two different current levels are used. When the disk is flush against the valve seats on the cylinder head, the gas pressure and the permanent magnet force both need to be overcome in order to lift the disc. Once the disc has been separated from the seats, there is no differential gas pressure across it. The permanent magnet force also decreases since the distance between the magnets and the discs increases. Therefore, a smaller magnetic force is needed to keep the disc open. In addition, a smaller current is required to generate the required magnetic field since the air gap between the disc and the valve yoke is smaller. Hence, a high current is used to pull the disc open, and after a specified time, a smaller holding current is used to keep it open. A specially designed current supply with a fast response was used to supply the two current levels for each of the valves.

Seals were made to seal the joints between:

- The high pressure flanges and the high-pressure chamber
- The cylinder head and the outlet valve, and the cylinder head and the inlet valve

High-pressure helium from the heat-exchanger coils enters the plenum chamber through the two-inlet flanges. The high-pressure gas enters the displacement volume when the intake valve is opened. It expands and does work on the piston, pushing it up. When the exhaust valve is opened, the low-pressure cool gas flows into the low-pressure side of the heat exchanger.

3.1.2 Valve Leaks

Experiments on the expander showed that there were significant leaks in the system even at room temperature, and the leak rates increased at they got colder. Even at temperatures as high as 190 K, the leak rates were as high as 15-40 % of the total flow rate through the expander. There were two major sources of leaks in the system:

- Leaks past the valve seats - high-pressure gas leaking past the intake valve into the displacement volume, and gas in the displacement volume leaking past the exhaust valve to the low-pressure side of the heat exchanger.
- Leaks past the cold-end seals, which led to the working fluid bypassing the displacement volume altogether.

In order to diagnose the leaks past the valve seats, a jig was constructed for static testing of the valves (Fig 3.2). The cylinder head together with the valve disc to be tested, and a Kapton seal on the side to be tested, is inserted into the circular groove and covered with a cover. Eight compression screws are used to provide the sealing force for the Kapton seal. Experiments with a solid stainless steel piece with the same shape and dimensions as the cylinder head proved that the sealing force was enough to prevent leaks past the Kapton seal even at 77 K. The rig is pressurised with helium and soap bubbles from the leaks past the valve seats can be observed through the ports. The inlet ports are accessible through a hole in the cover and the exhaust ports are accessible through three slots cut into the side of the rig.

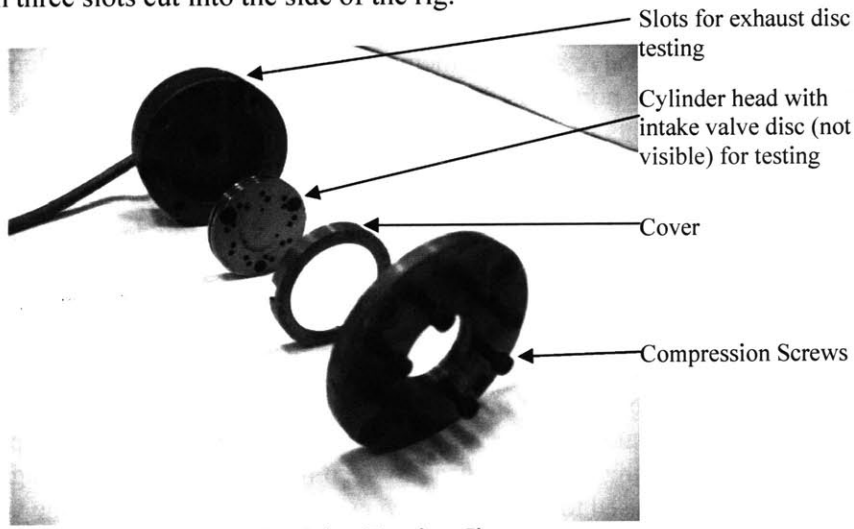

Figure 3.2: Valve Testing Jig

The design of the cylinder underwent several iterations to come up with a configuration that would have low leak rates associated with it at 77 K. In the first iteration, the Kel-F valve seats were crimped into the valve ports. When this was found to leak, a similar design, but with a

smaller valve seat area, was used. The purpose of the reduced area was to increase the sealing pressure. In the next design, Kel-F seats were machined and epoxied into the valve ports. However, the use of a cutting tool introduced large stresses in the seats, which were later noted to have deformed. In addition, thermal contraction of the constrained seats was suspected to have led to warpage of the sealing surfaces at low temperatures. In the final iteration, the Kel-F seats were epoxy-glued into shallow counterbores in the cylinder head. The seats were very nearly unconstrained and it was hoped that the smaller seat-height would result in smaller thermal strains. This design was found to have very low leak rates (less than 0.1 slm, compared to expander flow rates of the order of 10 slm) even at 77 K.

It was extremely important to keep the cylinder head and the valve discs scratch-free, since areas of the order of 0.002 * 0.002 in^2 were all that were needed to have leak rates of the order of 1 slm (assuming a choked-flow with a stagnation pressure of 145 psi and a stagnation temperature of 150 K). However, since the cold head was assembled by hand and not in necessarily clean environs, there were two possible sources of scratches along the valve discs and the valve seats. As there was no system to assemble the head and valve discs coaxially, the valve discs had to be pushed laterally, across the valve seats, for alignment. There was also always the possibility that a foreign particle would land on the discs or seats and cause indentations. The uncertainties associated with the assembly procedure need to be removed to ensure that the valves stay leak-free.

3.1.3 Cold End Seal Leaks

The material originally chosen to make these seals was 0.005 inch thick Kapton. The sealing force for the two large seals came from 16 #4-40 screws. The sealing force for the two smaller seals came from 4 #2-56 screws. In order to reduce the leaks past the large seals by increasing the sealing force, the size of the compression screws was increased to #5-40 and then #8-32, but that did not solve the problem. Teflon and Ultra High Molecular Weight Polythene were tried as gasket materials, but to no avail. It was then decided to use indium as the sealing material.

To make the small seals, indium wire 1.5 mm in diameter was compressed to make indium strips. A number 47 drill was used to make the internal diameter of the seal (Fig.3.3a). The outer diameter was made by clamping the strip between two pieces of plastic annuli of the required outer diameter and cutting away the excess material (Fig. 3.3b). A number 47 drill was used to align the two annuli and the sandwiched indium strip.

Indium strips about 0.004 inches thick were tried but were found to leak at 77 K. However, when the thickness of the strips was increased to about 0.008 inches, the small seals were found to seal properly at 77 K.

The large indium seals were made out of indium wire 0.5 mm in diameter. Jigs were made to fit the wire into the steps cut out into the cylinder head (Fig 3.4). Indium wire was squeezed into the steps using a screwdriver. With indium occupying the steps on both sides of the cylinder head, the cold end was then assembled without the compression cup. A special jig was constructed to uniformly compress the two large indium seals and squeeze out the excess material from within the steps (Fig 3.5). The excess indium was cut off with a blade. Following this, the jig was

removed and the compression cup was placed over the cold end. The compression screws were then tightened to compress the indium to its final thickness. The two inlet high-pressure flanges were then inserted into their respective grooves in the high-pressure chamber. On each side, the four screws were tightened to compress the small indium seals.

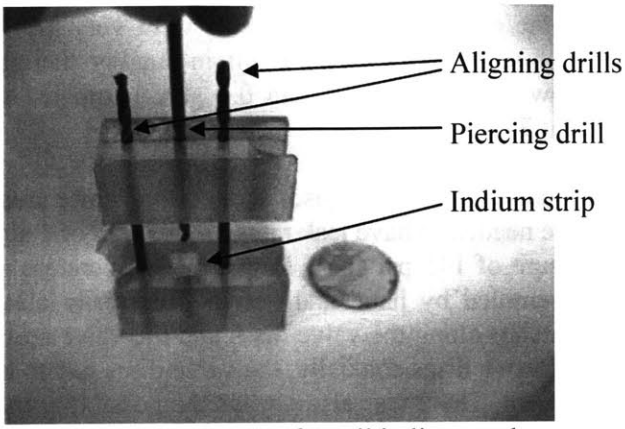

Figure 3.3a: Jig for ID of small indium seal

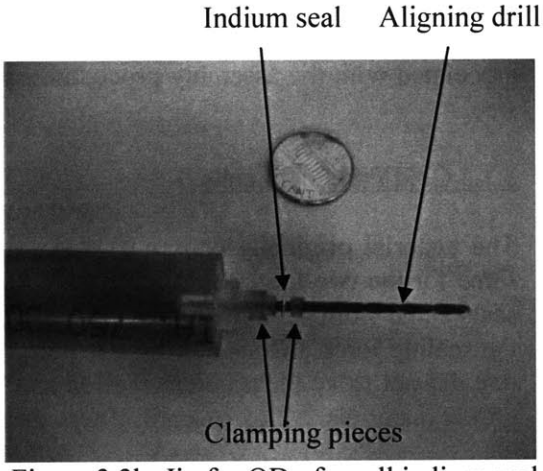

Figure 3.3b: Jig for OD of small indium seal

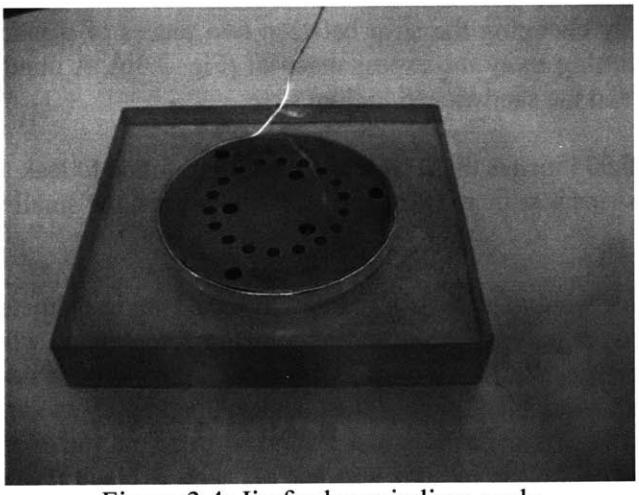
Figure 3.4: Jig for large indium seals

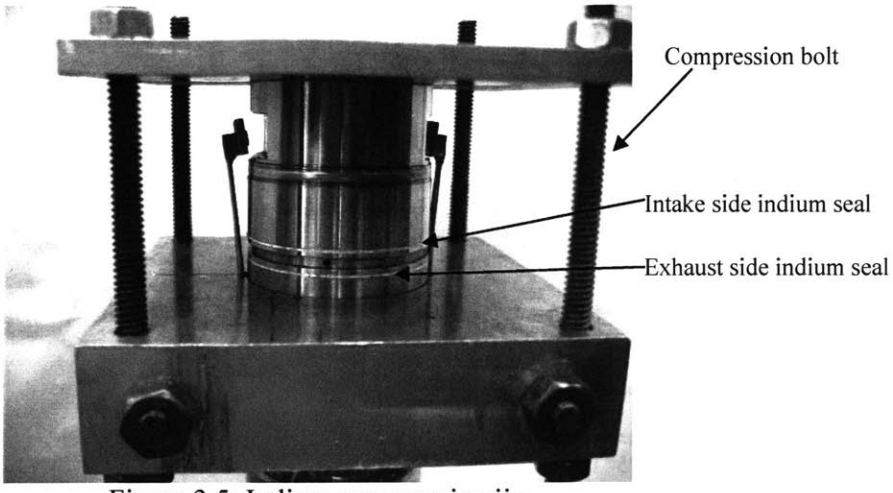

Figure 3.5: Indium compression jig

When tested for leaks, the inlet side indium seal was found to be reasonably tight at 77 K, with a leak rate of only about 0.06 slm (less than 1% of the expander flow rate) when subjected to a pressure difference of 140 psi. However, the outlet side indium seal did not seal well and had leak rates of the order of 2.5 slm (about 25% of the expander flow rate) when subjected to a pressure difference of 140 psi. Both indium seals had negligible leak rates at room temperature.

The relatively tight inlet side indium seal indicates that indium can work as a low temperature seal. One of the major differences between the inlet side seal and the outlet side seal is the thickness of the stainless steel piece sealing against the cylinder head – the inlet side stainless steel piece is 0.050 inches thick and has a lip 0.087 inches thick near the sealing surface, while the outlet side stainless steel piece is just 0.025 inches thick (Fig 3.6). This thin-walled piece (304SS) was originally epoxied to the solenoid quality stainless steel (430SS) making the outlet solenoid valve; however, the epoxy was known to have cracked. This resulted in the 304SS piece having very little rigidity. A pressure of 140 psi could have caused the thin wall to expand radially outwards, and slip on the indium seal, thus causing leaks.

Another possible cause of the leaks is the difference in thermal expansion coefficients of 430SS and 304SS. The thermal expansion coefficient of 304SS is about 1.6 times that of 430SS[6]. Therefore, the 304SS tends to contract more than 430SS. The thermal strain associated with the cooling of 304SS from 300 K to 80 K is 0.0029. The corresponding thermal strain for 430SS was estimated to be about 0.0018.

One of the sealing surfaces is the cylinder head, which is made of 304SS and contracts radially by about 0.0026 inches. The other sealing surface is the outlet side thin wall, which, when unconstrained, contracts by the same amount. However, the wall is constrained by the 430SS magnetic yoke, around which it forms a ring. As the wall is about 20 times thinner than the magnetic yoke, it is reasonable to model the 430SS piece as being rigid. Therefore, the wall contracts only as much as the 430SS allows it – about 0.0016 inches radially. There is a relative motion of about 0.001 inches between the two sealing surfaces (which are 0.025" wide) as they cool down from 300 K to 80 K, which could cause the seal to start leaking.

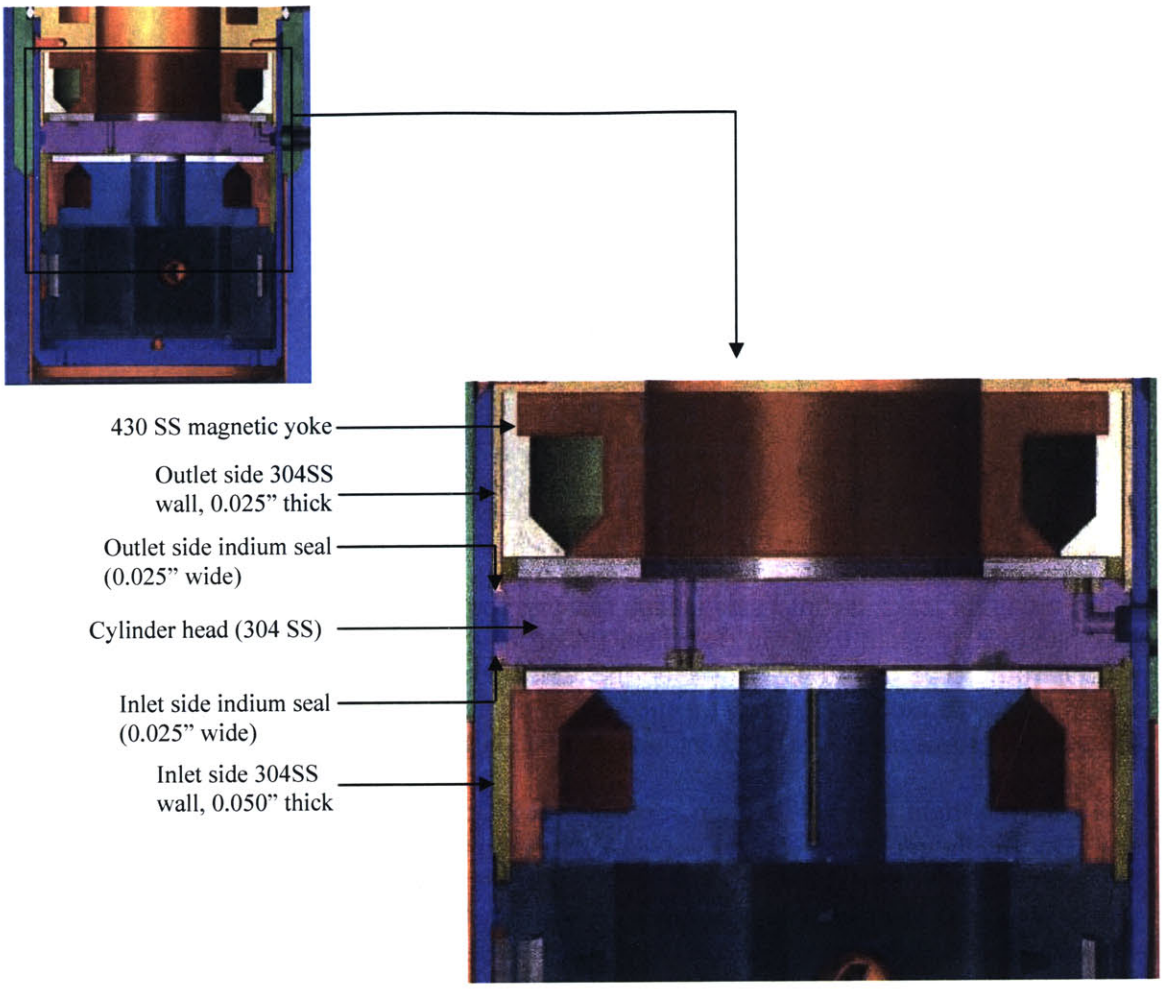

Figure 3.6: Indium seals and relative rigidities of intake and exhaust walls

Even though the exact reason for the leakage past the outlet side seal was uncertain, it seemed fairly certain that it was related to the flexibility of the outlet side wall. This needs to be kept in mind while designing cold heads for future prototypes of the expander.

3.1.3.1 Valve disc lift

The switch from Kapton to Indium had a significant effect on the valve impedance. The cold end had originally been designed for a valve lift of 0.011 inches in order to match the valve port diameter of 0.045 inches. However, the thickness of the Indium seal (about 0.001 inches after compression) was less than that of the Kapton (about 0.004 inches after compression). This reduced the valve lift by about 0.003 inches to 0.008 inches. At the same time, the valve port diameter was increased to 0.060 inches. This required a valve lift of 0.015 inches. Therefore, the valve lift was only half of what it needed to be. This resulted in a redesign of the cylinder head, whereby the steps were reduced by 0.007 inches each.

3.2 Heat Exchanger

The heat exchanger was sized by C.L.Hannon[1] and constructed by AMTI. It was made by winding two coils of finned copper tubing around a G10 tube that slipped over the cylinder assembly. These coils serve as the high-pressure passages of the heat exchanger. The low-pressure passage of the heat exchanger was created by heat shrinking a tube of Teflon onto the finned tubing. The low-pressure helium flows across the fins, between the heat shrink and the G10 wall.

The finned tubing has an internal diameter of 0.040 inches and an external diameter of 0.063 inches. The fins are 0.150 inches in diameter, 0.007 inches thick and are spaced at 60 fins per inch. Each finned coil is about 350 inches in length

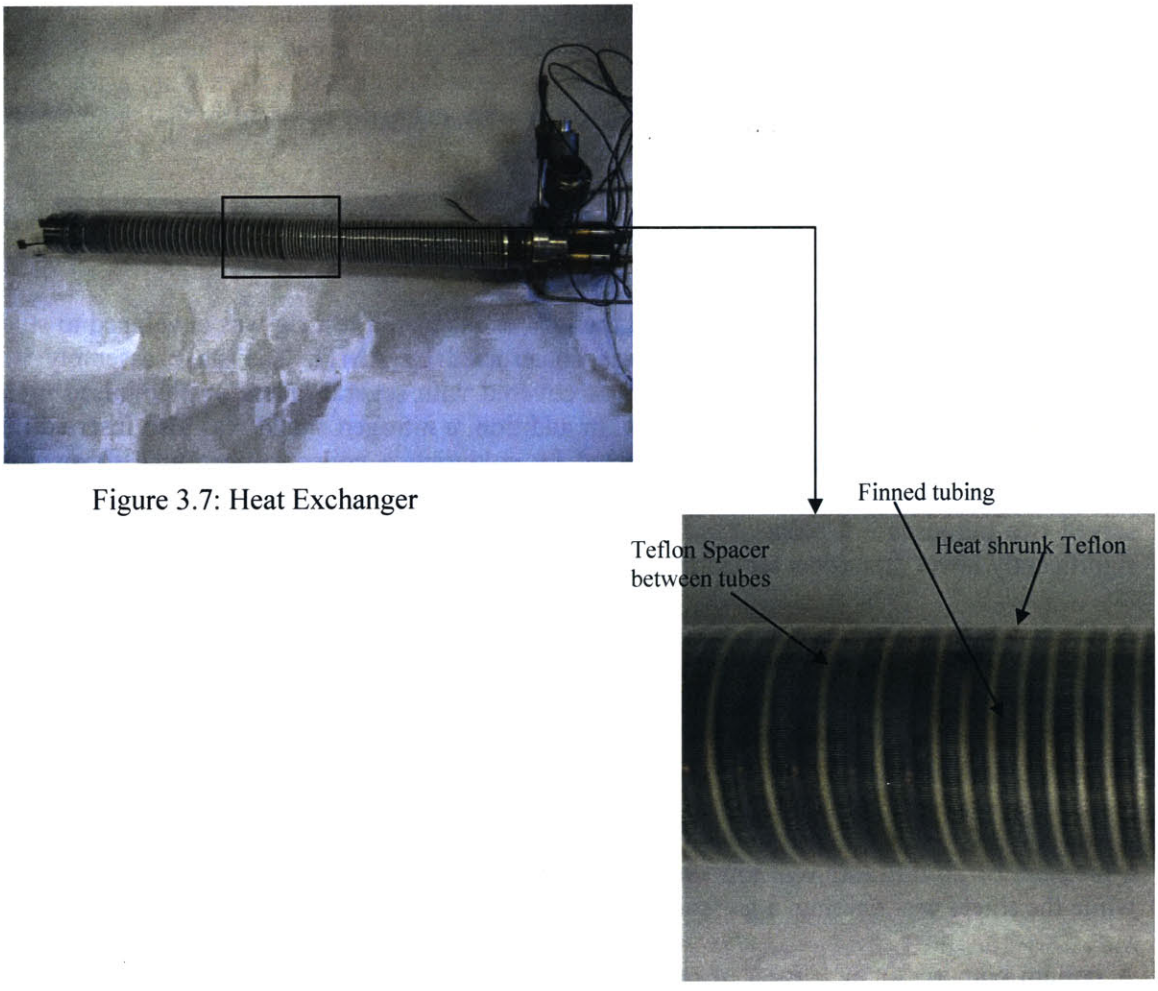

Figure 3.7: Heat Exchanger

3.3 Warm End Valves

DC operated solenoid valves manufactured by Clippard Instruments Laboratories were originally used to control the flow between the warm volume and the four reservoirs. The electromagnetic

force actuates a flexure-spring to open the valve. The valves were designed to withstand a maximum pressure of about 150 psi, which placed a restriction on the maximum pressure in the cycle. The Clippard valves were later replaced by Kip valves, which can withstand pressures of upto 250 psi.

Needle throttle valves were originally installed between the warm end solenoid valves and the warm displacement volume. They were put in to control the flow-rate of helium between the warm volume and the reservoirs, since it was felt that the flow-resistance of the warm-end passages was too low. However, after some testing, it was discovered that the flow-passages in the warm end had a significant flow-resistance, and the throttles only exacerbated it. Therefore, the throttle needles were backed out of their respective orifices. The warm-end valve pressure drop tests are described in Appendix E.

In order to drive the pressure in reservoir A closer to the high pressure and the pressure in D closer to the low pressure, throttle valves were added at the warm end – to bleed gas from the high-pressure line to A, and from D to the low-pressure line. These valves were always kept open during operation. During operation, the valves were manually adjusted so that the pressures in A and D could be maintained at appropriate levels.

3.4 Flow System

After the manufacture of the expander and the heat exchanger, a test rig was developed to study the performance of the stage. The rig was constructed by AMTI. The stage assembly was inserted in a vacuum can. The assembly was covered with several layers of aluminised mylar sheet in order to minimise radiation losses. In addition, a nitrogen shield was also inserted into the vacuum can. The shield was constructed by soldering a coiled copper tube to an open cylinder made of copper sheet. Liquid nitrogen was passed through this coil. The nitrogen shield served two purposes – it reduced the radiation losses when the expander was at a temperature significantly lower than room temperature, and it helped improve the vacuum in the vacuum can.

A schematic of the flow circuit is shown in Figure 3.8.

A pre-cooling line was incorporated into the system. By running cold helium vapour through it and into the low-pressure side of the heat exchanger, the 3rd stage of the proposed cryocooler could be simulated.

A vacuum pump was run continuously to maintain the vacuum in the can. It was found that while a pressure of 20 millitorr was low enough to keep the outer wall of the can from getting cold while the shield was running, a pressure of 40 millitorr caused condensation on the outer walls.

A helium compressor was used to provide high-pressure gas to the stage assembly. The high pressure and low pressure in the system were set by pressure regulators that were part of the compressor system. As the compressor output was much greater than the flow-rates required by the expander, a large fraction of the compressor flow was made to bypass the expander through a series of pressure regulators.

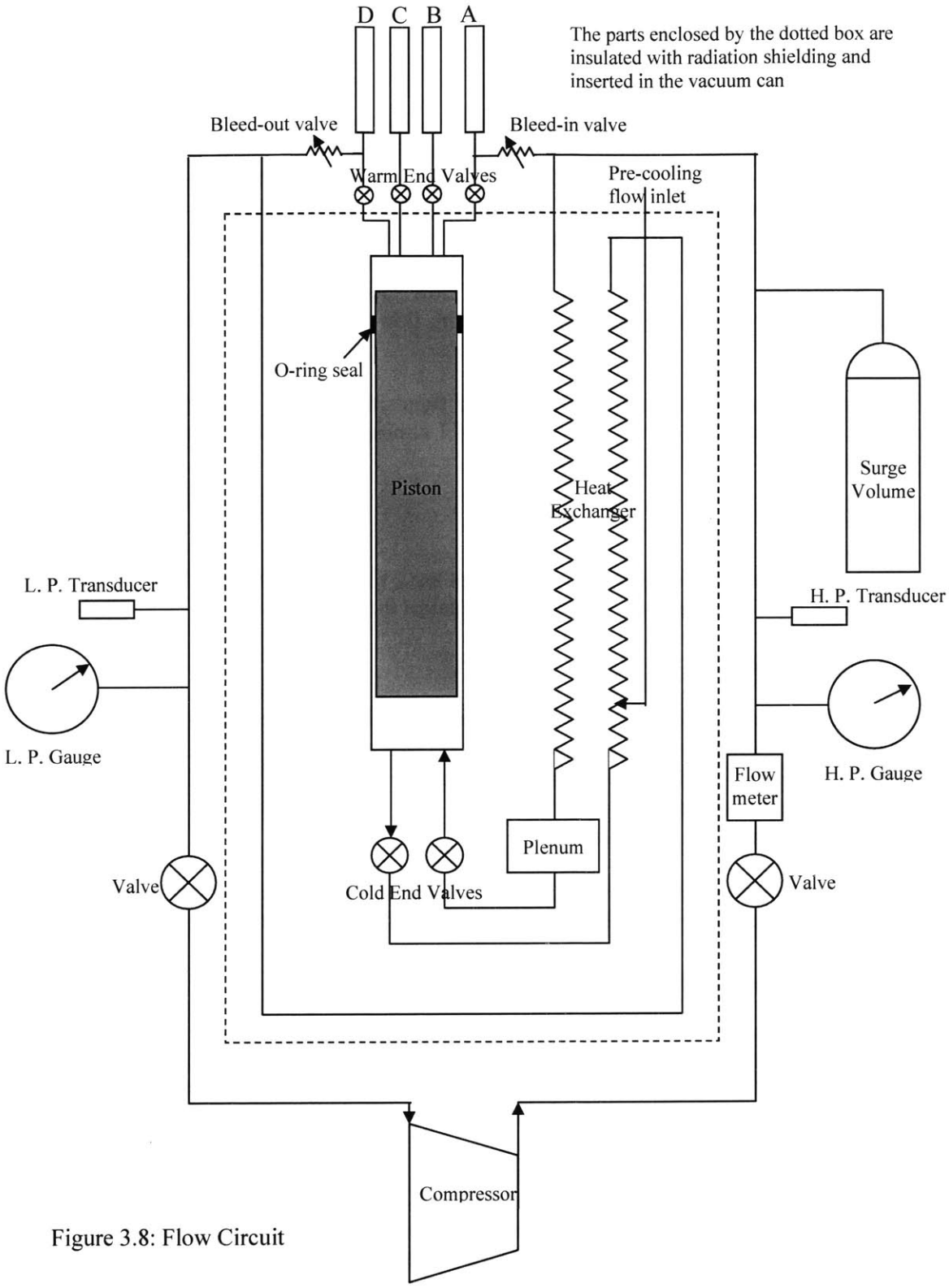

Figure 3.8: Flow Circuit

3.5 Instrumentation

3.5.1 Flow rate measurement

An MKS Type 1179A Mass-Flo Controller was used in conjunction with an MKS Type 247D Readout to measure the total helium flow rate through the system. The meter measures the flow rate by heating of gas stream and sensing the thermal mass movement. This type of meter is not well suited to the pulsatory flow which is a consequence of the cold valves being open for only a fraction of the cycle time, and the low capacitance in the system. In order to get a reasonably accurate averaged flow-rate measurement, the capacitance of the flow-loop was substantially increased by adding a surge volume between the flow meter and the cold valves. Another limitation of the flow-meter was that it prevented the flow-rate from exceeding a certain set point.

The flow meter measures the flow rate in units of standard litres per minute (slm), i.e., the volume flow rate in litres per minute at a pressure of 1 atmosphere and a temperature of 273 K. The conversion from Kg/s to slm is given below:

$$\dot{m}(Kg/s) = 2.98 * 10^{-6} Q(slm) \qquad \ldots(3.1)$$

During the heat exchanger effectiveness measurement tests, a rotameter was used to measure the pre-cooling flow rate. The rotameter was calibrated against the MKS flow meter.

3.5.2 Pressure measurement

Pressure transducers were used to measure the pressure at the following locations:

- The inlet of the high-pressure side of the heat exchanger
- The outlet of the low-pressure side of the heat exchanger
- The four warm-end reservoirs
- The pressure in the warm volume

Pressure gauges were installed at the inlet of the high-pressure side of the heat exchanger and the outlet of the low-pressure side of the heat exchanger in order to calibrate the transducers.

3.5.3 Temperature measurement

Lakeshore Silicon Diode Thermometers (DT-470-SD-13) were used to measure the temperature at various points in the cycle (Figure 3.9). They were calibrated against a pre-calibrated DT-470-SD-13 Thermometer. These thermometers have a range of 4 K–325 K. A four-lead measurement system was employed wherein two leads supply an excitation current of 10μA and the two other leads measure the voltage drop across the sensor.

A Lakeshore Model 218 Temperature Monitor was used to read the temperatures. The instrument, which supplies the excitation current and converts the voltage measurement into a temperature measurement, can only handle eight thermometers at any time. This was not a major issue during zero-load balanced-flow expander operation, since pre-cooling temperatures and

load-heater temperatures were not required. However, during testing of the pre-cooling loop, cables had to be manually switched every few minutes to monitor all the temperatures. This also messed up the temperature data logging function, which is described later, since some locations on the temperature monitor were now being alternately used for two thermometers.

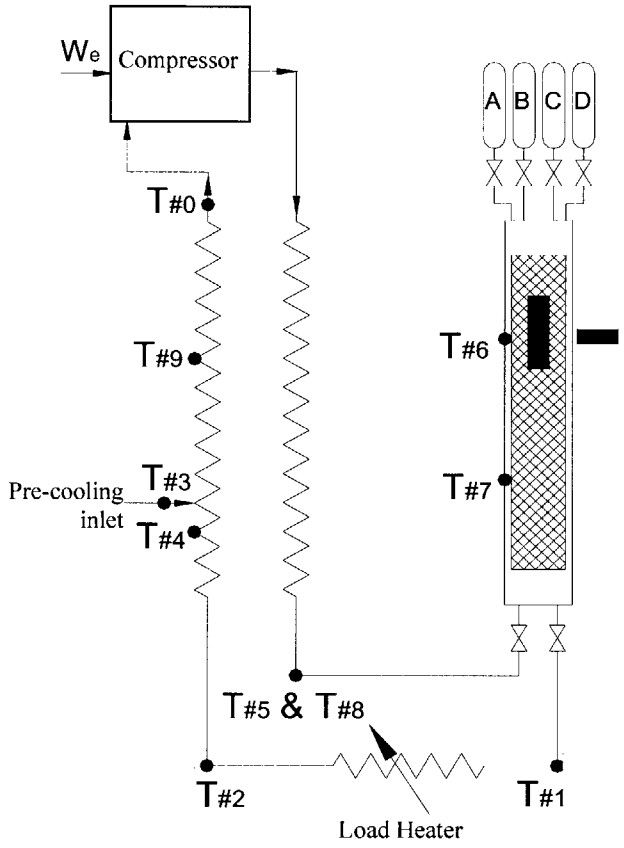

Figure 3.9: Location of Thermometers
(Image courtesy AMTI)

3.5.4 Piston Position Measurement

The piston position is measured using three Hall Effect sensors mounted on the cylinder. The Hall effect states that if a magnetic field is applied to a conductor, a voltage is generated transverse to the current flow direction in the conductor. The piston contains a stack of permanent magnets. The Hall effect sensors were mounted so that they were equidistant from the topmost and bottommost position of the magnets in the piston. This was done to ensure that the sensor output always stayed in the linear range.

3.6 The Piston Seal and Blow-by Leaks

The piston was constructed from a G10 tube with a phenolic cap. The stack of permanent magnets was originally suspended in the tube and kept in place with the help of foam. The foam did not do a good job of holding the magnets in place – the stack was found to change position due to piston motion and slip out of the linear range of the sensors. To remedy this, a new stack of magnets was integrated into the piston cap.

In order to ensure that the blow-by past the piston between the warm and cold volumes was kept to a minimum, the piston was a tight fit with the cylinder. The clearance between the cylinder and piston was of the order of 0.001 inches, though it was higher at the cold end. A lubricated rubber O-ring was inserted in a groove in the piston near the warm end to provide the sealing. However, it was found that during removal of the piston from the cold end, the lubricant residue got smeared all over the cylinder and increased the friction between the piston and the cylinder. To prevent this from happening again, the piston was subsequently always removed and reinserted through the warm end. In addition, an O-ring made from paper towels smeared with a few drops of oil was also inserted, in another groove. The purpose of this O-ring was to slowly release lubricant to the rubber ring.

Tests were performed to measure the blow-by past the piston. To measure the blow-by from the cold volume to the warm volume, one of the solenoid valves between the warm volume and one of the reservoirs was kept open. The cold intake valve was then opened and the pressure in the warm reservoir was recorded as a function of time. To measure the blow-by from the warm volume, the cold exhaust valve was kept open. One of the warm reservoirs was pressurised and the corresponding solenoid valve was opened. The pressure in the reservoir was recorded as a function of time.

With a new O-ring, the measured blow-by rates at room temperature were low. Flow rates of less than 0.1 slm were observed. These were negligible in comparison to expander flow rates of the order of 4 slm at room temperature.

After several weeks of experiments on the expander, though, the blow-by from the warm volume to the cold volume increased significantly. With a pressure differential of about 130 psi across the piston, blow-by rates as high as 5 slm were observed. However, with pressure differentials of 20 psi, the rates decreased to about 0.2 slm. Since there is never a significant pressure differential across the piston except when the piston is at the topmost or bottommost position, the blow-by was still within acceptable limits. By this time, the real-time hardware was operational and the expander was being run at higher frequencies, and thus with higher flow rates. Therefore, the effect of piston blow-by was further reduced. The blow-by from the cold volume to the warm volume was still negligibly small.

3.7 Computer Interface

The control program for the expander was written in Labview by B.Krass of AMTI. The original Labview program ran on a Windows XP operating system. The control and data logging were

both done by the same computer. That, coupled with the fact that Windows tends to allocate CPU time to various processes according to its own whims and fancies, meant that the control program was not nearly as fast as it needed to be to ensure that the expander ran smoothly. Later, the data logging function was transferred to a separate computer. This improved the performance slightly, but it was still not fast enough. The program ran at loop rates varying from 2 milliseconds to 20 milliseconds, when they needed to be consistently about 1 millisecond. Finally, a switch was made to National Instruments' Real Time Hardware to control the expander. A National Instruments SCB-100 I/O connector block was used to interface the input and output signals with the PCI 6031E data acquisition card in the real time instrument. The card receives analog signals from the pressure transducers and the position sensor and sends digital signals to open and close the valves.

With the real time instrument, the computer has more of a supervisory role. The real time system, which communicates with the "host" computer through an Ethernet cable, interfaces with the data acquisition hardware. The real time hardware runs two loops. The normal priority loop transfers data between the real time system and the host computer. The time-critical loop monitors all the real time input data and makes decisions regarding the opening and closing of valves. The second computer continues to act as a data-logging machine, and stores pressure and position data, as well as temperature data.

3.7.1 Control Functions

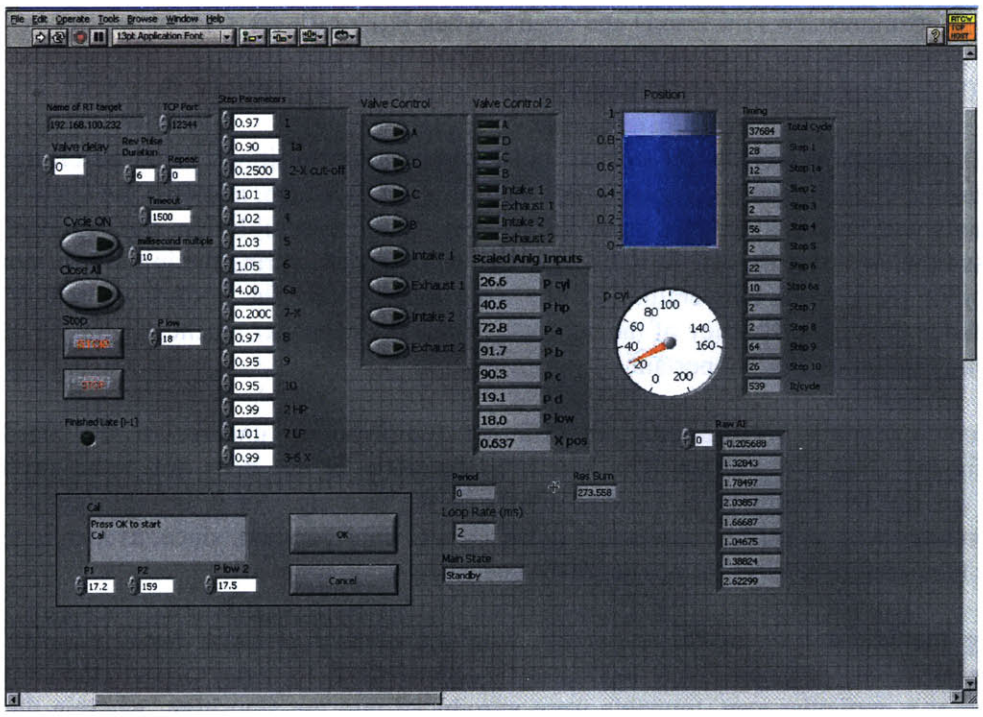

Figure 3.10: Control Program
(Virtual Instrument developed by B.Krass of AMTI)

Figure 3.10 shows a screenshot of the control program virtual instrument. It displays various cycle parameters – the pressures, piston position and the time taken by each individual process. It also allows modifications to the cycle parameters. In addition, it allows manual control of the four warm end valves and the cold end valves. It also includes a subroutine for calibration of all the pressure transducers and the position sensor.

The function of the control program is to send signals to open and close the two cold-end and the four warm-end valves. It does this on the basis of the input data (reservoir pressures, piston position, system high pressure and system low pressure) and certain specified constants. The most basic control program ran the following algorithm with the specified process-ending conditions:

Step 1 (Recompression 4): Close A and start inlet valve opening current when $P_{cyl} > c_1 P_A$ ($c_1 < 1$)
Step 1.1: Switch from opening current to holding current after a specified amount of time
Step 1a (Blow-in): Open warm valve A when $P_{cyl} > c_{1a} P_{high}$ ($c_{1a} < 1$) OR when $x_{piston} > x_{cut\text{-}off}$
Step 2 (Intake): Close cold inlet valve when $x_{piston} > x_{cut\text{-}off}$
Step 3 (Expansion 1): Close A and open B when $P_{cyl} < c_3 P_A$ ($c_3 > 1$)
Step 4 (Expansion 2): Close B and open C when $P_{cyl} < c_4 P_B$ ($c_4 > 1$)
Step 5 (Expansion 3): Close C and open D when $P_{cyl} < c_5 P_C$ ($c_5 > 1$)
Step 6 (Expansion 4): Close D and start exhaust valve opening current when $P_{cyl} < c_6 P_D$ ($c_6 > 1$)
Step 6.1: Switch from opening current to holding current after a specified amount of time
Step 6a (Blow-out): Open D when $P_{cyl} < c_{6a} P_{low}$ ($c_{6a} > 1$) OR when $x_{piston} < x_{recompression}$
Step 7 (Exhaust): Close cold exhaust valve when $x_{piston} < x_{recompression}$
Step 8 (Recompression 1): Close D and open C when $P_{cyl} > c_8 P_D$ ($c_8 < 1$)
Step 9 (Recompression 2): Close C and open C when $P_{cyl} > c_9 P_C$ ($c_9 < 1$)
Step 10 (Recompression 3): Close B and open C when $P_{cyl} > c_{10} P_B$ ($c_{10} < 1$)

The 10 constants as well as the cut-off and recompression positions could be changed at any point during cycle operation. They control the timing of each step, and thus the cycle frequency. Constants with values close to 1 drive the process nearly to equilibrium, but, by increasing the process time, decrease the rate of work done by the expander. During the initial cool-down of the cryocooler from room temperature to operating temperature, the cool-down rate is of more importance than the efficiency of the expander. Once the expander reaches operating conditions, efficiency becomes more important.

Different operating requirements at different temperatures underscore the need for an "intelligent" control algorithm. The algorithm currently in use does not make any decisions based on the temperatures at various points in the test rig. As it is, algorithms involving temperatures will be hard to implement in the current configuration, since, as mentioned before, all the temperature sensors cannot be monitored at the same time.

During the initial runs of the expander, with the control program running in a Windows environment, the expander cycle tended to be inconsistent. In order to prevent the cycle from stalling at a particular step, timeouts were introduced into the algorithm, wherein the program closed all open valves and started from the 1st step in case a particular step took more than a specified amount of time to complete. With the switch to the real time hardware system, the

inconsistency associated with the cycle reduced dramatically and the timeout condition became superfluous.

The use of mechanical valves to control the warm-end bleeds into reservoir A and out of reservoir D created some control issues. The pressures in A changes constantly due to the bleed-in and during the intake, 1st expansion and final compression. Similarly, the pressure in D constantly changes due to the bleed-out and during the final expansion, exhaust and the 1st compression. The changing pressures make it difficult to precisely control the bleed-flows. If the two bleed-flows are not exactly matched, the total amount of mass in the warm end increases or decreases with time (depending on which of the two bleed-flows is higher). Ultimately, the cycle may get to a point where the pressure in A(D) is so high(low) that the intake(exhaust) process cannot be completed, because the pressure difference across the piston is insufficient to move it.

A temporary solution to the problem was the addition of extra conditions to steps 2 and 7. The modified conditions were as follows:
Step 2 (Intake): Close cold inlet valve when $x_{piston} > x_{cut\text{-}off}$ OR $P_A > c_A P_{high}$
Step 7 (Exhaust): Close cold exhaust valve when $x_{piston} < x_{recompression}$ OR $P_D < c_D P_{low}$

The OR condition serves two purposes – it prevents the cycle from stalling on any of these steps, and it helps drive the pressures in A and D back (a shorter intake/exhaust process reduces the amount of gas going into A/out of D). However, it is not a permanent solution as the cycle tends to fall into a stall-work-stall-work loop. A better solution would be the replacement of the mechanical valves by some sort of electronic throttle valves which could be controlled by the Labview program. Another possible solution is the use of pressure regulators to maintain the pressures in A and D, but again, these would need to be electronically controlled, since different operating conditions call for different operational parameters.

3.7.2 Data Logging Functions

Figure 3.11 shows a screenshot of the monitoring program virtual instrument. It displays pressure-position, as well as pressure-time and position-time graphs of the expander cycles. It includes provisions to write all the cycle pressures and position data over an expander cycle at 1 millisecond intervals to a log file. The monitoring program also interfaces with the Lakeshore temperature monitor and displays all the temperatures. It allows the user to write the temperatures averaged over a time period specified by the user to a second log file.

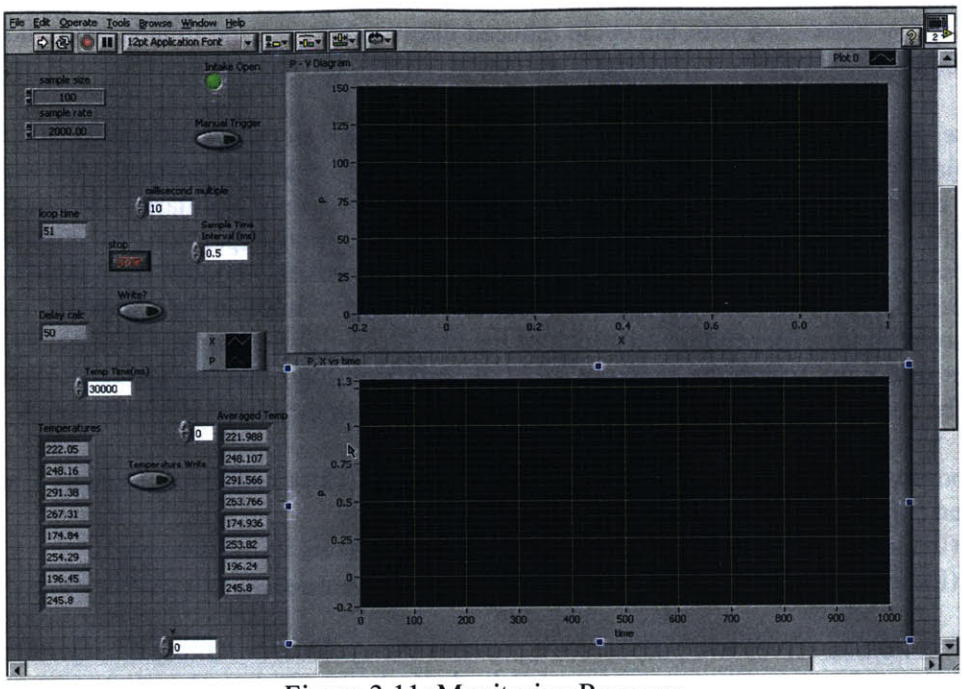

Figure 3.11: Monitoring Program
(Virtual Instrument developed by B.Krass of AMTI)

CHAPTER 4 – HEAT EXCHANGER ANALYSIS

Experiments were done to determine whether the performance of the heat exchanger was as per design specifications. In the first series of experiments, the heat transfer characteristics of the heat exchanger were determined. In the next set of experiments, the pressure drop through the high-pressure and low-pressure passages was studied.

4.1 Heat Exchanger Effectiveness Measurement

The heat exchanger had been designed to have an NTU of 60. The actual effectiveness of the heat exchanger was determined by running the heat exchanger with an unbalanced flow. This was done by running some helium through the pre-cooling line. The pre-cooling flow was supplied by bleeding some helium off the main high-pressure flow line, cooling it down in a helium dewar and sending it through a transfer line to the pre-cooling location. The MKS flow meter measured the total helium flow through the system. A rotameter was used to measure the flow-rate of the pre-cooling flow. A schematic of the system is shown in Figure 4.1.

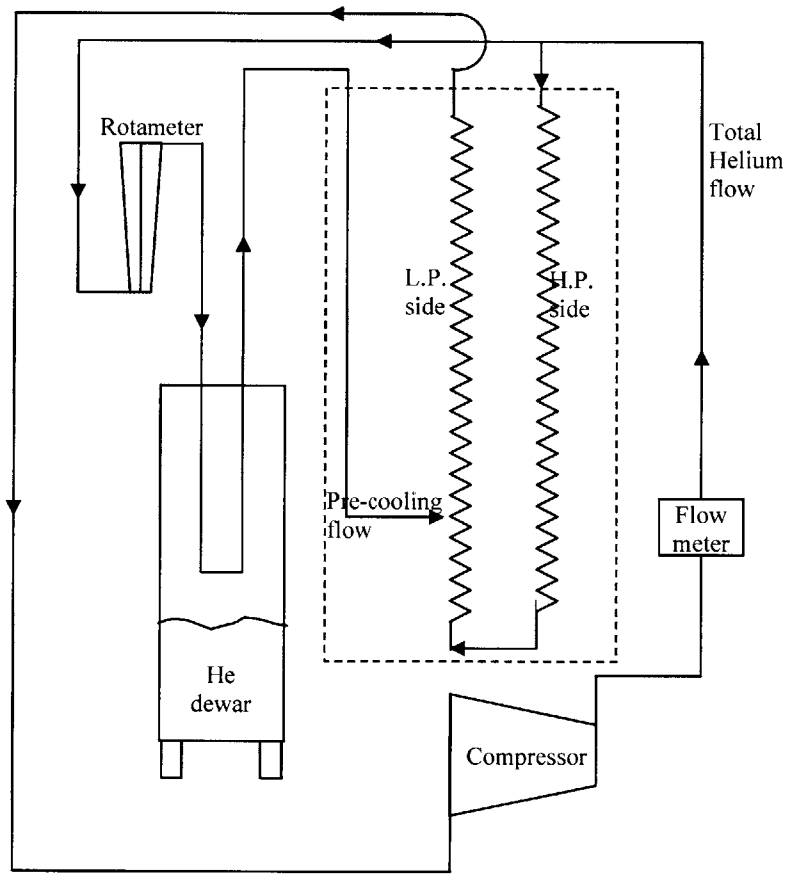

Figure 4.1: Heat Exchanger Effectiveness Test

Temperature measurements were taken at the following locations:

- the top of the heat exchanger,
- the middle of the heat exchanger
- the bottom of the heat exchanger
- the pre-cooling inlet

Both cold end valves were kept open throughout the experiment. Therefore, at steady state, the temperature at the exit of the high-pressure side was equal to the temperature at the inlet of the low-pressure side of the heat exchanger.

Initially, no helium was run through the high-pressure side of the heat exchanger. All the flow was routed through the dewar. The pre-cooling flow was maintained at about 15 slm in order to cool the heat exchanger down. When the heat exchanger had cooled sufficiently (T_{high} = 227.7 K, T_{mid} = 60.6 K, T_{low} = 117.3 K and T_{pc} = 58.2 K), the pre-cooling flow was decreased and the main flow was turned on. The heat exchanger was then allowed to go to steady state and the experiment was run until the liquid helium in the dewar ran out.

The steady state temperatures and flow rates are tabulated in Table 4.1

Table 4.1: Heat Exchanger NTU Experiment – Steady-state properties

Total Flow Rate	16.5 slm = $4.46*10^{-5}$ Kg/s
Pre-cooling Flow Rate	1.90 slm = $5.13*10^{-6}$ Kg/s
Temperature at high-end of heat exchanger	278.06 K
Temperature at middle of heat exchanger	173.40 K
Temperature at low-end of heat exchanger	163.71 K
Pre-cooling inlet temperature	162.16 K

A steady-state steady-flow First Law analysis for the entire heat exchanger leads to the following equation (neglecting external heat leaks) (Fig. 4.2):

$$m_t(T_h) = m_{pc}(T_{pc}) + m_m(T_h + \Delta T_{high}) \quad \ldots(4.1)$$
$$16.5(278.06) = 1.9(162.16) + 14.6(278.06 + \Delta T_{high})$$
$$\Delta T_{high} = 15.08 \text{ K}$$

The temperature difference at the top of the heat exchanger was determined to be 15.08 K. Therefore, the temperature at the inlet of the high-pressure side of the heat exchanger was 293.14 K. This agreed with a measurement of about 21 degrees Celsius made by a thermocouple attached to the inlet line

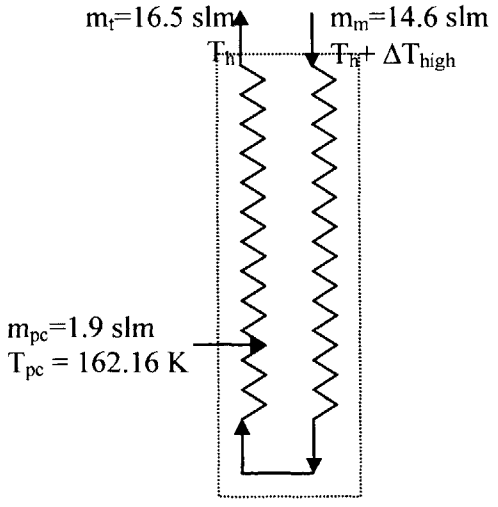

Figure 4.2: Mass and energy flows across heat exchanger boundary

A steady-state steady-flow First Law analysis for the heat exchanger between the top of the heat exchanger and an intermediate point downstream of the pre-cooling inlet yields the following (neglecting external heat leaks) (Fig. 4.3):

$$m_m(293.14) - m_t(278.06) = m_m(T_i+\Delta T) - m_t(T_i) \quad \ldots(4.2)$$
$$1.9T_i - 14.6\,\Delta T = 308.146$$
$$\Delta T = 0.13T_i - 21.106$$

At the location of the middle temperature sensor (T_9 in Fig. 3.9),
$T_i = T_{mid} = 173.4$ K
Therefore, $\Delta T_{mid} = 1.436$ K

The temperature difference between the hot stream and the cold stream at the location of the middle temperature sensor is 1.436 K.

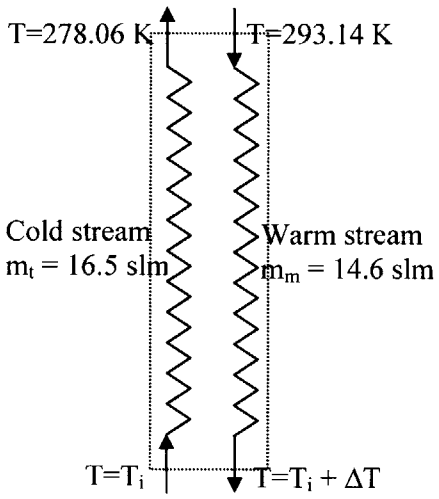

Figure 4.3: Mass and energy flows across heat exchanger boundary

4.1.1 Estimation of heat exchanger NTU

The NTU for the portion of the heat exchanger between the top and the middle temperature sensors can be calculated from the following formula[7], since both the hot- and cold-stream flow rates, as well the temperature differences at the ends are known.

$$\frac{UA}{m_m C_p} = \frac{-\ln\left(\frac{\Delta T_{high}}{\Delta T_{mid}}\right)}{\frac{m_m C_p}{m_t C_p} - 1} = \frac{-\ln\left(\frac{15.08}{1.436}\right)}{\frac{14.6}{16.5} - 1} = 20.42 \quad \ldots(4.3)$$

The NTU for the whole heat exchanger was extrapolated from this result, since it is reasonable to assume that the heat transfer coefficient does not change much across the length of the heat exchanger.

$$\frac{NTU_{top-middle}}{NTU_{whole}} = \frac{Area_{top-middle}}{Area_{whole}} = \frac{Length_{top-middle}}{Length_{whole}} = 0.55 \quad \ldots(4.4)$$

The NTU for the whole heat exchanger was determined to be about 37 (at a main flow rate of $4.5*10^{-5}$ Kg/s and a pre-cooling flow rate of $5.1*10^{-6}$ Kg/s). This is about two-thirds the design NTU of about 60 (at a main flow rate of $5*10^{-5}$ Kg/s and a pre-cooling flow rate of $3*10^{-6}$ Kg/s).

4.2 Pressure Drop Measurements

The large times associated with the intake and the exhaust strokes in preliminary expander runs led to concerns that the pressure drop across the heat exchanger was higher than what it was supposed to be. Experiments were performed to measure the pressure drop across the high-pressure and low-pressure sides of the heat exchanger.

In the first experiment, the cold end was assembled without the valve discs. With the compressor operational, helium was run through the system in a closed loop. Pressure gauges were used to measure the pressure at the following locations:

- The inlet of the high-pressure side of the heat exchanger (using the high-pressure gauge)
- In the cold end displacement volume. The pressure was measured using the transducer in the warm end displacement volume. Care was taken to ensure that the piston was not at the top- or bottom-dead centre.
- The inlet of the low-pressure side of the heat exchanger. A pressure gauge was installed at the pre-cooling location.
- The exit of the low-pressure side of the heat exchanger (using the low-pressure gauge)

The flow rate through the system was controlled by manually changing the amount of bypass through the compressor. The results are tabulated below.

Table 4.2: Pressures at different points in the expander circuit

Mass flow rate (slm)	$P_{high,\ inlet}$ (psig)	$P_{cylinder}$ (psig)	$P_{low,inlet}$ (psig)	$P_{low,\ exit}$ (psig)
0.89	14	11	11	10
2.19	16	8.5	8.5	7.5
4.37	28	10.5	10.5	10
6.43	34	7	7	6
9.17	43	4	4	3
12.19	57	6.5	6.5	5.5
14.91	66	4.5	4.5	3
18.20	79	4.5	4.5	3
19.62	85	3.5	3.5	2

The major drop in pressure is between the inlet to the high-pressure side of the heat exchanger and the displacement volume. This consists of the drop through the high-pressure side of the heat exchanger, through the Cu-Ni tubes which connect the heat exchanger to the high-pressure reservoir, and the drop across the inlet valve ports.

Each heat exchanger coil has an internal diameter of 0.040 inches and a length of approximately 350 inches. Each Cu-Ni tube has an internal diameter of 0.035 inches and a length of about 2.5 inches. As there are two Cu-Ni tubes for each heat exchanger coil, the flow through each Cu-Ni tube is only half the flow through the HX coil. The L/D^4 ratio of the heat exchanger coil is 82 times that of a single Cu-Ni tube. Therefore, it is reasonable to assume that all the pressure-drop across the Cu-Ni tubes is negligible in comparison to the pressure drop across the high-pressure side of the heat exchanger. The inlet valve ports are 0.060 inches in diameter and only 0.25

inches in length. Therefore, the pressure drop through the valve ports is also negligible in comparison to the heat exchanger pressure drop

It was clear that the maximum pressure drop in the helium loop occurred across the high-pressure side of the heat exchanger. In the next experiment, the two heat exchanger coils were tested individually. One of the purposes of this experiment was to determine whether both coils had similar pressure-drop characteristics or whether one of the coils was much worse than the other, possibly because of a blockage of some sort.

In this experiment, the helium was not run in a closed loop. The cold end was disassembled. High-pressure helium entered the inlet of the heat exchanger coil being tested and was directly vented to the atmosphere at the exit of the high-pressure side (through the Cu-Ni tubes leading to the inlet flange). The results are tabulated in Table 4.3.

Table 4.3: Pressure-drop across the individual heat-exchanger coils.

"Left side" H/X coil		"Right side" H/X coil	
Mass flow rate (slm)	Inlet pressure (psig)	Mass flow rate (slm)	Inlet pressure (psig)
1.03	12	1.00	12
2.93	30	2.97	32
6.62	58	6.51	64
10.41	88	10.08	92
14.01	110	14.07	124
16.31	124		

The data indicates that the two coils had similar pressure drops across them.

To determine whether the flow through the coils was laminar or turbulent, the Reynolds Numbers associated with the flow rates were calculated. They are tabulated in Table 4.4.

$$\mathrm{Re} = \frac{\rho UD}{\mu} = \frac{\rho QD}{\mu A} = \frac{4\dot{m}D}{\mu\pi D^2} = \frac{4\dot{m}}{\mu\pi D} \qquad \ldots(4.5)$$

The viscosity of helium at 300 K is $2*10^{-5}$ Ns/m^2.

Using Eq. 3.1, $$\mathrm{Re} = \frac{4*2.98*10^{-6}*Q}{(2*10^{-5})*\pi*(0.04*0.0254)} = 186*Q \qquad \text{(Q is in slm)} \qquad \ldots(4.6)$$

Table 4.4: Reynolds Numbers at measured flow rates

"Left side" H/X coil		"Right side" H/X coil	
Flow rate (slm)	Reynolds Number	Flow rate (slm)	Reynolds Number
1.03	191	1.00	186
2.93	545	2.97	553
6.62	1230	6.51	1211
10.41	1936	10.08	1874
14.01	2605	14.07	2617
16.31	3032		

For a straight tube, the transition from laminar to turbulent flow takes place at Reynolds Numbers of about 2000-3000. However, the heat exchanger coils are not straight – they are helical tubes and the transition to turbulent flow may take place over a range of Reynolds Numbers.

4.2.1 Correlations for pressure drop for an ideal gas flow through a circular tube

Theoretical correlations were developed for the pressure drop for laminar and turbulent ideal gas flows through a circular tube

4.2.1.1 Laminar flow pressure drop for an ideal gas flow through a straight circular tube at constant temperature

$$\frac{dp}{dx} = \frac{128\mu\dot{m}}{\pi D^4 \rho} = \frac{128\mu\dot{m}RT}{\pi D^4 p} \Rightarrow pdp = \frac{128\mu\dot{m}RT}{\pi D^4}dx \quad \text{(Using the ideal gas law } \rho = \frac{p}{RT}\text{)} \qquad \ldots(4.7)$$

$$\Rightarrow \frac{p_{in}^{\ 2} - p_{out}^{\ 2}}{2} = \frac{128\mu\dot{m}RTL}{\pi D^4} \qquad \ldots(4.8)$$

$$p_{in}^{\ 2} - p_{out}^{\ 2} \propto \dot{m}$$

For a laminar flow, the difference between the squares of the pressures at the inlet and the outlet is proportional to the flow rate.

4.2.1.2 Turbulent flow pressure drop for an ideal gas through a straight circular tube at constant temperature

$$\Delta p = f\rho\frac{L}{D}\frac{\overline{V}^2}{2} = f\rho\frac{L}{D}\frac{\dot{m}^2}{2\rho^2 A^2} = f\frac{L}{D}\frac{\dot{m}^2}{2\rho A^2} = f\frac{L}{D}\frac{\dot{m}^2 RT}{2pA^2} \qquad \ldots(4.9)$$

$$2pdp = \frac{f}{D}\frac{\dot{m}^2 RT}{A^2}dx \qquad \ldots(4.10)$$

$$\Rightarrow p_{in}^{\ 2} - p_{out}^{\ 2} = \frac{f}{D}\frac{\dot{m}^2 RT}{A^2}L = \frac{16f}{D}\frac{\dot{m}^2 RT}{\pi^2 D^4}L = \frac{16RTL}{\pi^2 D^5}f\dot{m}^2 \qquad \ldots(4.11)$$

Mills[8] gives the following formula for the friction factor for a smooth walled straight circular tube $f = (0.79 * \ln \mathrm{Re} - 1.64)^{-2}$ ...(4.12)

$p_{in}^{\ 2} - p_{out}^{\ 2} \propto \dot{m}^2$ (since the friction factor is very weakly dependent on flow rate)

For a turbulent flow, the difference between the squares of the pressures at the inlet and the outlet is proportional to the square of the flow rate.

4.2.2 Comparison of Experimental Results with Correlations

The data in Table 4.3 is used to calculate the value of $p_{in}^{\ 2} - p_{out}^{\ 2}$ at the measured flow rates. The

difference between the squares of the pressures and the corresponding flow rate is tabulated below for each coil.

Table 4.5: Variation of flow rate with difference of squared pressures

Left side (P_{out} = 0 psig)			Right side (P_{out} = 0 psig)		
Flow rate (slm)	P_{in} (psig)	$P_{in}^2 - P_{out}^2$ (Pa^2)	Flow rate (slm)	P_{in} (psig)	$P_{in}^2 - P_{out}^2$ (Pa^2)
1.03	12	2.36E+10	1.00	12	2.36E+10
2.93	30	8.47E+10	2.97	32	9.34E+10
6.62	58	2.41E+11	6.51	64	2.84E+11
10.41	88	4.91E+11	10.08	92	5.31E+11
14.01	110	7.29E+11	14.07	124	9.04E+11
16.31	124	9.04E+11			

The experimental results were then compared with the theoretical correlations for laminar and turbulent flows.

For a laminar flow at 300 K, $p_{in}^{\ 2} - p_{out}^{\ 2} = 8.33 * 10^{15} \dot{m} = 2.47 * 10^{10} * Q$ (Q in slm) ...(4.13)

For a turbulent flow at 300 K,

$p_{in}^{\ 2} - p_{out}^{\ 2} = 8.17 * 10^{21} f\dot{m}^2 = 7.25 * 10^{10} * (0.79 * \ln \mathrm{Re} - 1.64)^{-2} Q^2$ (Q in slm) ...(4.14)

Figures 4.4 and 4.5 show that the experimental results agree well with the laminar flow correlation for flow rates of less than 5 slm and with the turbulent flow correlation for flow rates of more than 5 slm.

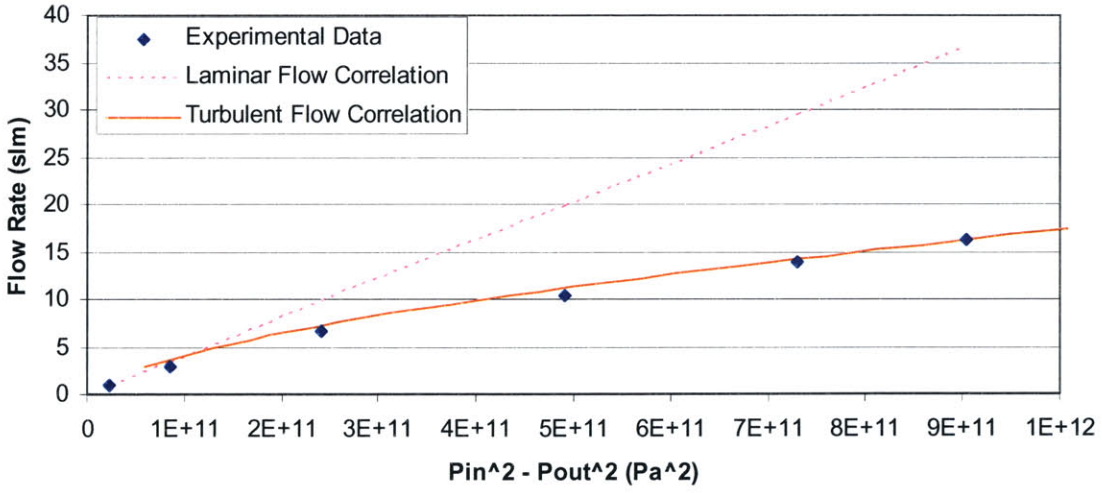

Figure 4.4: Comparison of experimental data with flow correlations for 1st coil (Left side)

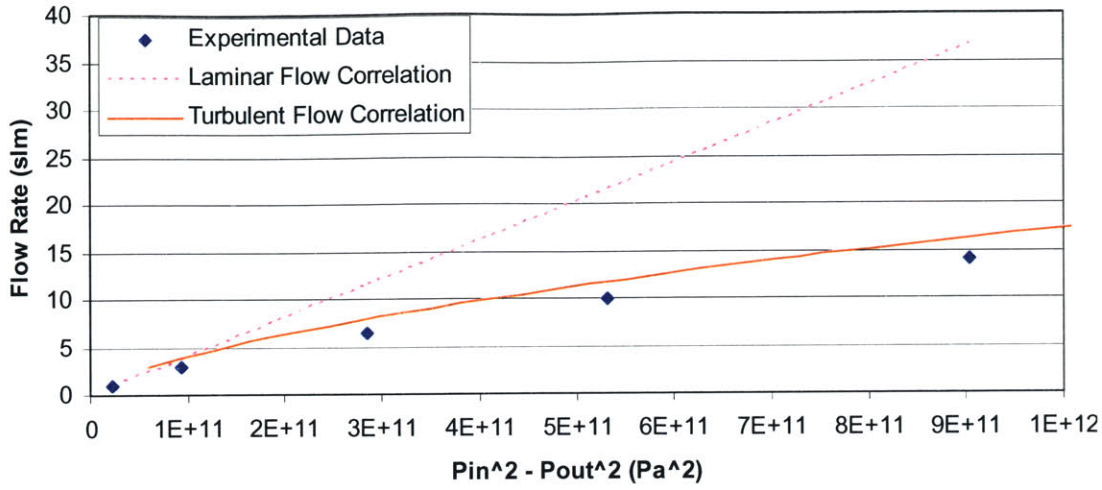

Figure 4.5: Comparison of experimental data with flow correlations for 2nd coil (Right side)

4.2.3 Predicted Pressure Drop at Operating Conditions

Since the laminar and turbulent flow pressure-drop correlations agree well with the experimental data, they are used to predict the pressure drop through the high-pressure side of the heat exchanger during operating conditions.

The correlations developed in Section 4.2.1 are modified slightly to account for the change in temperature over the heat exchanger. In addition, during operation, the pressures at the inlet and the exit of the high-pressure side of the heat exchanger are not expected to be too dissimilar and can both be approximated by an average pressure.

4.2.3.1 Laminar flow

From Equation 4.8, $pdp = \frac{128\mu\dot{m}RT}{\pi D^4}dx$

$$p_{in}^{\ 2} - p_{out}^{\ 2} = \frac{256\mu\dot{m}R}{\pi D^4}\int T dx \qquad \ldots(4.15)$$

The following equation expresses the viscosity of helium as a function of temperature[9]:

$\mu = 5.023 * 10^{-7} * T^{0.647}$ where μ is in Ns/m^2 and T is in K. ...(4.16)

If the heat exchanger is at a uniform temperature,

$$p_{in}^{\ 2} - p_{out}^{\ 2} = 2.074 * 10^6 QT^{1.647} \qquad \ldots(4.17)$$

If the heat exchanger is not at a uniform temperature,

$$p_{in}^{\ 2} - p_{out}^{\ 2} = 2.074 * 10^6 Q\frac{\int T^{1.647}dx}{L} \qquad \text{(T in K, pressures in Pa, Q in slm)} \qquad \ldots(4.18)$$

For a balanced flow heat exchanger, the temperature profile is linear.

$$p_{in}^{\ 2} - p_{out}^{\ 2} = 2.074 * 10^6 Q \frac{\int T^{1.647} dT}{T_{out} - T_{in}} \quad \ldots(4.19)$$

$$p_{in}^{\ 2} - p_{out}^{\ 2} = 2.074 * 10^6 Q \frac{T_{out}^{2.647} - T_{in}^{2.647}}{2.647(T_{out} - T_{in})} \quad \ldots(4.20)$$

4.2.3.2 Turbulent flow

From Equation 4.11, $2pdp = \frac{f}{D}\frac{\dot{m}^2 RT}{A^2}dx$

$$p_{in}^{\ 2} - p_{out}^{\ 2} = \frac{\dot{m}^2 R}{DA^2}\int fTdx \quad \ldots(4.21)$$

If the heat exchanger is at a uniform temperature,

$$p_{in}^{\ 2} - p_{out}^{\ 2} = 2.42 * 10^8 * Q^2 fT = 2.42 * 10^8 * Q^2 (0.79 * \ln \mathrm{Re} - 1.64)^{-2} T \quad \ldots(4.22)$$

(T in K, pressures in Pa, Q in slm)

If the heat exchanger is not at a uniform temperature,

$$p_{in}^{\ 2} - p_{out}^{\ 2} = 2.42 * 10^8 * Q^2 \frac{\int fTdx}{L} \quad \ldots(4.23)$$

For a balanced flow heat exchanger, the temperature profile is linear.

$$p_{in}^{\ 2} - p_{out}^{\ 2} = 2.42 * 10^8 * Q^2 \frac{\int fTdT}{T_{out} - T_{in}} \quad \ldots(4.24)$$

(T in K, pressures in Pa, Q in slm)

$$(p_{in} - p_{out})(p_{in} + p_{out}) = 2.42 * 10^8 * Q^2 \frac{\int (0.79 * \ln \mathrm{Re} - 1.64)^{-2} TdT}{T_{out} - T_{in}}$$

$$\Rightarrow 2(\Delta p)(p_{avg}) = 2.42 * 10^8 * Q^2 \frac{\int (0.79 * \ln \frac{3.73 * 10^{-3} Q}{\mu} - 1.64)^{-2} TdT}{T_{out} - T_{in}}$$

Using Eq. 4.16,

$$(\Delta p)(p_{avg}) = 1.21 * 10^8 * Q^2 \frac{\int \left(0.79 * \ln\left(\frac{Q * 10^7}{5.023 * T^{0.647}}\right) - 6.06\right)^{-2} TdT}{T_{out} - T_{in}} \quad \ldots(4.25)$$

4.2.3.3 Pressure drop predicted by correlations at various operating conditions

The following table presents the calculated pressure drops in the high-pressure passages of the heat exchanger at various operating conditions.

Table 4.6: Predicted pressure drop at various operating conditions

Cold End Temp (K)	Total Avge.Flow Rate (slm)	Avge.Flow Rate (slm) through one coil	$\Delta p * p_{avg}$ (assuming laminar) (Pa^2)	$\Delta p * p_{avg}$ (assuming turbulent) (Pa^2)	p_{avg} (psi)	Δp (assuming laminar)	Δp (assuming turbulent)
Expander at 300 K (Windows-based control – 0.8 Hz)							
300	3	1.5	$1.86*10^{10}$	$1.04*10^{10}$	130	3.02 psi	1.68 psi
Expander at 150 K, flow-balanced H/X (Windows-based control – 0.7 Hz)							
150	6	3	$2.36*10^{10}$	$2.00*10^{10}$	130	3.82 psi	3.25 psi
Expander at 300 K (Real-time control – 1.7 Hz)							
300	6	3	$3.72*10^{10}$	$2.90*10^{10}$	150	5.23 psi	4.07 psi
Expander at 150 K, flow-balanced H/X (Real-time control – 1.4 Hz)							
150	12	6	$4.72*10^{10}$	$6.00*10^{10}$	140	7.08 psi	9.06 psi

These results will be discussed in detail in the next chapter.

4.2.3.4 Comparison of predicted pressure drop with design pressure drop at 10 K

The expander design flow-rate at 10 K is $94*10^{-6}$ Kg/sec (about 35 slm) with a 5% heat exchanger pre-cooling flow rate. At this flow rate, the high-pressure side pressure drop according to the design calculations is 60 kPa, or about 9 psi, for a high pressure of 220 psi. Using a constant friction factor for simplicity of calculation, the turbulent flow correlation (Eq. 4.23) predicts a pressure drop of about 14 psi. The constant friction factor chosen is based on the viscosity at 300 K and leads to an overestimation of the pressure drop. The calculation indicates that the heat exchanger does perform according to design specifications.

However, during cool-down to operating temperature, the cryocooler is expected to run with a much higher flow rate. Since the pressure drop varies with the square of the flow rate, it is not insignificant at these higher flow rates.

CHAPTER 5 – EXPERIMENTATION

Initial tests on the stage assembly were basically restricted to troubleshooting exercises. The focus was on integrating the control program with all the electronics and instrumentation in order to get the expander to run consistently. Emphasis was laid on the proper operation of the cold electromagnetic valves. Tests were done to determine the duration and magnitude of the opening and holding current pulses required by the intake and exhaust valves to open and close consistently. One major issue was the duration of the opening current pulse. Since the Labview program was not very high on Windows' list of priorities, during certain cycles, the signal to start the opening current came a few milliseconds later than it was supposed to. However, if the signal to switch from the opening current to the holding current came at the right time, it meant that the opening current had not been run for long enough to actually open the valve. Therefore, the valve failed to open. In order to remedy this, the opening current duration had to be increased. This was detrimental to the performance of the expander since it led to a larger heat leak into the cold end because of Joule heating, but it could not be helped. The opening current was run for 20 milliseconds at this early stage of testing. Later, with the use of the Real-Time instrument, an opening current duration of 6-8 milliseconds was enough for consistent operation.

Once the electronics issues were sorted out, the expander-heat exchanger assembly was run as a cryocooler with no heat load other than the heat leak down the heat exchanger, from the surroundings and due to the ohmic heating of the valves. The expander was run at pressure ratios much lower than the 15:1 ratio at which the proposed cryocooler is supposed to run. There were two reasons for this. The Clippard valves at the warm end could hold pressures only up to about 150 psi. Secondly, the clearance volume in the cylinder was so high that it was not possible to get large volume ratios during expansion without reducing the intake flow.

With a clearance volume that was about 25% of the total displacement volume, a cut-off volume of 0.20 implies that the volume ratio over which the cold gas expands is only 1.25/0.45 or about 2.8. Using the PV^{γ} = constant relation for an adiabatic expansion, this translates to a required pressure ratio of only about 5.5.

The compressor low-pressure was typically set at about 18 psia (absolute pressure in psi). The high-pressure was varied, but was always kept below 140 psia. With the pressure differential required to force flow into and out of the displacement volume, the expander effectively ran between pressures of 125 psia and 25 psia at room temperature.

At this point, Kapton gaskets were being used as the cold end seals. Experiments would show that these did not work well at low temperatures. These were later replaced by indium seals.

5.1 Expander Efficiency Measurements

With the electronic issues sorted out, the expander could be operated at room temperature consistently. The parameters determined from the expander model were used to run the expander. By making slight changes to the values of these parameters, it was possible to obtain

P-V diagrams that expanded the gas from the high-pressure down to the pressure in reservoir D. However, the blow-in and blow-out associated with these cycles were significant.

Experiments were done at room temperature to measure the efficiency of the expander. The efficiency of the expander is typically defined as the actual temperature difference across the expander divided by the temperature difference across a reversible expander with the same inlet and exhaust pressures and inlet temperature. In this case, the efficiency of the expander was calculated as the specific work done by the expander divided by the specific work done by an ideal expander. The specific work done was calculated on the basis of the total mass flow (including leakage flow) through the system. This measure of efficiency does not take the heat leak into the cold end into account.

The expander was run at high-pressure-to-low-pressure ratios of 7.5:1 and 6:1. At each pressure ratio, the expander was run at various combinations of cut-off and recompression volumes and the warm end mass was adjusted to ensure that the piston exactly made full stroke (i.e., when the piston reached the topmost position, the pressure in the cylinder was equal to the pressure of the lowest pressure reservoir at the warm end).

At a pressure ratio of 7.5:1, the expander ran consistently for cut-off volumes between 0.3 and 0.4 and recompression volumes between 0.2 and 0.5. At the lower pressure ratio of 6:1, the cycle was not consistent at the lower range of cut-off volumes but became consistent at cut-off volumes greater than 0.35.

The expander efficiency was calculated at different operating conditions. The calculations are shown in Appendix D. Two separate data runs were done. The values from two different runs are tabulated below. Efficiencies of 70-90% were obtained from the first run. Efficiencies of 55-75% were obtained from the second run. However, the accuracy of these measurements, especially the first set, was under question since the flow rate as measured by the MKS flow meter tended to fluctuate quite a bit.

Table 5.1: Data from first run

Cut-off Volume	Recompression Volume	Expander Efficiency (%) with a pressure ratio of 7.5:1
0.30	0.22	72.2
0.35	0.22	82.8
0.35	0.30	80.3
0.40	0.22	89.4

Table 5.2: Data from second run

Cut-off Volume	Recompression Volume	Expander Efficiency (%) with a pressure ratio of 6:1	Expander Efficiency (%) with a pressure ratio of 7.5:1
0.35	0.2	60.0	72.8
0.35	0.3	52.6	69.0
0.35	0.4	38.6	59.5
0.40	0.2	69.8	75.6
0.40	0.3	68.7	74.1
0.40	0.4	59.0	69.8
0.40	0.5	48.2	59.9

Figure 5.1 shows the pressure-position diagram of a cycle running with a high pressure of 132.2 psi (pressure ratio = 7.5:1), a cut-off volume of 0.35 and a recompression volume of 0.3.

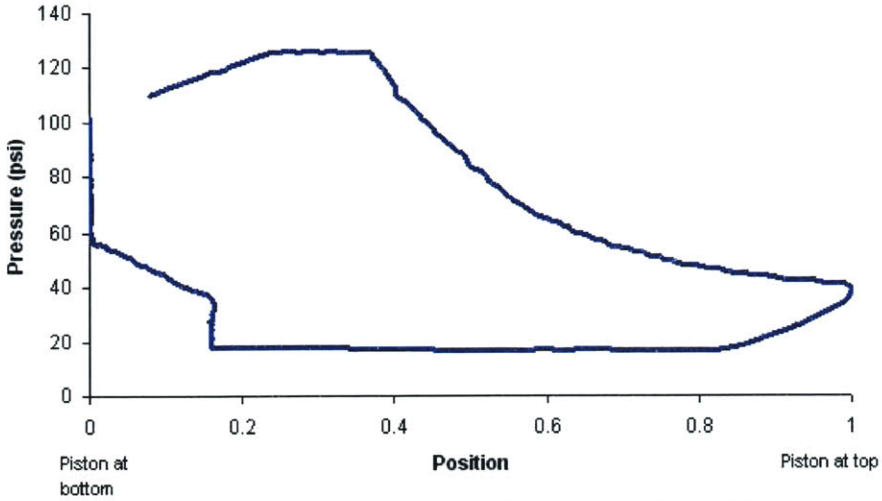

Figure 5.1: Room temperature pressure-position diagram $X_{co} = 0.35$, $X_{rc} = 0.3$

The graph indicates that the helium expands from about 125 psia to about 41 psia. This is because the mass in the warm end redistributed itself so that the pressure in reservoir A was only 107 psia, while the pressure in reservoir D was as high as 36 psia. This resulted in long blow-in and blow-out processes. Although the static models indicated that it was possible to operate the cycle with the pressure in A quite close to the high pressure and the pressure in D quite close to the low pressure, it proved very difficult to achieve this in practice. Increasing the amount of gas in the warm end did increase the pressure in A, but also increased the pressure in D. Similarly, decreasing the amount of gas in the warm end did not work (At this point, the warm end throttles had not been installed).

Another noticeable problem with the graph is the point at which the exhaust stops. The signal to close the exhaust valve was supposed to have been given when the piston reached a position of 0.3. However, the exhaust continued until the piston reached a position of about 0.16. The delay between the point at which the signal ought to have been sent by the control program to close the exhaust valve and the actual closing of the exhaust valve was as high as 22 milliseconds. When the intake stroke was investigated, it was found that the intake valve also took about 20 milliseconds to close. The problem with the intake valve is not readily apparent from the P-V graph, since the piston velocity was a lot lower during intake than during exhaust. The data seemed to imply that there were major timing problems with the control program running on a Windows machine.

Another issue, not immediately apparent from the graph above, but from the P-V graphs of cycles running with a lower recompression volume, was that of leaks. Figure 5.2 shows the pressure-position diagram of a cycle running with a high pressure of 132.2 psi (pressure ratio = 7.5:1), a cut-off volume of 0.35 and a recompression volume of 0.2. Following the closing of the exhaust valve (late as usual), it can be seen that despite the pressure in the cylinder increasing, as

expected, the piston actually starts to move up. This happens even though reservoir D, at a pressure of 35 psia, is open to the warm volume during this process (the first recompression). For the piston to move up during this process, the pressure in the cold end must have been higher than the pressure in the warm end. It was hypothesised that high-pressure gas was leaking into the displacement volume.

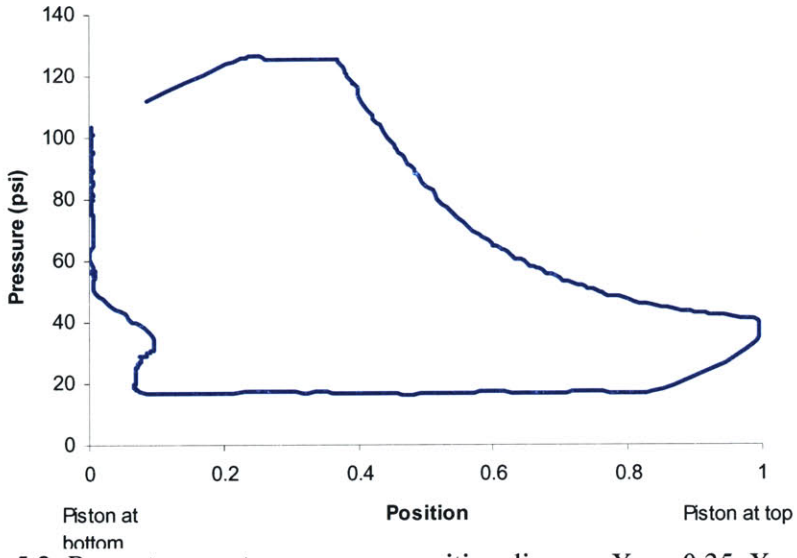

Figure 5.2: Room temperature pressure-position diagram $X_{co} = 0.35$, $X_{rc} = 0.2$

A series of leak tests were performed to estimate the magnitude and location of the leaks. With the high-pressure and low-pressure maintained at 132 psia and 17.5 psia respectively, the leak rate through the expander with both valves closed was as high as 0.22 slm, nearly 10% of the average flow rate through the expander while it was running. The leak rate increased to about 0.4 slm with one of the valves open. These leaks were pretty big, especially at room temperatures; as the expander cooled and the working fluid got denser, the leaks would only get larger.

5.2 Experiments with warm-end throttles

In order to drive the pressure in A up and the pressure in D down, high-pressure gas was bled into reservoir A, while gas from reservoir D was bled to the low-pressure side of the circuit. Mechanical valves were used to throttle the flow into and out of A and D respectively.

The warm end bleed made a significant difference to the performance of the expander. Figure 5.3 shows the P-V graph of the expander with the bleeds operational. It became possible to run the cycle at lower cut-off volumes. The blow-in and blow-out associated with the cycle reduced considerably. The working fluid expanded from about 130 psia to about 30 psia, a significant improvement over what had been achieved earlier.

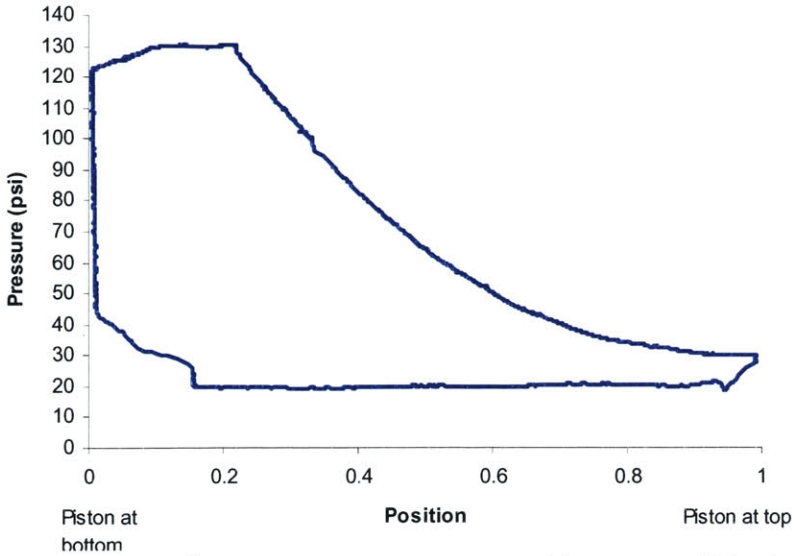

Figure 5.3: P-V diagram at room temperature with warm-end bleeds

With the expander running well at room temperature, it was decided to let the expander cool down and test its performance at lower temperatures. Over the course of a number of runs, it was observed that the expander cooled down to about 190 – 200 K, before consistently stalling at the exhaust step. For a comparison, the P-V graphs of the expander running at the same high pressure at 225 K and 191 K are shown in Figures 5.4a and 5.4b.

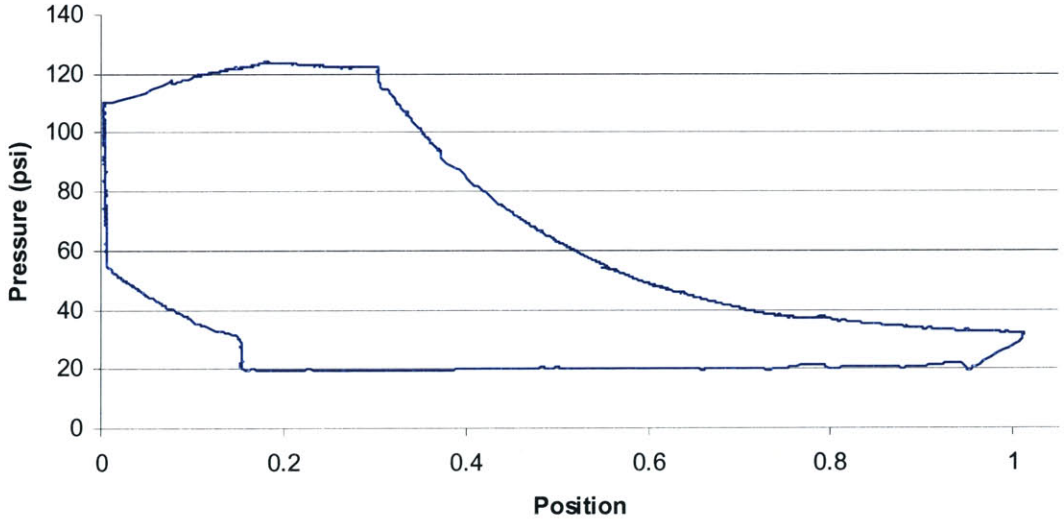

Figure 5.4a: P-V diagram at 225 K

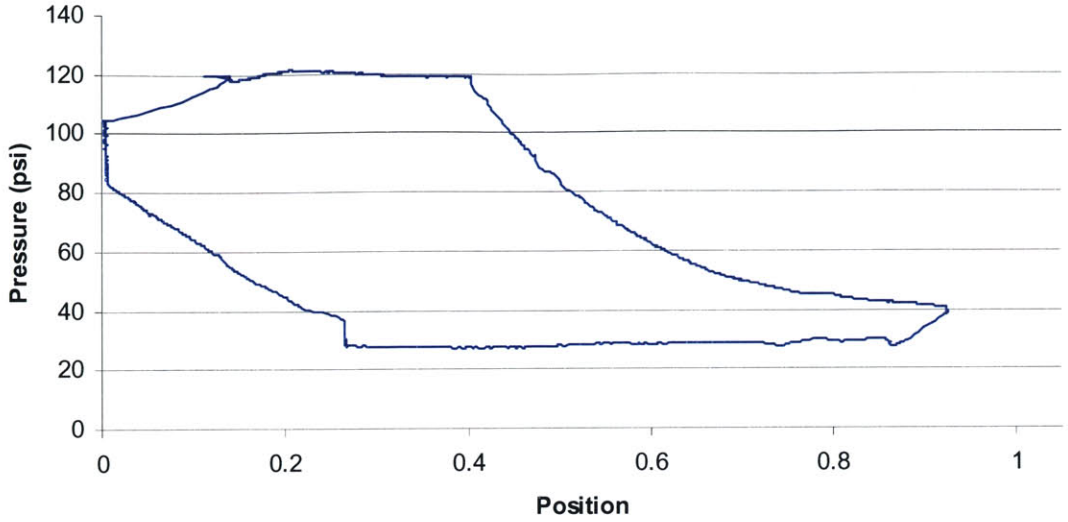

Figure 5.4b: P-V diagram at 191 K

As the expander cooled from about 220 K to about 190 K, the time taken by the expander to exhaust the cold gas kept increasing. The pressure in the cylinder during the exhaust step steadily increased. To keep the cycle operational, the pressure in reservoir D had to be increased in order to drive the piston down. The figures show that while the cylinder pressure was about 20 psia during exhaust at 225 K, it rose to 30 psia during exhaust at 190 K. This had the effect of reducing the effective pressure ratio over which the working fluid could expand.

Another indication that the pressure in the cold displacement volume was not decreasing during exhaust was the point at which the exhaust valve closed and the recompression started. Both the graphs above had the same recompression volume. While the exhaust valve closed at about X = 0.17 at 225 K, it closed at about X = 0.25 at 190 K. This made it clear that the piston was moving a lot slower at 190 K, despite the fact that the pressure in the warm end was much higher at this temperature.

There were two explanations for this behaviour at 190 K. The leaks past the intake and exhaust valves had not been eliminated and were, as expected, increasing with decreasing temperature. It was likely that below 200 K, the leak past the intake valve had increased to an extent which was preventing the displacement volume from pressuring down. It is also seen from the two graphs that the pressure during the intake stroke decreases from 225 K to 190 K. This could be attributed to leaks past the exhaust valve. The exhaust valve leaks, though, did not seem to be as big of an issue as the intake valve leaks at this point.

The leak tests that followed these runs agreed with the hypothesis. The intake valve leak was measured at about 2.25 slm at 190 K, while the exhaust valve leak was about 0.72 slm at the same temperature. These were very substantial when compared with the cycle flow rate of about 5 slm. At 230 K, the valve leaks were much lower, with the intake valve at 0.26 slm and the exhaust valve at 0.07 slm.

In an effort to combat the leaks by increasing the sealing force on the valve seats, a new cylinder head was manufactured with a smaller valve seat area (at this point, the valve seats were still being crimped into the valve ports).

The second explanation for the pressure not dropping during exhaust was increased piston friction. Since there was no pressure meter at the cold end, it was quite possible that the pressure in the cold displacement volume was decreasing during exhaust, but the piston friction was responsible for the piston not moving down. Indeed, when the piston was removed from the cylinder, it was seen that the piston was smeared with oil all along its length. The piston and cylinder were thoroughly cleaned with acetone. The piston O-ring near the warm end was replaced. O-rings made of paper towel were inserted into an annular groove near the top of the piston and were smeared with a few drops of oil. To prevent the piston and cylinder getting smeared again, the piston was inserted into the cylinder from the warm end instead of the cold end, as had been done previously.

At the time, it was theorised that a large pressure-drop in the low pressure passage of the heat exchanger could also be responsible for the pressure not dropping during the exhaust. Although the heat exchanger had been designed with a negligible pressure drop in the low-pressure side, no tests had yet been carried out to confirm the design parameters. The heat exchanger tests performed subsequently indicated that the low-pressure side pressure drop was very small.

The newly lubricated piston made a significant difference to the performance of the expander. The problem with the exhaust stroke did not appear until a much lower temperature. Figure 5.5 shows a P-V graph at 160 K. The pressure during the exhaust stroke falls to about 23 psia – not as low as the 20 psi near room temperature, but an improvement over the previous run.

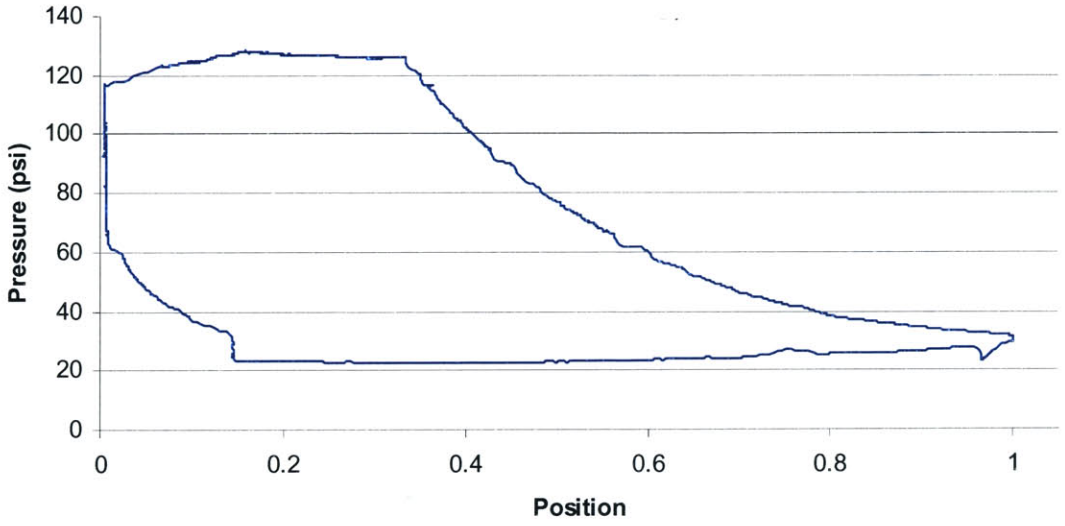

Figure 5.5: P-V diagram at 160 K

The expander cooled down to about 135 K, at which point the magnitude of the leaks made proper operation almost impossible. A measurement of leak rates at temperatures between 150

and 200 K showed that the replacement of the cylinder head had not made any difference to the leaks in the system. At this point, further testing of the expander was postponed and efforts were made to understand the cause of the leaks in the system and develop techniques to remedy them. These exercises have already been described in Section 3.1.

5.3 Expander Testing with Real-Time hardware

The replacement of the Kapton seals with indium seals significantly reduced the leakage past the seals. In addition, the new method of manufacturing the cylinder head, with the Kel-F seats glued to the cylinder head rather than crimped into the valve ports, reduced the leaks past the valves.

The switch from the Windows-based control program to the real-time hardware improved the cycle performance. As mentioned before, program loop rates decreased from 2-20 milliseconds to about 1 millisecond. This ensured that the opening and closing of the cold valves could be controlled more precisely. Experiments showed that the lag between the signal to open/close the cold valves and the actual opening/closing was less than 10 milliseconds, down from the more than 20 milliseconds with the Windows-based program.

The faster control program allowed for the expander to be run at a higher frequency. While the expander could not be run at faster than 1 Hz with a decent P-V graph with the Windows-based program, frequencies of up to 2 Hz were obtained with the real-time instrument. The faster expander cycle led to a higher rate of work extraction from the working fluid and hence a higher cooling rate (Figure 5.6).

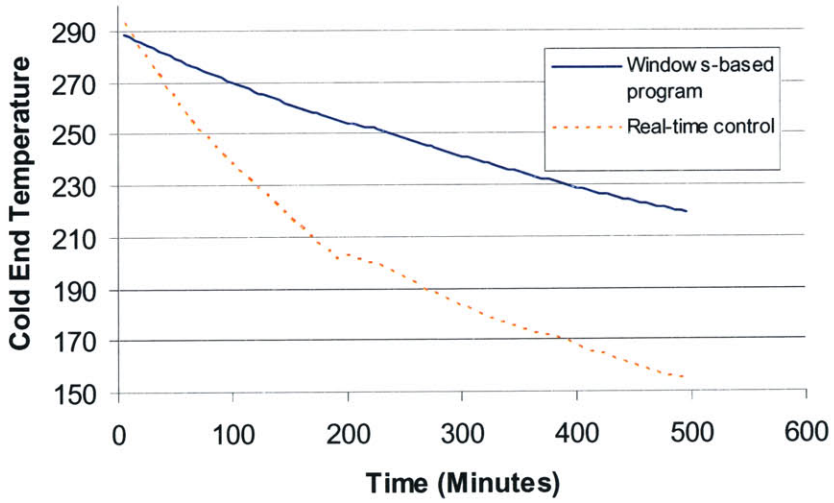

Figure 5.6: Cooling Rate Comparison

Previous experiments had raised concerns about the flow impedance of the heat exchanger. However, the whole issue of large heat exchanger pressure drops had tended to get clouded by the large leak rates. With the lower leak rates, a better understanding of heat-exchanger impedance was obtained.

It was noted that at room temperature, the piston still moved upwards during the first recompression, before starting downwards again. It had been hypothesised that high leak rates were responsible for this phenomenon; however, the tiny room temperature leak rates in the current system precluded that theory.

Pressure-time and position-time graphs at three different temperatures – 279 K, 187 K and 153 K – are shown in Figures 5.7a, 5.7b and 5.7c respectively, with the blow-in and intake strokes highlighted. At 279 K, the time taken to complete the blow-in and intake strokes was of the order of 50 milliseconds. At 153 K, the time taken was as high as 300 milliseconds. In the P-V graph at 153 K, it is seen that there is a preliminary spike in pressure, which is followed by a slow increase in pressure and position up to the end of the intake stroke. At 187 K, both kinds of cycles were observed – one with a blow-in/intake-stroke duration of 60 milliseconds and the other with a blow-in/intake-stroke duration of 300 milliseconds. This indicates that in some cycles, the pressure in the plenum was just high enough to complete the blow-in; in others, the plenum pressure was not high enough and additional flow through the heat exchanger passages was required to drive the pressure up. The fact that both kinds of cycles were observable at 187 K indicated that the pressure drop in the high-pressure passages of the heat exchanger and/or leaks were beginning to play a significant role.

As the expander and the heat exchanger cool down, the mass flow rate increases since the density of the working fluid increases with temperature. The increased mass flow rate is responsible for a larger pressure drop through the heat exchanger.

From Equation 4.23, $(\Delta p)(p_{avg}) \propto fTQ^2$

The pressure drop is directly proportional to the average temperature in the heat exchanger, but is also proportional to the square of the mass flow rate. The mass flow rate is inversely proportional to the temperature. Therefore, the pressure drop is actually inversely proportional to the temperature. The result is that the pressure at the exit of the high-pressure side of the heat-exchanger reduces with decreasing temperature. Therefore, with decreasing temperature, the intake stroke takes increasingly longer, as it takes more time for pressure to build up in the displacement volume and push the piston up.

As the expander cooled, it became increasingly difficult to operate at high intake pressures. The trend of decreasing "cycle maximum pressures" is obvious from the three figures. The parameters in the control program had to be appropriately modified (in particular, the blow-in process was stopped at a lower cylinder pressure) in order to keep the cycle going.

In order to keep the expander operating at an acceptable cycle maximum pressure, the high-pressure at the compressor discharge was increased to compensate for the pressure drop. This helped matters to some extent. However, the lengthening duration of the intake stroke reduced the rate of work done by the expander. The temperature bottomed out around 107 K, at which point the rate of expander work was only enough to balance the heat leak into the cold end.

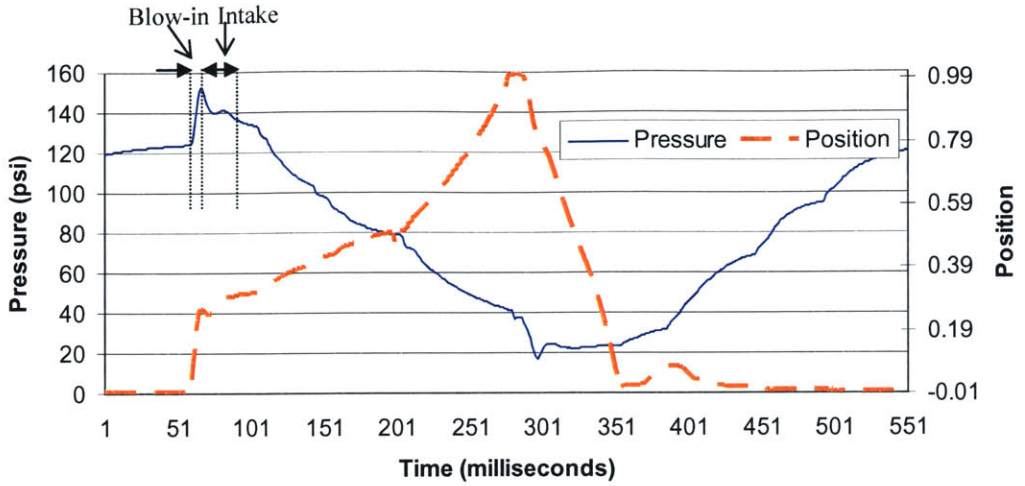

Figure 5.7a: P-t and V-t graphs at 279 K

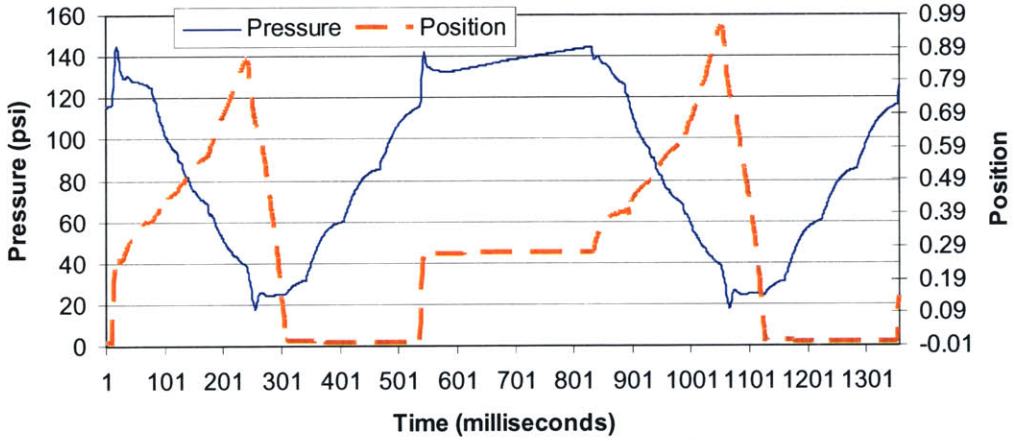

Figure 5.7b: P-t and V-t graphs at 187 K

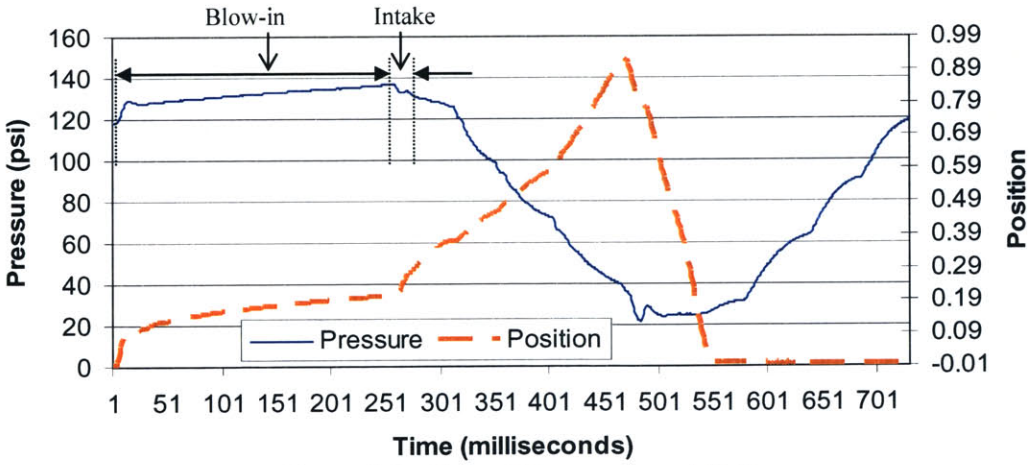

Figure 5.7c: P-t and V-t graphs at 153 K

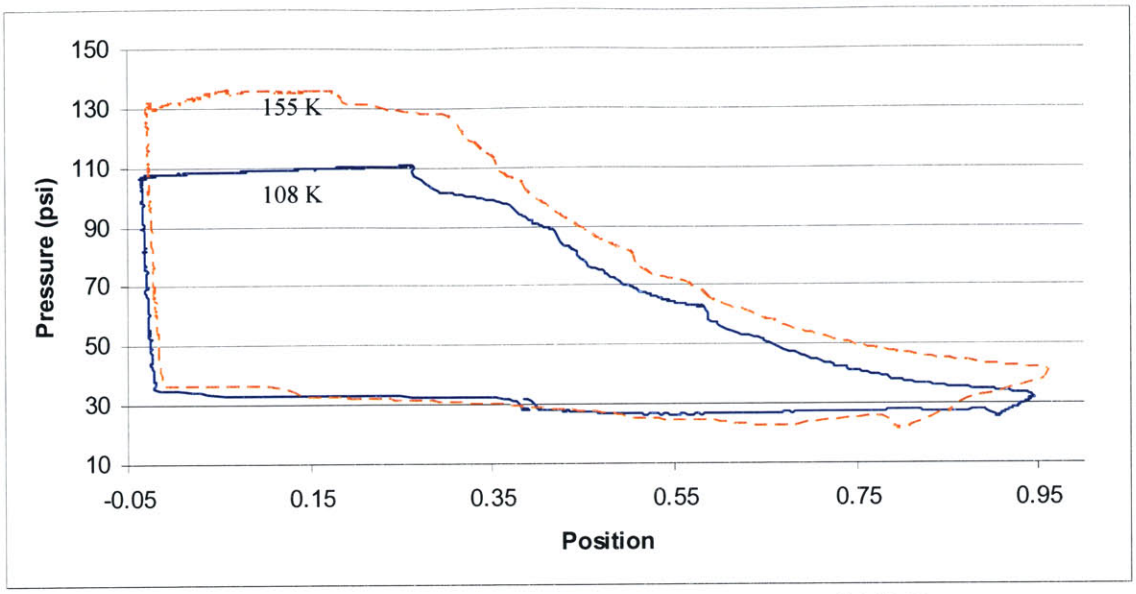

Figure 5.8: A comparison of P-V graphs at 155 K and 108 K

A comparison of the P-V graphs at 155 K and 108 K (Fig. 5.8) shows that the decrease in the maximum cylinder pressure was responsible for the decrease in expander work. In addition, the blow-in and intake strokes took nearly 1.1 seconds to complete at 108 K, which raised the cycle time to about 1.7 seconds, and further reduced the rate of work done by the expander.

It is worth noting that the time taken by all the processes except the blow-in and intake hardly changed from 300 K (about 0.5 seconds) to 110 K (about 0.6 seconds). The blow-in/intake stroke time, on the other hand, increased from about 50 milliseconds at 300 K to about 300 milliseconds at 150 K to 1100 milliseconds at 110 K. This resulted in a threefold decrease in expander frequency and a corresponding threefold reduction in the rate of work done by the expander.

Although the predicted heat-exchanger pressure drop does increase from 5.2 psi at 300 K to 9 psi at 150 K (Table 4.6), it is not nearly as high as the increase seen during experiments. Experimental data showed that the pressure at the end of the intake stroke was decreased from 140 psi at 279 K to 130 psi at 153 K. In the experiments described in section 5.2, the pressure at the end of the intake stroke changed from 120 psi to 117 psi from 300 K to 160 K. The predicted pressure drop only increased from 3 psi to 3.8 psi (Table 4.6).

These numbers suggested that the heat-exchanger pressure drop was not the only factor responsible for the deteriorating performance of the expander. A dynamic analysis of the expander, explained in the next chapter, indicated that a combination of high leak rates and high piston friction could have been responsible for the long blow-in/intake stroke durations. It was not immediately clear, though, why piston friction would have increased. A subsequent examination of the piston answered the question. The original stack of permanent magnets (suspended within the foam) had shifted downwards, and stressed a small part of the G10 tube,

causing it to expand radially. The 0.002" rise in diameter was responsible for increased friction between the piston and cylinder.

Another reason for the long intake duration was the size of the high-pressure plenum. The plenum is supposed to act as a flow capacitance, since the flow through the heat exchanger is continuous, while the flow into the displacement volume is pulsatory. The plenum volume was only twice the displacement volume, while similar capacitance volumes in the Collins Helium Liquefier are about 5 to 10 times the displacement volume. Due to large leakage flows, the small plenum is not able to supply enough high pressure gas for intake; the surplus gas must be supplied by flow through the heat exchanger.

With the original stack of magnets removed, piston friction reduced significantly and so did the blow-in/intake duration. Around 110 K, the duration was about 450 milliseconds, down from 1.1 seconds previously. The result was that the rate of work done by the expander increased and the stage cooled down to 76 K.

5.3.1 Heat Leak into the Cold End

To get an estimate of the heat leak into the cold end, the cool-down rate of the expander and the warm-up rate of the expander were calculated at the same temperature. The cool-down rate is proportional to the difference of the rate of work done by the expander, the rate of heat leak into the expander and heat exchanger losses. While the heat leak into the cold end is constant, the heat exchanger losses scale with the mass flow rate. The warm-up rate is proportional to the rate of heat leak only, since there is no flow through the heat exchanger during warm-up.

$$-\left(\frac{dT}{dt}\right)_{cooldown} \propto \dot{W}_{\exp} - \dot{Q}_{leak} - \dot{Q}_{heat\_ex\_loss} \qquad \ldots(5.1)$$

$$\left(\frac{dT}{dt}\right)_{warmup} \propto \dot{Q}_{leak} \qquad \ldots(5.2)$$

In the following analysis, the losses in the heat exchanger have been ignored.

At the same temperature, the two equations have the same constant of proportionality associated with them. Therefore, at the same temperature,

$$\frac{\dot{W}_{\exp} - \dot{Q}_{leak}}{-\left(\frac{dT}{dt}\right)_{cooldown}} = \frac{\dot{Q}_{leak}}{\left(\frac{dT}{dt}\right)_{cooldown}} \qquad \ldots(5.3)$$

The cold-end temperature is plotted as a function of time in Fig. 5.9. The expander started cooling down from 300 K. It cooled down to a temperature of 107 K, at which point the cold-end temperature stopped changing. The expander was then stopped and all valves were closed. The temperature of the cold end continued to be monitored in order to get an estimate of the warm-up rate. The kinks in the graph correspond to points at which the expander stopped running and had

to be restarted. The restarts were typically accompanied by a change in the parameters and an increase in the high pressure to overcome the heat exchanger pressure drop.

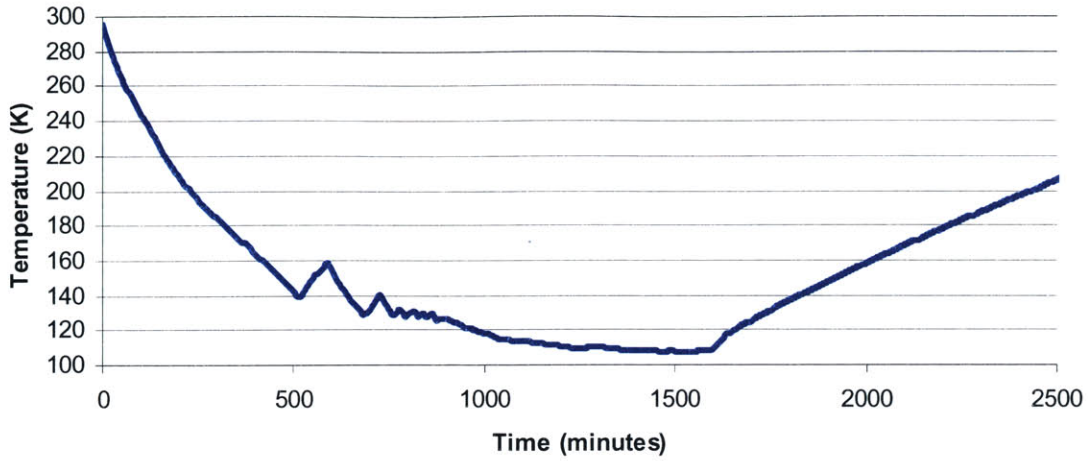

Figure 5.9: Cold End Temperature vs Time

The warm-up rates at various temperatures are tabulated below. The table indicates that the warm-up rate does not change significantly over the 125 K – 200 K temperature range.

Table 5.3: Warm-up rate as a function of temperature

Temperature(K)	dT/dt (K/minute)
125	0.120
150	0.108
175	0.096
200	0.090

To calculate the rate of work done by the expander at a particular temperature, the area under the P-V graph was determined and divided by the cycle time. This was done at two temperatures, 155.6 K and 148.1 K. The cool-down rates and the corresponding warm-up rates at these temperatures are listed in Table 5.4. P-V cycle data was recorded at several other temperatures but was not used in this analysis, since the frequent stop-starts were responsible for uneven cooling and hence inconsistent cool-down rates around those temperatures.

Table 5.4: Cool-down and warm-up rates at temperatures at which consistent data was available

Temperature(K)	Cool-down dT/dt (K/minute)	Warm-up dT/dt (K/minute)
155.6	0.194	0.104
148.1	0.220	0.108
108.2(min. temp.)	≈0	

To ensure that the rate of expander work was consistent at a particular temperature, the rate of work was calculated from two sets of data about 5-6 cycles apart and compared (the expander work calculation is explained in Appendix D).

Table 5.5: Rate of expander work

	Rate of expander work (cycle 1)			Rate of expander work (cycle 2)		
Temperature(K)	Cycle P-V work	Cycle time (secs)	Work Rate (W)	Cycle P-V work	Cycle time (secs)	Work Rate (W)
155.6	4.79 J	0.800	5.99	4.88 J	0.810	6.02
148.1	5.02 J	0.762	6.58	4.91 J	0.750	6.55
108.2	3.68 J	1.712	2.15	3.66 J	1.725	2.12

The rate of expander work was determined to be 6.00 W at 155.6 K and 6.56 W at 148.1 K. These values were used along with the cool-down and warm-up rates in Table 5.4 to determine the heat leak from Eq. 5.3. The data at 155.6 K yielded a heat leak rate of 2.09 W, while the data at 148.1 K yielded a heat leak rate of 2.16 W.

In order to confirm the heat leak rate, the expander work rate at 108 K was calculated. Since this was the lowest temperature attained, the expander work was just enough to balance the heat leak into the cold end. The calculated work rate (and hence the heat leak rate) of about 2.14 W was consistent with the 155.6 K and 148.1 K data.

CHAPTER 6 – DYNAMIC MODELLING OF EXPANDER

The static models developed in Chapter 2 do not adequately describe the performance of the expander. They assume the thermodynamic processes that make up the expander cycle to be quasi-static. These models are improved by incorporating the dynamics of the piston motion and the fluid flow through the warm and cold volumes. Since the blow-by past the piston was determined to be negligible in comparison to other flow rates in the expander, it was not incorporated into the model.

A program was written in Matlab to simulate the expander. Since the flow rates and piston speed depend on pressures and temperatures that are constantly changing, each of the 12 processes was broken up into a series of steps taking place over small time intervals. The intervals were small enough to ensure that the properties in the warm end and cold end could be assumed to be constant over that step.

Each of the individual steps consists of the following:

- All mass flows through the heat exchanger passages, cold and warm volumes are calculated from the constant properties (specifically, pressure and temperature).
- The pressures in the cold and warm ends, as well as the initial velocity of the piston are used to calculate the velocity, acceleration and final position of the piston.
- The final position of the piston is used to calculate the volume of helium in the cold end and the warm end.
- The equations developed in Chapter 2 are used to update the pressures and temperatures in the warm and cold volumes.
- If there is flow into or out of a warm reservoir, the pressure in the warm reservoir is updated.
- The pressures in reservoirs A and D are updated (these pressures change due to warm-end bleeds).
- The cold-end plenum pressure is updated.

The smaller steps associated with a particular process are repeated until the condition for switching from the current process to the next process is fulfilled. The switching conditions are the same as the ones used in the Labview control routine - ten constants, a cut-off volume and a recompression volume are specified.

The program starts with a set of specified initial properties and executes the expander processes. The cycle is repeated a specified number of times. It can be repeated until equilibrium is observed. Ten cycles are typically enough to reach a steady state solution.

6.1 Dynamic Models

6.1.1 Modelling of flow through warm and cold valves

The helium flow through the warm and cold valves was modelled as a choked flow. White[10] gives the following formula for choked flow through a nozzle:

$$\frac{\dot{m}}{A} = \frac{p_o}{\sqrt{RT_o}}\sqrt{\frac{2\gamma}{\gamma-1}r^{2/\gamma}\left(1-r^{(\gamma-1)/\gamma}\right)} \qquad \ldots(6.1)$$

where p_o and T_o are the stagnation pressure and temperature respectively, γ is the adiabatic constant for the gas and r is the ratio of the exit pressure and the stagnation pressure if the flow is subsonic and the ratio of the critical pressure and the stagnation pressure if the flow is sonic.

$$p_{crit} = p_o\left(\frac{2}{\gamma+1}\right)^{\frac{\gamma}{\gamma-1}} \qquad \ldots(6.2)$$

After the modification to the lift of the cold end valves, the minimum valve area corresponded to a valve port diameter of 0.060 inches. The minimum valve area at the warm end corresponded to a port diameter of 0.040 inches.

A function was written in Matlab, which, given the stagnation pressure and temperature, the pressure difference across the valve, returned the amount of mass passing through the valve in a specified amount of time. The code is given in Appendix F.

6.1.2 Modelling of flow through the high pressure passages of the heat-exchanger

The Matlab models originally developed modelled the cold-end plenum as a constant pressure reservoir. The timings for the intake stroke predicted by this model were orders of magnitude lower than those observed during experimental runs. In reality, the plenum chamber had a finite volume that was only about twice the displacement volume. In addition, the heat exchanger pressure-drop tests showed that the major flow resistance in the high-pressure side was the heat-exchanger tube (which was 0.040 inches in diameter and about 350 inches in length), and not the valve-port, which was 0.060 inches in diameter and 0.25 inches in length. In order to get a more accurate model of the intake stroke, the heat exchanger impedance was incorporated into the model.

The flow through the high-pressure passages of the heat-exchanger was modelled according to the correlations developed in Chapter 4. The mass flow rate through a single heat exchanger coil was calculated from both laminar and turbulent flow correlations (Eq. 4.8 and Eq. 4.11), and the lower value was used in the model. Figures 4.4 and 4.5 indicate that this approximation is valid.

$$\dot{m}_{hx} = 2 * \min\left(\frac{p_{hp}^{\,2} - p_{plenum}^{\,2}}{2}\frac{\pi D^4}{128\mu \mathrm{RTL}}, \sqrt{\frac{p_{hp}^{\,2} - p_{plenum}^{\,2}}{16RTL}\pi^2 D^5 f}\right) \qquad \ldots(6.3)$$

where p_{hp} is the pressure at the compressor discharge, p_{plenum} is the pressure in the high-pressure plenum, L is the length of a heat exchanger coil, D is the diameter of the heat exchanger coil, R is the gas constant for helium, T in the turbulent correlation is the average temperature in the heat exchanger, f is a friction factor for turbulent flow, and the product μT in the laminar correlation is the product of temperature and viscosity averaged over the heat exchanger.

6.1.3 Modelling of the piston motion

The forces acting on the piston are the pressure forces at the two ends, the weight of the piston, and the friction force. The static and dynamic friction forces were assumed to be equal. It was experimentally determined that the piston needed a pressure difference of about 3 psi to start moving.

A piston function written in Matlab, when given the pressure difference across the piston, the initial velocity, the initial position, returns the final position, velocity and acceleration of the piston, for a specified time step. The function calculates the net force acting on the piston, and hence the acceleration. Equations of motion are then used to calculate the final velocity and position of the piston. The code is given in Appendix F.

6.1.4 Modelling of the warm-end bleeds

It was assumed that the flow rate through the warm-end throttles varied with the square root of the pressure difference across the valve. Two initial constants of proportionality are calculated, one for each valve. These constants are representative of the flow-resistances of the valves.

$$\dot{m}_{bleedinA} = b_1\sqrt{p_{high} - p_A} \qquad \ldots(6.4a)$$

$$\dot{m}_{bleedoutD} = b_2\sqrt{p_D - p_{low}} \qquad \ldots(6.4b)$$

where b_1 and b_2 are the constants of proportionality, p_{high} and p_{low} are the pressures at the compressor discharge and suction respectively, and p_A and p_D are the pressures in reservoirs A and D respectively.

The initial values of the constants are based on the estimated flow rates required to keep the pressures in A and D constant and the approximate pressure differences across the valves. The flow-rate estimates were made by running the program without the bleed-valve model and noting the change in mass of reservoirs A and D over a cycle.

After every expander cycle, the two constants are increased, decreased or kept the same, depending on the pressures in the reservoirs. The constant b_1 is updated according to the following algorithm:

If $P_A > P_{A,required}$ *and* P_A *has increased over the last cycle (i.e. too much bleed)*
decrease b_1

If $P_A < P_{A,required}$ *and* P_A *has decreased over the last cycle (i.e. too little bleed)*
increase b_1

The constant b_2 is updated in a similar way, the only difference being that it is increased if the pressure in D is too high and decreased if the pressure in D is too low.

6.2 Simulation Results

The program is designed to analyse the expander at a particular cold-end temperature. Therefore, the cold end temperature must be specified along with certain other cycle constants (compressor

inlet pressure, compressor exit pressure, switching condition constants, warm-end reservoir temperature) before running the expander loop. The average heat exchanger temperature is required to calculate the flow-rate through the high-pressure passages. In a balanced flow configuration, however, the average temperature is simply the mean of the inlet temperature (300 K) and the cold end temperature.

A time-step of 0.1 milliseconds was used in the program. A time-step of 0.01 milliseconds did not produce a significant change in the P-V diagram. However, the ten-fold decrease in the time-step increased the program run-time by a factor of 100.

A P-V diagram is shown in Figure 6.1. The pressures and piston position over a cycle are plotted as a function of time in Figure 6.2. The cycle constants used are given in Table 6.1.

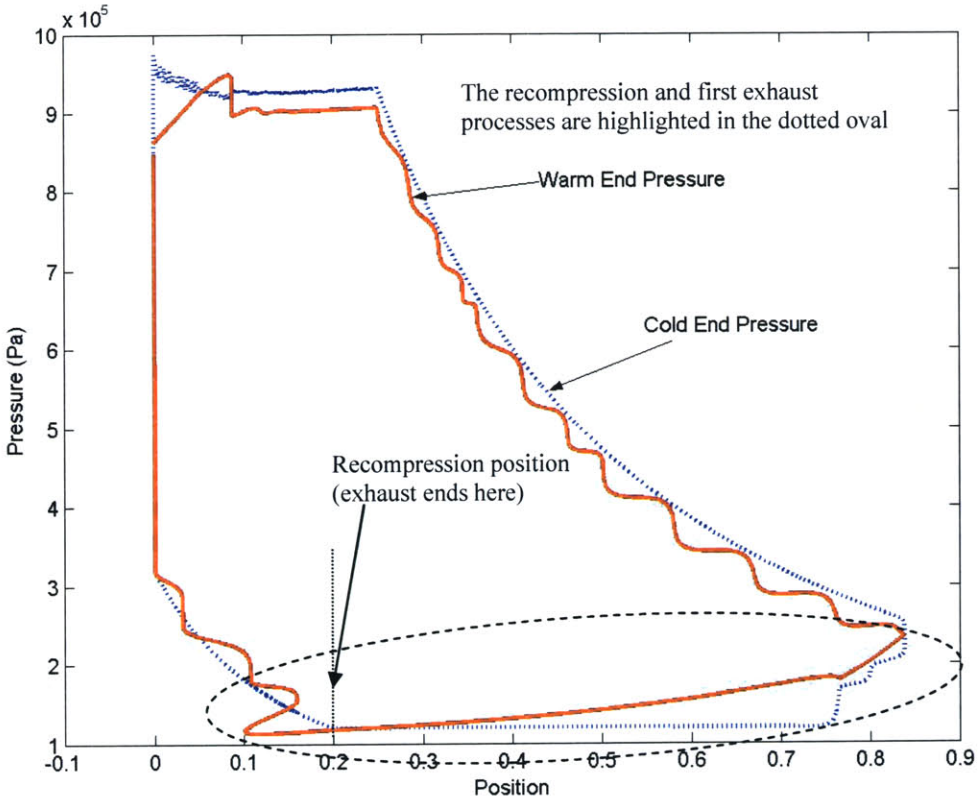

Figure 6.1: Simulated Pressure-Position Diagram

The P-V diagram obtained from the program is very similar to experimentally observed P-V diagrams. The one major difference is the 'waviness' seen in the warm-end pressure during the expansion and recompression processes.

Table 6.1: Cycle constants

Compressor exit pressure	10 atm
Compressor inlet pressure	1.2 atm
Cold End temperature	300 K
Average heat exchanger temperature	300 K
Cut-off position	0.25
Recompression position	0.2
Initial reservoir pressures (A and D held nearly constant through bleeds)	9 atm, 6 atm, 4.5 atm, 1.8 atm
Switching condition constts – c_1, c_{1a}, c_3, c_4, c_5, c_6, c_{6a}, c_8, c_9, c_{10}	0.97, 0.92, 1.01, 1.02, 1.03, 1.5, 1.2, 0.95, 0.95, 0.97

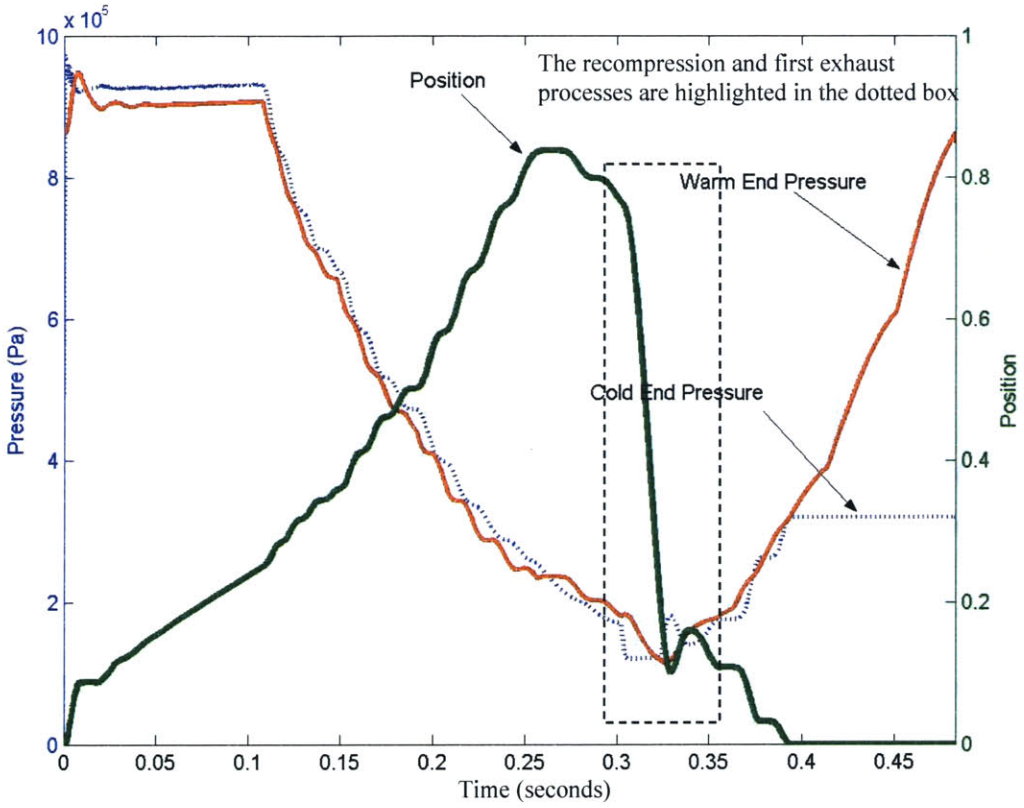

Figure 6.2: Warm end pressure, Cold end pressure and position as a function of time

During the expansion processes, there is a pressure difference across the piston which causes it to accelerate upwards. The rapid acceleration expands the gas in the cold end very quickly. It also causes the gas in the warm end to expand very slowly even though the warm end is open to one of the reservoirs. This results in the pressure differential across the piston dropping to a very low value and a rapid deceleration of the piston due to friction. The piston continues to move up due to inertia; however, the warm end pressure decreases very slowly. When the piston decelerates to a very low velocity, the warm end pressure begins to decrease more rapidly as gas flows into the

warm reservoir. The cold end pressure on the other hand, decreases very slowly due to the low velocity. This builds up the pressure differential across the piston and the process is repeated. The cold end pressure, warm end pressure, piston position, velocity and acceleration over a part of the expansion process are plotted as functions of time in Figure 6.3. It can be seen that the acceleration varies about a mean of about zero. The velocity oscillates, but never goes to zero. The cold end and warm end pressures alternate between fast and slow rates of expansion and are always out of sync with each other. The cold end pressure is always in sync with the piston position, since they are related by the adiabatic relation $PV^{\gamma} = constant$. This is why the cold end pressure does not appear to fluctuate in Fig. 6.1.

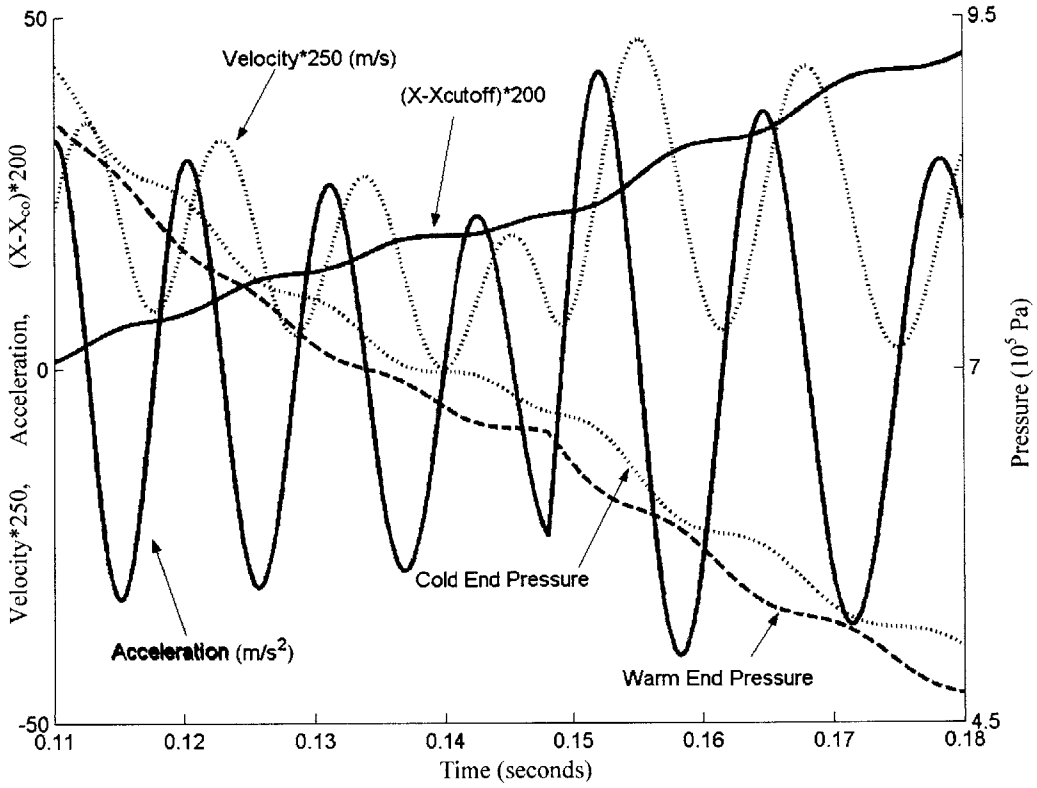

Figure 6.3: Cold-end pressure, warm-end pressure, and piston position, velocity and acceleration as a function of time during expansion

The same phenomenon is observed during the recompression processes.

The simulation helped explain the behaviour of the expander during the exhaust and the first recompression processes. The P-V diagrams obtained during experiments showed that the warm-end pressure continued to decrease even when the piston was past the recompression volume. It had previously been assumed that the reason for this was a delay associated with the closing of the exhaust valve. However, the simulation results indicated that this was not the case. In Figure 6.1, it can be seen that the warm end pressure keeps decreasing past the recompression volume,

just like in the experiments. It can also be seen that the cold end pressure starts increasing as soon as the recompression volume is hit. During the final stages of the exhaust, the piston has a large downward velocity (Fig. 6.2) as a result of the high pressure differential across it in the early stages of the exhaust. The rapid descent of the piston prevents the warm end pressure from rising even after the cold exhaust valve has closed.

It had also been noted that the piston moved up during the first recompression. It had previously been assumed that this was due to leaks past the cold intake valve which were driving the cold volume pressure up. However, the model proved that this was a consequence of the high piston velocity during exhaust. As soon as the exhaust valve is closed, the pressure in the cold volume begins to rise rapidly. The high downward velocity piston velocity, which prevents the warm volume pressure from rising, is also responsible for the sharp rise in cold volume pressure. This leads to a large upward pressure differential across the piston. The large pressure differential causes the downward moving piston to decelerate and accelerate upwards. The upward motion results in an expansion of the gas in the cold end. At the same time, the flow from reservoir D into the warm end as well as the upward moving piston cause the warm end pressure to increase. After a few milliseconds, the pressure differential is reversed. The piston changes direction again and starts moving downwards to complete the remainder of the recompression processes.

At 300 K, the timings predicted by the program for the expansion and recompression processes were less than those observed during experiments. It was apparent that the choked flow model used for flows between the warm end and the reservoirs underestimated the combined impedance of the flow-passages in the warm end cap and the solenoid valve. A four-fold decrease in the area available for flow (Eq. 6.1) yielded timings that were very close to the experimental data. The only effect the change had on the P-V diagram was to increase the number of warm end pressure oscillations - since the expansion time was greater and the natural frequency of the piston stayed the same, more oscillations were observed. The P-V diagram shown in Figure 6.1 was obtained with the reduced flow area.

6.3 Factors affecting the blow-in and intake stroke durations

A condensed version of the program was used to analyse the effect of the heat exchanger configuration, the plenum chamber size, leaks and piston friction on the duration of the blow-in and intake strokes at various temperatures. Of the twelve processes, only the blow-in and intake processes were retained in the program. Experiments had shown that the time associated with the remainder of the cycle stayed more-or-less constant around 500-600 milliseconds. Therefore, instead of analysing the remaining processes in detail, they were replaced by a constant-time plenum-refill process. This process, like the others, was broken into small time-steps. In each time step, the mass flow through the high-pressure passages of the heat exchanger was calculated and the plenum pressure updated. The process was continued until the individual time-steps added up to a total time of 0.5 seconds. At the end of every cycle (consisting of the blow-in, intake and refill processes), the conditions in the cold end and warm end were reinitialised to the same value. This was done to simulate a state of equilibrium.

The program was run at two different cold-end temperatures – 300 K and 100 K. A compressor exit pressure of 10 atm was used for the simulation. The pressure in reservoir A was set at 9 atm. The cycle constants for the blow-in and intake strokes (c_{1a} and the cut-off volume, respectively) were kept the same as before. These values were very close to the actual parameter values during expander operation. None of the other constants were required for this program - the blow-in and intake stroke timings are only affected by the pressure in reservoir A and the pressure in the cold-end plenum at the beginning of the blow-in.

It was observed that it took about 5-6 cycles for the blow-in/intake stroke durations to settle down to a constant value. At 300 K, the predicted blow-in/intake stroke time was about 130 milliseconds. It increased to 250 milliseconds at 100 K. The change was not nearly as drastic as that observed during experiments, even though it did suggest deteriorating heat exchanger performance. To ascertain the effect of leaks on stroke timings at low temperature, leak rates of the order of those observed at about 110 K (about 4 slm) were incorporated into the model. With leak rates, the blow-in/intake time only increased to about 400 milliseconds, still well below the 1 second observed during the experiments described in Section 5.3.

The effect of piston friction on the blow-in/intake stroke timing was then studied. It was found that an increase in the piston friction from 3 psi to 6 psi increased the duration to over 800 milliseconds. It was, therefore, concluded that the combination of higher leak rates and increased piston friction was largely responsible for the poor performance of the cycle at lower temperatures.

In the final expander cool-down test, with the piston friction problem having been rectified, blow-in/intake stroke durations of about 450 milliseconds were observed at 100 K. This data was consistent with the "leaks only" model which predicted a blow-in/intake time of 400 milliseconds.

When the full expander program was run with the increased piston friction condition, it was found that the duration of the remainder of the cycle hardly changed – only the blow-in and intake strokes took longer. This was consistent with the experimental data, and justified the assumption made in the condensed expander program (that of constant time taken by the remainder of the cycle).

The effect of increasing the number of heat exchanger coils on the blow-in/intake stroke durations was then studied. It was found that increasing the number of heat exchanger coils from 2 to 4 resulted in a huge decrease in duration at 100 K, from 800 milliseconds to 170 milliseconds. In the absence of the increased piston friction, the duration decreased to 115 seconds. In the absence of leaks, it decreased even further to 102 seconds.

In the next series of simulations, the effects of increasing the size of the cold-end plenum were studied. Increasing the size of the plenum does lead to an improvement, especially if piston friction is low.

The blow-in/intake valve duration results are summarised in Table 6.2.

These results indicate that the heat exchanger impedance is not a limiting factor at temperatures of about 100 K if leak rates and piston friction are kept within reasonable limits. As the final expander test proved, it is not difficult to keep the piston friction low. On the other hand, if the relatively large leak rates continue to persist, configuration changes may be necessary. Although doubling the number of heat exchanger coils will make a significant difference to the expander work rate, it will cut the NTU in half and increase heat exchanger losses. Increasing the plenum volume, on the other hand, will increase the expander work rate while keeping heat exchanger losses low.

Table 6.2: Blow-in/intake stroke duration

Model	Duration with present configuration	Duration with 4 high-pressure coils	Duration with plenum volume doubled	Duration with plenum volume quadrupled
300 K	130 ms	65 ms	85 ms	60 ms
100 K	250 ms	105 ms	170 ms	100 ms
100 K with leaks	400 ms	115 ms	330 ms	250 ms
100 K with piston friction doubled	430 ms	145 ms	370 ms	300 ms
100 K with leaks and piston friction doubled	800 ms	170 ms	745 ms	725 ms

CHAPTER 7 – CONCLUSIONS

The objective of this project was to study the behaviour of a single stage of a 10 K cryocooler through modelling and experimental testing. The third stage of the cryocooler was manufactured and tested. Static models were developed to help determine operational parameters for the expander. Dynamic models were later developed to get a better understanding of the various expander processes.

Over the course of the project, several design issues which need to be rectified in future iterations of the expander were identified. The cold end needs to be redesigned to ensure better sealing and to reduce the dead volume. The current magnitudes of leaks in the system are extremely detrimental to the performance of the expander. They are responsible for an increased mass flow through the heat exchanger and consequently, larger heat exchanger losses. In addition, they increase the heat leak into the cold end. By increasing the duration of the intake stroke, they are also responsible for a reduced expander work rate. Analytical models predicted that an increase in the size of the cold-end plenum would help remedy the problem of increased intake-stroke duration to some extent.

The large dead volume prevents the expander from being run at compressor pressure ratios above about 9:1, while the machine was originally designed for pressure ratios of 15:1.

When run as a refrigerator with no heat load, the stage cooled from room temperature down to 76 K. At this point, a combination of cold-end leaks and heat exchanger impedance reduced the expander work rate to an extent where it could not overcome heat leaks into the cold end.

Once these issues have been sorted out, several experiments can be performed to further characterise the performance of the expander. The expander rig has a load heater, which can be used to determine the cooling capacity of the expander at various temperatures. The pre-cooling line will also allow the stage to be run as the third stage of the proposed cryocooler.

The dynamic model developed to simulate the expander was primarily used to gain a better understanding of the expander processes and to identify the factors responsible for the compromised performance of the expander during initial testing. It was used to suggest design changes for future prototypes. It can also be used to optimise expander performance. The expander can be optimised by determining sets of cycle constants appropriate for specific operating conditions.

The model can also be used to develop a better control routine. The control routine currently in use does not have provisions to make changes to cycle constants or the capability to manipulate the pressures in the warm end reservoirs. An intelligent control routine will contain algorithms that are capable of modifying these constants based on the temperature at various points in the stage and recent cycle data. These algorithms can be easily incorporated into the expander model and tested analytically. As an example, the current iteration of the expander model contains a rudimentary algorithm that simulates control of the warm end bleed flow and serves to maintain the pressures in reservoirs A and D at desired levels.

Several improvements can be made to the expander model. The choked flow models for flow through the warm end are simplistic, since they do not take into account the tiny flow-passages that lead from the warm displacement volume to the reservoirs. The impedance of the passages and the solenoid valves need to be experimentally measured and a better flow model developed for use.

At this point, the expander model can only be used to analyse the cycle at a particular temperature and does not provide any information about cool-down rates. By incorporating the heat capacity of the cold end and the cold-end heat-leak into the model, this information can be obtained.

REFERENCES

1. Hannon, C.L., Gerstmann, J., Traum, M., Brisson, J.G., Smith Jr, J.L., "Development of a Medium-Scale, Collins-type 10 K Cryocooler", Cryocoolers 12, Kluwer Academic/ Plenum Publishers, New York, 2003, pp. 587-594

2. Crunkleton, J.A., "A New Configuration for a Small-Capacity, Liquid Helium Temperature Cryocooler", Doctoral Thesis, Massachusetts Institute of Technology, September 1987

3. Ceridon, K.M., "Remote Cooling using Cold Electromagnetic Valves to Drive an External Flow Loop on a Gifford-McMahon Cryocooler", Master's Thesis, Massachusetts Institute of Technology, June 2001

4. Jones, R.E., "Design and Testing of Experimental Free-Piston Cryogenic Expander", Master's Thesis, Massachusetts Institute of Technology, February 1999

5. Traum, M.J., "Development of a Cold End and High-Efficiency Valves for a One-Watt 10 Kelvin Cryocooler", Master's Thesis, Massachusetts Institute of Technology, June 2003

6. http://www.azom.com/details.asp?ArticleID=996
   http://www.azom.com/details.asp?ArticleID=965

7. Cravalho, E.G. and Smith Jr., J.L., Engineering Thermodynamics, Massachusetts Institute of Technology, Cambridge, MA, 1992

8. Mills, A.F., Basic Heat and Mass Transfer, Irwin, Chicago, 1995, pp. 235-236

9. Scott, R.B., Cryogenic Engineering, D. Van Nostrand Co., Princeton, New Jersey, 1959

10. White, F.M., Fluid Mechanics, 5th Edition, McGraw-Hill, New York, 2003

APPENDIX A: EQUATIONS FOR DETERMINATION OF STATE IN THE EXPANDER CYCLE

A1. Cold End (Ideal cycle)

Equations for three unknowns at each stage are given. The fourth unknown can be calculated from the equation $PX=mT$.

State 1a:

$$P_{1a} = P_h \qquad X_{1a} = 1 + X_{cc} + X_{cw} - X_{1a,warm}$$

$$m_{1a} = \frac{(P_{1a}X_{1a} - P_1X_1) + [m_1(T_{1a} - T_1)]_{warm}}{T_{in}\gamma} + m_1$$

State 2:

$$P_2 = P_h \qquad X_2 = X_{co} + X_{cc} \qquad m_2 = \frac{P_2X_2 - P_{1a}X_{1a}}{T_{in}} + m_{1a}$$

State 3:

$$P_3 = P_a \qquad X_3 = X_2\left(\frac{P_2}{P_3}\right)^{\left(\frac{1}{\gamma}\right)} \qquad T_3 = T_2\left(\frac{P_3}{P_2}\right)^{\left(\frac{\gamma-1}{\gamma}\right)}$$

State 4:

$$P_4 = P_b \qquad X_4 = X_3\left(\frac{P_3}{P_4}\right)^{\left(\frac{1}{\gamma}\right)} \qquad T_4 = T_3\left(\frac{P_4}{P_3}\right)^{\left(\frac{\gamma-1}{\gamma}\right)}$$

State 5:

$$P_5 = P_c \qquad X_5 = X_4\left(\frac{P_4}{P_5}\right)^{\left(\frac{1}{\gamma}\right)} \qquad T_5 = T_4\left(\frac{P_5}{P_4}\right)^{\left(\frac{\gamma-1}{\gamma}\right)}$$

State 6:

$$P_6 = P_d \qquad X_6 = X_5\left(\frac{P_5}{P_6}\right)^{\left(\frac{1}{\gamma}\right)} \qquad T_6 = T_5\left(\frac{P_6}{P_5}\right)^{\left(\frac{\gamma-1}{\gamma}\right)}$$

State 6a:

$$P_{6a} = P_l \qquad X_{6a} = 1 + X_{cc} + X_{cw} - X_{6a,warm} \qquad m_{6a} = \frac{P_6X_{6a}}{T_6}\left(\frac{P_{6a}}{P_6}\right)^{\left(\frac{1}{\gamma}\right)}$$

$$T_{out} = \frac{[m_6(T_6 - T_{6a})]_{warm} + m_6T_6 - m_{6a}T_{6a}}{(m_6 - m_{6a})\gamma}$$

State 7:

$P_7 = P_l$ $\quad X_7 = X_{rc} + X_{cc}$ $\quad T_7 = T_{6a}$

$T_{out} = T_{6a}$

$$P_{rc} = P_7\left(\frac{X_7}{X_{cc}}\right)^{\gamma} \qquad T_{cc} = \frac{P_{cc}X_{cc}}{m_7}$$

State 8:

$m_8 = m_7$

If $P_d > P_{rc}$ $\quad P_8 = P_{rc}$ $\quad X_8 = X_{cc}$

Else $\quad P_8 = P_d$ $\quad X_8 = X_7\left(\frac{P_7}{P_8}\right)^{\left(\frac{1}{\gamma}\right)}$

State 9:

$m_9 = m_7$

If $P_c > P_{rc}$ $\quad P_9 = P_{rc}$ $\quad X_9 = X_{cc}$

Else $\quad P_9 = P_c$ $\quad X_9 = X_8\left(\frac{P_8}{P_9}\right)^{\left(\frac{1}{\gamma}\right)}$

State 10:

$m_{10} = m_7$

If $P_b > P_{rc}$ $\quad P_{10} = P_{rc}$ $\quad X_{10} = X_{cc}$

Else $\quad P_{10} = P_b$ $\quad X_{10} = X_9\left(\frac{P_9}{P_{10}}\right)^{\left(\frac{1}{\gamma}\right)}$

State 1:

$m_1 = m_7$

If $P_a > P_{rc}$ $\quad P_1 = P_{rc}$ $\quad X_1 = X_{cc}$

Else $\quad P_1 = P_a$ $\quad X_1 = X_{10}\left(\frac{P_{10}}{P_1}\right)^{\left(\frac{1}{\gamma}\right)}$

A2. Warm End

State 1a:

$$P_{1a} = P_h \qquad X_{1a} = X_1\left(\frac{P_1}{P_{1a}}\right)^{\left(\frac{1}{\gamma}\right)} \qquad T_{1a} = T_1\left(\frac{P_{1a}}{P_1}\right)^{\left(\frac{\gamma-1}{\gamma}\right)}$$

State 2:

$$P_2 = P_h \qquad X_2 = 1 + X_{cc} + X_{cw} - X_{co} \qquad T_2 = T_{1a}$$

State 3:

$$P_3 = P_a \qquad X_3 = 1 + X_{cc} + X_{cw} - X_{3,cold} \qquad m_3 = \frac{P_2 X_3}{T_2}\left(\frac{P_3}{P_2}\right)^{\left(\frac{1}{\gamma}\right)}$$

State 4:

$$P_4 = P_b \qquad X_4 = 1 + X_{cc} + X_{cw} - X_{4,cold} \qquad m_4 = \frac{P_3 X_4}{T_3}\left(\frac{P_4}{P_3}\right)^{\left(\frac{1}{\gamma}\right)}$$

State 5:

$$P_5 = P_c \qquad X_5 = 1 + X_{cc} + X_{cw} - X_{5,cold} \qquad m_5 = \frac{P_4 X_5}{T_4}\left(\frac{P_5}{P_4}\right)^{\left(\frac{1}{\gamma}\right)}$$

State 6:

$$P_6 = P_d \qquad X_6 = 1 + X_{cc} + X_{cw} - X_{6,cold} \qquad m_6 = \frac{P_5 X_6}{T_5}\left(\frac{P_6}{P_5}\right)^{\left(\frac{1}{\gamma}\right)}$$

State 6a:

$$P_{6a} = P_l \qquad X_{6a} = X_6\left(\frac{P_6}{P_{6a}}\right)^{\left(\frac{1}{\gamma}\right)} \qquad T_{6a} = T_6\left(\frac{P_{6a}}{P_6}\right)^{\left(\frac{\gamma-1}{\gamma}\right)}$$

State 7:

$$P_7 = P_l \qquad X_7 = 1 + X_{cc} + X_{cw} - X_{rc} \qquad m_7 = \frac{P_7 X_7 - P_{6a} X_{6a}}{T_d} + m_{6a}$$

State 8:

$$P_8 = P_d \qquad X_8 = 1 + X_{cc} + X_{cw} - X_{8,cold}$$

$$m_8 = \frac{P_8 X_8 - P_7 X_7 + (P_8 X_8 - P_7 X_7)_{cold}}{T_d \gamma} + m_7$$

State 9:

$$P_9 = P_c \qquad X_9 = 1 + X_{cc} + X_{cw} - X_{9,cold}$$

$$m_9 = \frac{P_9 X_9 - P_8 X_8 + (P_9 X_9 - P_8 X_8)_{cold}}{T_c \gamma} + m_8$$

State 10:

$$P_{10} = P_b \qquad X_{10} = 1 + X_{cc} + X_{cw} - X_{10,cold}$$

$$m_{10} = \frac{P_{10} X_{10} - P_9 X_9 + (P_{10} X_{10} - P_9 X_9)_{cold}}{T_b \gamma} + m_9$$

State 1:

$$P_1 = P_a \qquad X_1 = 1 + X_{cc} + X_{cw} - X_{1,cold}$$

$$m_1 = \frac{P_1 X_1 - P_{10} X_{10} + (P_1 X_1 - P_{10} X_{10})_{cold}}{T_a \gamma} + m_{10}$$

A3. Cold End (Modified for Non-Ideal cycles)

State 3:

$$X_3 = \max\left(X_2 \left(\frac{P_2}{P_a}\right)^{\left(\frac{1}{\gamma}\right)}, 1 + Xcc \right) \qquad P_3 = P_2 \left(\frac{X_2}{X_3}\right)^{\gamma} \qquad T_3 = T_2 \left(\frac{P_3}{P_2}\right)^{\left(\frac{\gamma-1}{\gamma}\right)}$$

State 4:

$$X_4 = \max\left(X_3 \left(\frac{P_3}{P_b}\right)^{\left(\frac{1}{\gamma}\right)}, 1 + Xcc \right) \qquad P_4 = P_3 \left(\frac{X_3}{X_4}\right)^{\gamma} \qquad T_4 = T_3 \left(\frac{P_4}{P_3}\right)^{\left(\frac{\gamma-1}{\gamma}\right)}$$

State 5:

$$X_5 = \max\left(X_4 \left(\frac{P_2}{P_c}\right)^{\left(\frac{1}{\gamma}\right)}, 1 + Xcc \right) \qquad P_5 = P_4 \left(\frac{X_4}{X_5}\right)^{\gamma} \qquad T_5 = T_4 \left(\frac{P_5}{P_4}\right)^{\left(\frac{\gamma-1}{\gamma}\right)}$$

State 6:

$$X_6 = \max\left(X_5 \left(\frac{P_2}{P_d}\right)^{\left(\frac{1}{\gamma}\right)}, 1 + Xcc \right) \qquad P_6 = P_5 \left(\frac{X_5}{X_6}\right)^{\gamma} \qquad T_6 = T_5 \left(\frac{P_6}{P_5}\right)^{\left(\frac{\gamma-1}{\gamma}\right)}$$

APPENDIX B: CHANGE IN PRESSURE OF GAS IN A RESERVOIR

Consider a reservoir k that is open during the process i to i+1.

Mass in reservoir $m = \frac{P_{res}V_{res}}{RT_{res}}$

Change in mass of the reservoir $\Delta m = -\left(\frac{P_{i+1}V_{i+1}}{RT_{i+1}} - \frac{P_iV_i}{RT_i}\right)$

$$\frac{\Delta m}{m} = -\left(\frac{P_{i+1}V_{i+1}}{T_{i+1}} - \frac{P_iV_i}{T_i}\right)\frac{T_{res}}{V_{res}P_{res}}$$

$$P_{i+1} = \frac{P^*_{i+1}}{P^*_{in}}P_{in} \qquad P_{res} = \frac{P^*_{res}}{P^*_{in}}P_{in} \qquad T_{i+1} = \frac{T^*_{i+1}}{T^*_{res}}T_{res} \qquad V_{i+1} = X^*_{i+1}V_{swept}$$

Substituting,

$$\frac{\Delta m}{m} = -\left(\frac{P^*_{i+1}X^*_{i+1}}{T^*_{i+1}} - \frac{P^*_iX^*_i}{T^*_i}\right)\frac{P_{in}V_{swept}T^*_{res}}{P^*_{in}T_{res}}\frac{T_{res}P^*_{in}}{V_{res}P^*_{res}P_{in}}$$

$$\Rightarrow \frac{\Delta m}{m} = \left(m^*_i - m^*_{i+1}\right)\frac{V_{swept}T^*_{res}}{V_{res}P^*_{res}}$$

As the temperature of the reservoir is assumed to be constant, the pressure in the reservoir is directly proportional to the amount of mass in the reservoir. The new reservoir pressure can thus be calculated from the change in mass over a process.

$$\therefore P_{res,new} = \frac{m_{res,new}}{m_{res,old}}P_{res,old} \qquad \Rightarrow P_{res,new} = \left(1 + \frac{\Delta m_{res}}{m_{res,old}}\right)P_{res,old}$$

APPENDIX C: CYCLE STABILITY - CONVERGENCE TO A STEADY STATE

The table below shows the results of two cycle stability runs with different initial conditions. It shows that the reservoir pressures at steady state depend only on the sum of the warm-end reservoir pressures (i.e., the total mass in the warm end) and not on the initial reservoir pressures.

Cut-Off Volume = 0.23, Recompression Volume = 0.1,
Sum of reservoir pressures = 23.5 * P_{out}

No. of cycles	P_a/P_{out}	P_b/P_{out}	P_c/P_{out}	P_d/P_{out}	P_a/P_{out}	P_b/P_{out}	P_c/P_{out}	P_d/P_{out}
0	9.000	7.000	5.000	2.500	8.000	6.500	6.000	3.000
5	9.049	6.982	4.941	2.528	8.129	6.611	5.694	3.066
10	9.093	6.967	4.897	2.543	8.269	6.673	5.482	3.076
15	9.128	6.956	4.866	2.550	8.396	6.712	5.330	3.061
20	9.157	6.948	4.842	2.553	8.509	6.740	5.221	3.031
25	9.180	6.943	4.825	2.553	8.607	6.761	5.138	2.994
30	9.199	6.940	4.811	2.550	8.693	6.778	5.075	2.954
35	9.215	6.938	4.801	2.547	8.768	6.794	5.026	2.913
40	9.228	6.937	4.792	2.543	8.833	6.808	4.987	2.873
45	9.239	6.937	4.786	2.538	8.890	6.821	4.954	2.835
50	9.249	6.937	4.780	2.534	8.939	6.833	4.927	2.800
55	9.257	6.938	4.776	2.529	8.983	6.844	4.905	2.768
60	9.264	6.939	4.772	2.525	9.021	6.855	4.885	2.739
65	9.270	6.940	4.769	2.522	9.054	6.865	4.869	2.712
70	9.275	6.941	4.766	2.518	9.084	6.874	4.855	2.688
75	9.279	6.942	4.764	2.515	9.110	6.882	4.842	2.666
80	9.283	6.942	4.762	2.512	9.133	6.889	4.831	2.647
85					9.153	6.896	4.822	2.629
90					9.171	6.902	4.813	2.614
95					9.187	6.907	4.806	2.600
100					9.201	6.912	4.799	2.587
105					9.214	6.916	4.794	2.576
110					9.225	6.920	4.789	2.566
115					9.235	6.924	4.784	2.558
120					9.243	6.927	4.780	2.550
125					9.251	6.930	4.777	2.543
130					9.258	6.932	4.773	2.537
135					9.264	6.934	4.771	2.531
140					9.270	6.936	4.768	2.526
145					9.274	6.938	4.766	2.522
150					9.279	6.940	4.764	2.518
155					9.282	6.941	4.762	2.514

APPENDIX D: EXPANDER EFFICIENCY

Work done by an ideal expander = $\frac{P_1V_1 - P_2V_2}{\gamma - 1}$

For an ideal gas, W = $\frac{mRT_1 - mRT_2}{\gamma - 1}$

Specific work done by an ideal expander $\frac{W}{m} = \frac{RT_1}{\gamma - 1}\left(1 - \frac{T_2}{T_1}\right) = \frac{RT_1}{\gamma - 1}\left(1 - \left(\frac{P_2}{P_1}\right)^{\frac{\gamma-1}{\gamma}}\right)$

For Helium, R = 2078.5 J/Kg K, γ = 1.667

Therefore, ideal specific work $\frac{W}{m} = 3118T_1\left(1 - \left(\frac{P_2}{P_1}\right)^{0.4}\right)$

Work done by the expander = $\int PdV$

= (Area under P-V graph)*(Scaling factor for P)*(Scaling factor for V)

where scaling factor for P = 101325/14.7 = 6892.86 Pa/psi
and scaling factor for V = 11.86 * 10^{-6} m^3 (expander swept volume, based on a cylinder diameter of 0.96 inches and a stroke length of 1 inch)

Therefore, work done by expander = (Area under P-V graph) * 0.08175

Specific work done by expander= Work done by expander / (t * total mass flow rate)
where t is the cycle time

Mass flow rate $\dot{m} = \frac{P_{ref}\left(\dot{V}\frac{10^{-3}}{60}\right)}{RT_{ref}}$, where $\dot{V}$ is the measured flow rate in standard litres/minute, P_{ref} and T_{ref} are the reference pressure and temperature at which the flow meter is calibrated.

For the flow meter being used, P_{ref} = 1 atm = 101325 Pa and T_{ref} = 273 K

$\dot{m} = 2.976 * 10^{-6}(\dot{V})$

Specific work done by expander = (0.08175/2.976*10^{-6}) * Area under P-V graph / (t*$\dot{V}$) = 2.747*10^4 * (Area under P-V graph) / (t*$\dot{V}$)

APPENDIX E: WARM-END VALVE PRESSURE DROP TESTS

In order to measure the pressure drop across the needle throttles, helium was made to flow from reservoir A into the cylinder and from the cylinder to the atmosphere. In one experiment, the needle throttle was left in place. In the second experiment, the needle throttle at the outlet was completely backed out so that the pressure drop was only due to the resistance of the flow passages.

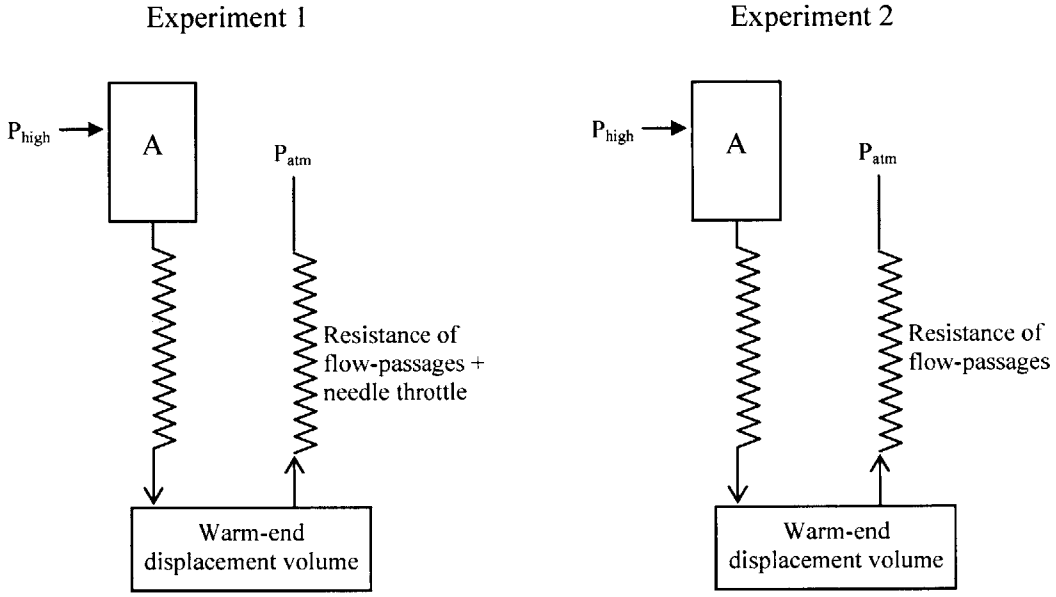

	Experiment 1	Experiment 2
P_{high} (psia)	52.3	50.5
P_A (psia)	50	48.3
$P_{disp\ vol}$ (psia)	27.7	24.3

The results show that the presence of the throttle increases the pressure drop by about 30%.

APPENDIX F: DYNAMIC EXPANDER MODEL – MATLAB CODE

F1. Mass Flow Function

```
% FUNCTION FILE

function m = massflownewer(po,to,delp,cw,t_step)
gam = 5/3;
k = 5/3;
R = 2078;
Acoldin = (pi/4) * 0.0254^2 * 0.060^2;
Acoldout = (pi/4) * 0.0254^2 * 0.060^2;
Awarm = (pi/4) * 0.0254^2 * 0.040^2/4;
if cw == 1
   nozarea = 3 * Acoldin;
elseif cw == 2
   nozarea = Awarm;
else
   nozarea = 3 * Acoldout;
end
pcrit = po * (2/(gam+1))^(gam/(gam-1));
if (po-pcrit > delp)       %subsonic
   r = (po - delp)/po;
else                       %sonic
   r = pcrit/po;
end
m = t_step * nozarea*po*sqrt( (2*k * r^(2/k) * (1 - r^((k-1)/k))) / (k-1) ) / sqrt(R*to);
```

F2. Piston Motion Function

```
% FUNCTION FILE

function [s,v,a,t_step] = pistonnewer(delp,u,xi,t_step1)
t = t_step1;
Ap = (pi/4) * 0.0254^2 * 0.96^2;
mass = 0.2;
fst = 0.2e5 * Ap;
fdy = 0.2e5 * Ap;
f = fdy;
g = 9.8;
F = delp * Ap - mass * g;

if u > 0                   %since the friction force always opposes the velocity
   netf = F - fdy;
elseif u < 0
   netf = F + fdy;
                           %if the piston is initially at rest
elseif abs(F) < abs(f)
   netf = 0;
else
   netf = sign(F) * (abs(F) - f);
end
```

```
a = netf / mass;
v = u + a * t;
s = u * t + 0.5 * a * t^2;
to = 0;
t_step = t;

if abs(sign(u) - sign(a)) <= 1      %if u and a are not in different directions
   to = t;
else                %if u and a are in different directions, but a is NOT large enough to cause the velocity to drop to zero
   to = -u/a;
end

if to < t
   t_step = to;
   v = 0;
   s = u * to + 0.5 * a * to^2;
end

s=s/0.0254;

if s + xi> 1                    %if the piston reaches the top of the cylinder
   s = 1 - xi;
   v = 0;
elseif s + xi < 0               %if the piston reaches the bottom of the cylinder
   s = -xi;
   v = 0;
end
```

F3. Main Expander Program

```
clear all
hold on
%Cycle constants

%Step controllers
c1 = 0.97;
c1a = 0.92;
c3 = 1.01;
c4 = 1.02;
c5 = 1.03;
c6 = 1.1;
c6a = 1.5;
c8 = 0.95;
c9 = 0.95;
c10 = 0.97;
xco = 0.25;
xrc = 0.2;

gam = 5/3;
R = 2078;

%Dead Volumes
xcc = 0.25;
```

```
xcw = 0.25;

tr = 300;  %Reservoir temperatures
pmax = 10e5;  %Compressor exit pr.
pl = 1.2e5; %Compressor inlet pr.

vratio = 0.0925;      %Ratio of swept volume to reservoir volume
vr = 128.28e-6;       %Reservoir volume
vsw = vr*vratio;      %Swept volume
Ap = (pi/4) * 0.0254^2 * 0.96^2;              %Piston area
vhp = 1 * 1.4 * 0.0254^3;  %Cold Plenum Volume
%=========================
%initial values

pa = 9e5;
pb = 6e5;
pc = 4.5e5;
pd = 1.8e5;

%Bleed flow controllers
b1 = 5.4e-9;
b2 = 10e-9;

%Desired pressure levels in A and D
pas = 9e5;
pds = 1.8e5;

%Initial conditions in cylinder
pcc = pb;
xc = xcc;
tcc = 300;
mc = pcc*xc*vsw/(R*tcc);
pcw = pa;
xw = 1+xcw;
tcw = 300;
mw = pcw*xw*vsw/(R*tcw);

ph = 10e5; %Initial pressure in cold end plenum
u = 0;  %piston velocity
%=======================

t_step=1e-4;
totalcycles = 10;
ncycle = 1;
n=0;
pdold = pd;
paold = pa;

for ncycle=1:1:totalcycles

  if pa>pas
    if pa>paold
      b1 = 0.97*b1;
    end
  else
    if pa<paold
```

```
      b1 = 1.03*b1;
   end
end
if pd>pds
   if pd>pdold
      b2 = 1.03*b2;
   end
else
   if pd<pdold
      b2 = 0.97*b2;
   end
end

pdold = pd;
paold = pa;

t_step = 1e-4;

%Individual step times
t1a = 0;
t2 = 0;
t3 = 0;
t4 = 0;
t5 = 0;
t6 = 0;
t6a = 0;
t7 = 0;
t8 = 0;
t9 = 0;
t10 = 0;
t1 = 0;

cycletime = 0;

n = 0; %total no. of time steps in a cycle

%Flow rates in and out of cold end
mtotalout = 0;
mtotalin = 0;

%Variables tracking change in mass of reservoirs
delma = 0;
delmb = 0;
delmc = 0;
delmd = 0;

f = 0.05; %friction factor for turbulence
thxlow = 300; %cold plenum temperature
thx = (300+thxlow)/2; %averaged heat exchanger temperature
tin = thxlow; %cold plenum temperature
%--------------------
%Process 1-1a
while pcw < c1a*pmax
   %Process "dynamic variables"
   mhx1 = sqrt( (pmax^2 - ph^2)/(2.72e19*f*thx) );
   mhx2 = (pmax^2 - ph^2)/(2.778e13*thx);
```

```
    t_step=1e-4;
    mhpin = mhx1;
    if mhx1>mhx2
       mhpin = mhx2;
    end
    if ph>pmax
       mhpin = 0;
    end
    mhpin = 2*mhpin;

    [s,u,a,t_step] = pistonnewer(pcc-pcw,u,xc-xcc,t_step);        %Define a function piston that returns the amount
by which the piston moves - function of delta p and the initial velocity

    mhpin = mhpin*t_step;
    mcin = massflownewer(ph,tin,ph-pcc,1,t_step);     %Define a function massflow

    if ph-pcc<100
       mcin = 0;
    end

    %Recalculating parameters
    mc = mc + mcin;              %mw stays the same
    xc = xc + s;
    xw = xw - s;
    pcwo = pcw;
    pcw = pcw * (1+s/xw)^gam;
    pcc = ( mcin*tin*gam*R/vsw - (pcw*xw - pcwo*(xw+s)) + pcc*(xc-s) ) / xc;
    tcw = pcw*xw*vsw/(R*mw);      %Calculating temps
    tcc = pcc*xc*vsw/(R*mc);
    ph = ph + (mhpin-mcin)*R*thxlow/vhp; %Plenum pressure recalculated
    mtotalin = mtotalin + mcin;

    mabd = b1 * sqrt(pmax-pa) * t_step;
    mdbd = b2 * sqrt(pd-pl) * t_step;
    pa = pa + mabd*tr*R/vr;
    pd = pd - mdbd*tr*R/vr;

    t1a = t1a + t_step; %Time for this step only
    cycletime = cycletime + t_step;
    n=n+1;          %Number of iterations
    prco(n)=pcc;
    prwa(n)=pcw;
    pos(n)=xc;
    samay(n)=cycletime;
    acc(n)=a;
    vel(n)=u;
  end
  %====================
  t1a
  %--------------------
  %Process 1a-2
  while xc-xcc < xco
    %Process "dynamic variables"
    mhx1 = sqrt( (pmax^2 - ph^2)/(2.72e19*f*thx) );
    mhx2 = (pmax^2 - ph^2)/(2.778e13*thx);
```

```
  t_step=1e-4;
  mhpin = mhx1;
  if mhx1>mhx2
    mhpin = mhx2;
  end
  if pmax-ph<100
    mhpin = 0;
  end
  mhpin = 2*mhpin;

  [s,u,a,t_step] = pistonnewer(pcc-pcw,u,xc-xcc,t_step);
  mhpin = mhpin*t_step;

  mcin = massflownewer(ph,tin,ph-pcc,1,t_step);
  if ph-pcc<100
    mcin = 0;
  end

  mwout = massflownewer(pcw,tcw,pcw-pa,2,t_step);
  if pcw-pa<100
    mwout=0;
  end

  %Recalculating parameters
  mc = mc + mcin;
  mw = mw - mwout;
  xc = xc + s;
  xw = xw - s;
  pcw = pcw * ((mw/xw) / ( (mw+mwout)/(xw+s) ))^gam;
  pcc = ( (mcin*R*tin)/vsw + pcc*(xc-s) ) / xc;
  tcw = pcw*xw*vsw/(R*mw);      %Calculating temps
  tcc = pcc*xc*vsw/(R*mc);
  ph = ph + (mhpin-mcin)*R*thxlow/vhp;

  mtotalin = mtotalin + mcin;
  delma = delma + mwout;

  pa = pa + mwout*tr*R/vr;      %Updating pressure in reservoir a
  mabd = b1 * sqrt(pmax-pa) * t_step;
  mdbd = b2 * sqrt(pd-pl) * t_step;
  pa = pa + mabd*tr*R/vr;
  pd = pd - mdbd*tr*R/vr;

  t2 = t2 + t_step;
  cycletime = cycletime + t_step;
  n=n+1;
  prco(n)=pcc;
  prwa(n)=pcw;
  samay(n)=cycletime;
  pos(n)=xc;
  acc(n)=a;
  vel(n)=u;
end
%====================
t2
```

```
%-------------------
%Process 2-3
while pcw > c3*pa
   %Process "dynamic variables"
   mhx1 = sqrt( (pmax^2 - ph^2)/(2.72e19*f*thx) );
   mhx2 = (pmax^2 - ph^2)/(2.778e13*thx);

   t_step=1e-4;
   mhpin = mhx1;
   if mhx1>mhx2
      mhpin = mhx2;
   end
   if pmax-ph<100
      mhpin = 0;
   end
   mhpin = 2*mhpin;

   [s,u,a,t_step] = pistonnewer(pcc-pcw,u,xc-xcc,t_step);
   mhpin = mhpin*t_step;

   mwout = massflownewer(pcw,tcw,pcw-pa,2,t_step);
   if pcw-pa<100
      mwout=0;
   end

   %Recalculating parameters
   mw = mw - mwout;              %mc stays the same
   xc = xc + s;
   xw = xw - s;
   pcc = pcc * (1-s/xc)^gam;
   pcw = pcw * ( (mw/xw) / ( (mw+mwout)/(xw+s) ) )^gam;
   tcw = pcw*xw*vsw/(R*mw);      %Calculating temps
   tcc = pcc*xc*vsw/(R*mc);

   ph = ph + (mhpin)*R*thxlow/vhp;
   delma = delma + mwout;

   pa = pa + mwout*tr*R/vr;      %Updating pressure in reservoir a
   mabd = b1 * sqrt(pmax-pa) * t_step;
   mdbd = b2 * sqrt(pd-pl) * t_step;
   pa = pa + mabd*tr*R/vr;
   pd = pd - mdbd*tr*R/vr;

   t3 = t3 + t_step;
   cycletime = cycletime + t_step;
   n=n+1;
   prco(n)=pcc;
   prwa(n)=pcw;
   samay(n)=cycletime;
   pos(n)=xc;
   acc(n)=a;
   vel(n)=u;
end
%====================
t3
%-------------------
```

```
%Process 3-4
while pcw > c4*pb
   %Process "dynamic variables"
   mhx1 = sqrt( (pmax^2 - ph^2)/(2.72e19*f*thx) );
   mhx2 = (pmax^2 - ph^2)/(2.778e13*thx);

   t_step=1e-4;
   mhpin = mhx1;
   if mhx1>mhx2
      mhpin = mhx2;
   end
   if pmax-ph<100
      mhpin = 0;
   end
   mhpin = 2*mhpin;

   [s,u,a,t_step] = pistonnewer(pcc-pcw,u,xc-xcc,t_step);
   mhpin = mhpin*t_step;

   mwout = massflownewer(pcw,tcw,pcw-pb,2,t_step);
   if pcw-pb<100
      mwout=0;
   end

   %Recalculating parameters
   mw = mw - mwout;              %mc stays the same
   xc = xc + s;
   xw = xw - s;
   pcc = pcc * (1-s/xc)^gam;
   pcw = pcw * ( (mw/xw) / ( (mw+mwout)/(xw+s) ) )^gam;
   tcw = pcw*xw*vsw/(R*mw);       %Calculating temps
   tcc = pcc*xc*vsw/(R*mc);

   ph = ph + (mhpin)*R*thxlow/vhp;
   delmb = delmb + mwout;

   pb = pb + mwout*tr*R/vr;       %Updating pressure in reservoir b
   mabd = b1 * sqrt(pmax-pa) * t_step;
   mdbd = b2 * sqrt(pd-pl) * t_step;
   pa = pa + mabd*tr*R/vr;
   pd = pd - mdbd*tr*R/vr;

   t4 = t4 + t_step;
   cycletime = cycletime + t_step;
   n=n+1;
   prco(n)=pcc;
   prwa(n)=pcw;
   samay(n)=cycletime;
   pos(n)=xc;
   acc(n)=a;
   vel(n)=u;
end
%====================
t4
%--------------------
%Process 4-5
```

```
while pcw > c5*pc
   %Process "dynamic variables"
   mhx1 = sqrt( (pmax^2 - ph^2)/(2.72e19*f*thx) );
   mhx2 = (pmax^2 - ph^2)/(2.778e13*thx);

   t_step=1e-4;
   mhpin = mhx1;
   if mhx1>mhx2
      mhpin = mhx2;
   end
   if pmax-ph<100
      mhpin = 0;
   end
   mhpin = 2*mhpin;

   [s,u,a,t_step] = pistonnewer(pcc-pcw,u,xc-xcc,t_step);
   mhpin = mhpin*t_step;

   mwout = massflownewer(pcw,tcw,pcw-pc,2,t_step);
   if pcw-pc<100
      mwout=0;
   end

   %Recalculating parameters
   mw = mw - mwout;              %mc stays the same
   xc = xc + s;
   xw = xw - s;
   pcc = pcc * (1-s/xc)^gam;
   pcw = pcw * ( (mw/xw) / ( (mw+mwout)/(xw+s) ) )^gam;
   tcw = pcw*xw*vsw/(R*mw);      %Calculating temps
   tcc = pcc*xc*vsw/(R*mc);

   ph = ph + (mhpin)*R*thxlow/vhp;
   delmc = delmc + mwout;

   pc = pc + mwout*tr*R/vr;      %Updating pressure in reservoir b
   mabd = b1 * sqrt(pmax-pa) * t_step;
   mdbd = b2 * sqrt(pd-pl) * t_step;
   pa = pa + mabd*tr*R/vr;
   pd = pd - mdbd*tr*R/vr;

   t5 = t5 + t_step;
   cycletime = cycletime + t_step;
   n=n+1;
   prco(n)=pcc;
   prwa(n)=pcw;
   samay(n)=cycletime;
   pos(n)=xc;
   acc(n)=a;
   vel(n)=u;
end
%=====================
t5
%--------------------
%Process 5-6
while pcw > c6*pd
```

```
   %Process "dynamic variables"
   mhx1 = sqrt( (pmax^2 - ph^2)/(2.72e19*f*thx) );
   mhx2 = (pmax^2 - ph^2)/(2.778e13*thx);

   t_step=1e-4;
   mhpin = mhx1;
   if mhx1>mhx2
      mhpin = mhx2;
   end
   if pmax-ph<100
      mhpin = 0;
   end
   mhpin = 2*mhpin;

   [s,u,a,t_step] = pistonnewer(pcc-pcw,u,xc-xcc,t_step);
   mhpin = mhpin*t_step;

   mwout = massflownewer(pcw,tcw,pcw-pd,2,t_step);
   if pcw-pd<100
      mwout=0;
   end

   %Recalculating parameters
   mw = mw - mwout;              %mc stays the same
   xc = xc + s;
   xw = xw - s;
   pcc = pcc * (1-s/xc)^gam;
   pcw = pcw * ( (mw/xw) / ( (mw+mwout)/(xw+s) ) )^gam;
   tcw = pcw*xw*vsw/(R*mw);      %Calculating temps
   tcc = pcc*xc*vsw/(R*mc);

   ph = ph + (mhpin)*R*thxlow/vhp;
   delmd = delmd + mwout;

   pd = pd + mwout*tr*R/vr;      %Updating pressure in reservoir b
   mabd = b1 * sqrt(pmax-pa) * t_step;
   mdbd = b2 * sqrt(pd-pl) * t_step;
   pa = pa + mabd*tr*R/vr;
   pd = pd - mdbd*tr*R/vr;

   t6 = t6 + t_step;
   cycletime = cycletime + t_step;
   n=n+1;
   prco(n)=pcc;
   prwa(n)=pcw;
   samay(n)=cycletime;
   pos(n)=xc;
   acc(n)=a;
   vel(n)=u;
end
%=====================
t6
%--------------------
%Process 6-6a
while pcw > c6a*pl
   %Process "dynamic variables"
```

```
   mhx1 = sqrt( (pmax^2 - ph^2)/(2.72e19*f*thx) );
   mhx2 = (pmax^2 - ph^2)/(2.778e13*thx);

   t_step=1e-4;
   mhpin = mhx1;
   if mhx1>mhx2
      mhpin = mhx2;
   end
   if pmax-ph<100
      mhpin = 0;
   end
   mhpin = 2*mhpin;

   [s,u,a,t_step] = pistonnewer(pcc-pcw,u,xc-xcc,t_step);
   mhpin = mhpin*t_step;

   mcout = massflownewer(pcc,tcc,pcc-pl,2,t_step);
   if pcc-pl<100
      mcout=0;
   end

   mco = mc; tcco = tcc; tcwo = tcw;
   %Recalculating parameters
   mc = mc - mcout;              %mw stays the same
   xc = xc + s;
   xw = xw - s;
   pcw = pcw * (1+s/xw)^gam;
   pcc = pcc * ( (mc/xc) / ( (mc+mcout)/(xc-s) ) )^gam;
   tcw = pcw*xw*vsw/(R*mw);      %Calculating temps
   tcc = pcc*xc*vsw/(R*mc);

   %tout = -( mw*(tcw-tcwo) + mc*tcc - mco*tcco ) / (mcout * gam);   %Equation for outlet temperature
   %outenergy = mcout * tout;
   mtotalout = mtotalout + mcout;

   ph = ph + (mhpin)*R*thxlow/vhp;
   mabd = b1 * sqrt(pmax-pa) * t_step;
   mdbd = b2 * sqrt(pd-pl) * t_step;
   pa = pa + mabd*tr*R/vr;
   pd = pd - mdbd*tr*R/vr;

   t6a = t6a + t_step;
   cycletime = cycletime + t_step;
   n=n+1;
   prco(n)=pcc;
   prwa(n)=pcw;
   samay(n)=cycletime;
   pos(n)=xc;
   acc(n)=a;
   vel(n)=u;
end
%=======================
t6a
%--------------------
%Process 6a-7
while xc-xcc > xrc
```

```
%Process "dynamic variables"
mhx1 = sqrt( (pmax^2 - ph^2)/(2.72e19*f*thx) );
mhx2 = (pmax^2 - ph^2)/(2.778e13*thx);

t_step=1e-4;
mhpin = mhx1;
if mhx1>mhx2
   mhpin = mhx2;
end
if pmax-ph<100
   mhpin = 0;
end
mhpin = 2*mhpin;

[s,u,a,t_step] = pistonnewer(pcc-pcw,u,xc-xcc,t_step);
mhpin = mhpin*t_step;

mcout = massflownewer(pcc,tcc,pcc-pl,3,t_step);
if pcc-pl<100
   mcout = 0;
end

if abs(pcw-pd)<100
   mwin = 0;
elseif pcw>pd
   mwout = massflownewer(pcw,tcw,pcw-pd,2,t_step);
else
   mwin = massflownewer(pd,tr,pd-pcw,2,t_step);
end

%Recalculating parameters
mc = mc - mcout;
xc = xc + s;
xw = xw - s;
pcc = pcc * (mc/xc) / ( (mc+mcout)/(xc-s) );
if pcw<pd
   mw = mw + mwin;
   pcw = ( (mwin*R*tr)/vsw + pcw*(xw+s) ) / xw;
else
   mw = mw - mwout;
   pcw = pcw * ( (mw/xw) / ( (mw+mwout)/(xw+s) ) )^gam;
end

tcw = pcw*xw*vsw/(R*mw);       %Calculating temps
tcc = pcc*xc*vsw/(R*mc);

%tout = tcc;        %Outlet temperature
%outenergy = outenergy + mcout * tout;
mtotalout = mtotalout + mcout;

if pcw<pd
   delmd = delmd - mwin;
else
   delmd = demd + mwout;
end
```

```
    ph = ph + (mhpin)*R*thxlow/vhp;

    if pcw<pd
       pd = pd - mwin*tr*R/vr;       %Updating pressure in reservoir d
    else
       pd = pd + mwout*tr*R/vr;      %Updating pressure in reservoir d
    end
    mabd = b1 * sqrt(pmax-pa) * t_step;
    mdbd = b2 * sqrt(pd-pl) * t_step;
    pa = pa + mabd*tr*R/vr;
    pd = pd - mdbd*tr*R/vr;

    t7 = t7 + t_step;
    cycletime = cycletime + t_step;
    n=n+1;
    prco(n)=pcc;
    prwa(n)=pcw;
    samay(n)=cycletime;
    pos(n)=xc;
    acc(n)=a;
    vel(n)=u;
end
%====================
t7
%--------------------
%Process 7-8
while pcw < c8*pd
    %Process "dynamic variables"
    mhx1 = sqrt( (pmax^2 - ph^2)/(2.72e19*f*thx) );
    mhx2 = (pmax^2 - ph^2)/(2.778e13*thx);

    t_step=1e-4;
    mhpin = mhx1;
    if mhx1>mhx2
       mhpin = mhx2;
    end
    if pmax-ph<100
       mhpin = 0;
    end
    mhpin = 2*mhpin;

    [s,u,a,t_step] = pistonnewer(pcc-pcw,u,xc-xcc,t_step);

    mhpin = mhpin*t_step;
    mwin = massflownewer(pd,tr,pd-pcw,2,t_step);

    if pd-pcw<100
       mwin = 0;
    end

    %Recalculating parameters
    mw = mw + mwin;        %mc stays the same
    xc = xc + s;
    xw = xw - s;
    pcco = pcc;
    pcc = pcc * (1-s/xc)^gam;
```

```
   pcw = ( mwin*tr*gam*R/vsw - (pcc*xc - pcco*(xc-s)) + pcw*(xw+s) ) / xw;
   tcw = pcw*xw*vsw/(R*mw);        %Calculating temps
   tcc = pcc*xc*vsw/(R*mc);

   delmd = delmd - mwin;
   ph = ph + (mhpin)*R*thxlow/vhp; %Plenum pressure recalculated

   pd = pd - mwin*tr*R/vr;        %Updating pressure in reservoir d
   mabd = b1 * sqrt(pmax-pa) * t_step;
   mdbd = b2 * sqrt(pd-pl) * t_step;
   pa = pa + mabd*tr*R/vr;
   pd = pd - mdbd*tr*R/vr;

   t8 = t8 + t_step;
   cycletime = cycletime + t_step;
   n=n+1;
   prco(n)=pcc;
   prwa(n)=pcw;
   pos(n)=xc;
   acc(n)=a;
   vel(n)=u;
   samay(n)=cycletime;
end
%=====================
t8
%--------------------
%Process 8-9
while pcw < c9*pc
   %Process "dynamic variables"
   mhx1 = sqrt( (pmax^2 - ph^2)/(2.72e19*f*thx) );
   mhx2 = (pmax^2 - ph^2)/(2.778e13*thx);

   t_step=1e-4;
   mhpin = mhx1;
   if mhx1>mhx2
      mhpin = mhx2;
   end
   if pmax-ph<100
      mhpin = 0;
   end
   mhpin = 2*mhpin;

   [s,u,a,t_step] = pistonnewer(pcc-pcw,u,xc-xcc,t_step);

   mhpin = mhpin*t_step;
   mwin = massflownewer(pc,tr,pc-pcw,2,t_step);

   if pc-pcw<100
      mwin = 0;
   end

   %Recalculating parameters
   mw = mw + mwin;        %mc stays the same
   xc = xc + s;
   xw = xw - s;
   pcco = pcc;
```

```
   pcc = pcc * (1-s/xc)^gam;
   pcw = ( mwin*tr*gam*R/vsw - (pcc*xc - pcco*(xc-s)) + pcw*(xw+s) ) / xw;
   tcw = pcw*xw*vsw/(R*mw);       %Calculating temps
   tcc = pcc*xc*vsw/(R*mc);

   delmc = delmc - mwin;
   ph = ph + (mhpin)*R*thxlow/vhp; %Plenum pressure recalculated

   pc = pc - mwin*tr*R/vr;        %Updating pressure in reservoir d
   mabd = b1 * sqrt(pmax-pa) * t_step;
   mdbd = b2 * sqrt(pd-pl) * t_step;
   pa = pa + mabd*tr*R/vr;
   pd = pd - mdbd*tr*R/vr;

   t9 = t9 + t_step;
   cycletime = cycletime + t_step;
   n=n+1;
   prco(n)=pcc;
   prwa(n)=pcw;
   pos(n)=xc;
   samay(n)=cycletime;
   acc(n)=a;
   vel(n)=u;
end
%====================
t9
%--------------------
%Process 9-10
while pcw < c10*pb
   %Process "dynamic variables"
   mhx1 = sqrt( (pmax^2 - ph^2)/(2.72e19*f*thx) );
   mhx2 = (pmax^2 - ph^2)/(2.778e13*thx);

   t_step=1e-4;
   mhpin = mhx1;
   if mhx1>mhx2
      mhpin = mhx2;
   end
   if pmax-ph<100
      mhpin = 0;
   end
   mhpin = 2*mhpin;

   [s,u,a,t_step] = pistonnewer(pcc-pcw,u,xc-xcc,t_step);

   mhpin = mhpin*t_step;
   mwin = massflownewer(pb,tr,pb-pcw,2,t_step);

   if pb-pcw<100
      mwin = 0;
   end

   %Recalculating parameters
   mw = mw + mwin;        %mc stays the same
   xc = xc + s;
   xw = xw - s;
```

```
   pcco = pcc;
   pcc = pcc * (1-s/xc)^gam;
   pcw = ( mwin*tr*gam*R/vsw - (pcc*xc - pcco*(xc-s)) + pcw*(xw+s) ) / xw;
   tcw = pcw*xw*vsw/(R*mw);        %Calculating temps
   tcc = pcc*xc*vsw/(R*mc);

   delmb = delmb - mwin;
   ph = ph + (mhpin)*R*thxlow/vhp; %Plenum pressure recalculated

   pb = pb - mwin*tr*R/vr;         %Updating pressure in reservoir d
   mabd = b1 * sqrt(pmax-pa) * t_step;
   mdbd = b2 * sqrt(pd-pl) * t_step;
   pa = pa + mabd*tr*R/vr;
   pd = pd - mdbd*tr*R/vr;

   t10 = t10 + t_step;
   cycletime = cycletime + t_step;
   n=n+1;
   prco(n)=pcc;
   prwa(n)=pcw;
   pos(n)=xc;
   samay(n)=cycletime;
   acc(n)=a;
   vel(n)=u;
end
%=====================
t10
%--------------------
%Process 10-1
while pcw < c1*pa
   %Process "dynamic variables"
   mhx1 = sqrt( (pmax^2 - ph^2)/(2.72e19*f*thx) );
   mhx2 = (pmax^2 - ph^2)/(2.778e13*thx);

   t_step=1e-4;
   mhpin = mhx1;
   if mhx1>mhx2
      mhpin = mhx2;
   end
   if pmax-ph<100
      mhpin = 0;
   end
   mhpin = 2*mhpin;

   [s,u,a,t_step] = pistonnewer(pcc-pcw,u,xc-xcc,t_step);

   mhpin = mhpin*t_step;
   mwin = massflownewer(pa,tr,pa-pcw,2,t_step);

   if pa-pcw<100
      mwin = 0;
   end

   %Recalculating parameters
   mw = mw + mwin;         %mc stays the same
   xc = xc + s;
```

```
    xw = xw - s;
    pcco = pcc;
    pcc = pcc * (1-s/xc)^gam;
    pcw = ( mwin*tr*gam*R/vsw - (pcc*xc - pcco*(xc-s)) + pcw*(xw+s) ) / xw;
    tcw = pcw*xw*vsw/(R*mw);        %Calculating temps
    tcc = pcc*xc*vsw/(R*mc);

    delma = delma - mwin;
    ph = ph + (mhpin)*R*thxlow/vhp; %Plenum pressure recalculated

    pa = pa - mwin*tr*R/vr;        %Updating pressure in reservoir d
    mabd = b1 * sqrt(pmax-pa) * t_step;
    mdbd = b2 * sqrt(pd-pl) * t_step;
    pa = pa + mabd*tr*R/vr;
    pd = pd - mdbd*tr*R/vr;

    t1 = t1 + t_step;
    cycletime = cycletime + t_step;
    n=n+1;
    prco(n)=pcc;
    prwa(n)=pcw;
    pos(n)=xc;
    samay(n)=cycletime;
    acc(n)=a;
    vel(n)=u;
  end
  %====================
  t1
  pa
  pd
  n
  plot(pos-xcc,prwa)
  plot(pos-xcc,prco,'r')
  n=0;
end
```

F4. Condensed Expander Program for blow-in/intake stroke analysis

```
%Cycle constants

%Step controllers
c1a = 0.92;
xco = 0.25;

gam = 5/3;
R = 2078;

%Dead Volumes
xcc = 0.25;
xcw = 0.25;

tr = 300;   %Reservoir temperatures
pmax = 10e5;  %Compressor exit pr.
```

```
vratio = 0.0925;       %Ratio of swept volume to reservoir volume
vr = 128.28e-6;        %Reservoir volume
vsw = vr*vratio;       %Swept volume
Ap = (pi/4) * 0.0254^2 * 0.96^2;              %Piston area
vhp = 4 * 1.4 * 0.0254^3;  %Cold Plenum Volume
coils = 2;             %Number of heat ex. high pressure coils
%=========================
%initial values

pas = 9e5;
pa = pas;
pb = 6e5;

ph = 10e5; %Initial pressure in cold end plenum
u = 0;  %piston velocity
%=========================

t_step = 1e-4;
totalcycles = 6;
ncycle = 1;
n = 0;

for ncycle=1:1:totalcycles

   t1a = 0;
   t2 = 0;
   cycletime = 0;

   n = 0; %total no. of time steps in a cycle

   leak = 0*5.95e-6; %Leak rate
   f = 0.05; %friction factor for turbulence
   thxlow = 100; %cold plenum temperature
   thx = thxlow/2+150; %averaged heat exchanger temperature
   tin = thxlow;

   %Initial conditions in cylinder
   pcc = pb;
   xc = xcc;
   tcc = thxlow;
   mc = pcc*xc*vsw/(R*tcc);
   pcw = pa;
   xw = 1+xcw;
   tcw = 300;
   mw = pcw*xw*vsw/(R*tcw);

   %-------------------
   %Process 1-1a
   while pcw < c1a*pmax
      %Process "dynamic variables"
      mhx1 = sqrt( coils/2 *(pmax^2 - ph^2)/(2.72e19*f*thx) );
      mhx2 = coils/2 *(pmax^2 - ph^2)/(2.778e13*thx);

      t_step=1e-4;
      mhpin = mhx1;
      if mhx1>mhx2
```

```
    mhpin = mhx2;
  end
  if ph>pmax
    mhpin = 0;
  end
  mhpin = coils*mhpin;

  [s,u,a,t_step] = pistonnewer(pcc-pcw,u,xc-xcc,t_step);        %Define a function piston that returns the amount
by which the piston moves - function of delta p and the initial velocity

  mhpin = mhpin*t_step;
  mcin = massflownewer(ph,tin,ph-pcc,1,t_step);     %Define a function massflow

  if ph-pcc<100
    mcin = 0;
  end

  mcleak = leak*t_step;
  mcin = mcin-mcleak;
  mhpin = mhpin-mcleak;

  %Recalculating parameters
  mc = mc + mcin;              %mw stays the same
  xc = xc + s;
  xw = xw - s;
  pcwo = pcw;
  pcw = pcw * (1+s/xw)^gam;
  pcc = ( mcin*tin*gam*R/vsw - (pcw*xw - pcwo*(xw+s)) + pcc*(xc-s) ) / xc;
  tcw = pcw*xw*vsw/(R*mw);       %Calculating temps
  tcc = pcc*xc*vsw/(R*mc);
  ph = ph + (mhpin-mcin)*R*thxlow/vhp; %Plenum pressure recalculated
  mtotalin = mtotalin + mcin;

  t1a = t1a + t_step; %Time for this step only
  cycletime = cycletime + t_step;
  n=n+1;
  prco(n)=pcc;
  prwa(n)=pcw;
  pos(n)=xc;
  samay(n)=cycletime;
end
%==================
t1a
%-------------------
%Process 1a-2
while xc-xcc < xco
  %Process "dynamic variables"
  mhx1 = sqrt( coils/2 *(pmax^2 - ph^2)/(2.72e19*f*thx) );
  mhx2 = coils/2 *(pmax^2 - ph^2)/(2.778e13*thx);

  t_step=1e-4;
  mhpin = mhx1;
  if mhx1>mhx2
    mhpin = mhx2;
  end
  if pmax-ph<100
```

```
    mhpin = 0;
  end
  mhpin = coils*mhpin;

  [s,u,a,t_step] = pistonnewer(pcc-pcw,u,xc-xcc,t_step);
  mhpin = mhpin*t_step;

  mcin = massflownewer(ph,tin,ph-pcc,1,t_step);
  if ph-pcc<100
    mcin = 0;
  end

  mwout = massflownewer(pcw,tcw,pcw-pa,2,t_step);
  if pcw-pa<100
    mwout=0;
  end

  mcleak = leak*t_step;
  mcin = mcin-mcleak;
  mhpin = mhpin-mcleak;

  %Recalculating parameters
  mc = mc + mcin;
  mw = mw - mwout;
  xc = xc + s;
  xw = xw - s;
  pcw = pcw * ((mw/xw) / ( (mw+mwout)/(xw+s) ))^gam;
  pcc = ( (mcin*R*tin)/vsw + pcc*(xc-s) ) / xc;          % just check this, while i'm at it
  tcw = pcw*xw*vsw/(R*mw);       %Calculating temps
  tcc = pcc*xc*vsw/(R*mc);
  ph = ph + (mhpin-mcin)*R*thxlow/vhp;

  pa = pa + mwout*tr*R/vr;       %Updating pressure in reservoir a

  t2 = t2 + t_step;
  cycletime = cycletime + t_step;
  n=n+1;
  prco(n)=pcc;
  prwa(n)=pcw;
  samay(n)=cycletime;
  pos(n)=xc;
end
%====================
t2
%====================
%Refilling high-pressure reservoir
t1cycle = 0.5;
trefill = 0;
t_step = 1e-4;
while trefill < t1cycle
  mhx1 = sqrt(coils/2 * (pmax^2 - ph^2)/(2.72e19*f*thx) );
  mhx2 = coils/2 *(pmax^2 - ph^2)/(2.778e13*thx);
  mhpin = mhx1;
  if mhx1>mhx2
    mhpin = mhx2;
  end
```

```
    if pmax-ph<100
       mhpin = 0;
    end
    mhpin = coils*mhpin;
    mhpin = mhpin*t_step;
    mcleak = leak*t_step;
    mhpin = mhpin-mcleak;
    ph = ph + mhpin*R*thxlow/vhp;
    trefill = trefill + t_step;
  end

  %Reinitialising cylinder conditions
  pa=pas;
  pcc = pb;
  xc = xcc;
  tcc = thxlow;
  mc = pcc*xc*vsw/(R*tcc);
  pcw = pa;
  xw = 1+xcw;
  tcw = 300;
  mw = pcw*xw*vsw/(R*tcw);
  u = 0;
  ph
end
```